UNIVERSITÀ DEGLI STUDI DI MILANO
FACOLTÀ DI SCIENZE MATEMATICHE,
FISICHE E NATURALI

Corso di Laurea Magistrale in Fisica

A MICROSCOPIC MODEL FOR THE COLLECTIVE RESPONSE IN ODD NUCLEI

Relatore:
Prof. Gianluca COLÒ
Correlatore:
Prof.ssa Angela BRACCO
Correlatore:
Dott. Xavier ROCA-MAZA

Tesi di Laurea di:
Giacomo POZZI
Matricola n.772405
Codice Pacs: 21.60-n, 21.10-k, 21.65-f

Anno accademico 2010-2011

Contents

Introduction

One of the most outstanding problems in nuclear physics nowadays is the determination of the equation of state (EOS) of isospin-asymmetric nuclear matter, i.e., nuclear matter in which the number of neutrons exceeds the number of protons. In particular, it is of paramount importance to constrain the properties of the symmetry energy, which is an estimate of the energy cost to convert a proton into a neutron in symmetric nuclear matter. Knowledge of the nuclear symmetry energy, and in particular of its density dependence, is essential for solving many problems in nuclear physics, such as the dynamics of heavy-ion collisions and the structure of exotic nuclei (their masses, neutron and proton density distributions, mean radii, collective excitations). Besides, the symmetry energy deeply influences a number of important issues in astrophysics, such as the mass-radius relation of neutron stars, the nucleosynthesis during pre-supernova evolution of massive stars, the cooling of proto-neutron stars and the fractional moment of inertia of the neutron star crust [LCK08, SPL$^+$05].

Recently, two kinds of tools have been identified to constrain the properties of the symmetry energy. The first includes the study of the isospin effects in heavy-ion reactions with different entrance/exit channels. The second, instead, is related to the main features of giant resonances, which are a prime example of nuclear collective modes. In fact, even though the nucleus, to a first approximation, can be described as composed by independent particles moving in an average potential generated by all nucleons, it is a well-known fact that the residual interaction terms can give rise to collective excitations, that is, vibrations of the nucleus as a whole in which almost all the particles participate. As an example, the isovector giant dipole resonance (IVGDR) is an extremely collective mode in which neutrons and protons oscillate out of phase with a dipole pattern, and whose constrained energy is qualitatively found to be related to the symmetry energy at a certain subsaturation density. Recently, it has been claimed the pygmy dipole resonance (PDR), a low-energy peak which is found in the dipole response of several neutron-rich nuclei, to be a good constraint for the density dependence of the symmetry energy [K$^+$07, C$^+$10]. In fact, since this mode is thought to correspond to a resonant oscillation of the weakly bound neutron skin against the isospin-saturated proton-neutron core, one expects the total strength of the PDR to be closely related to the neutron skin thickness, i.e., the difference between the neutron and proton r.m.s. radii [Pie06]. The latter quantity is very important for the constraint of the symmetry energy since it has been empirically found to be closely related to the slope of the symmetry energy at the saturation density. The latter, in fact, directly affects the pressure of neutron rich matter and so, as a consequence, the thickness of the outermost neutron skin around the core. This picture holds if the PDR is confirmed to be a true collective mode: in recent years, great efforts have been devoted to the analysis of the collective character of the pygmy resonance and opposite conclusions were drawn [RN10], leaving the problem open and unsolved.

The interest in the present work stems from some recent Coulomb-excitation experiments at GSI (Darmstadt) which provided experimental data about the features of the PDR in ^{68}Ni and neighboring nuclei [W$^+$09]. A preliminary analysis of the recorded experimental data has claimed the pygmy dipole centroid in the odd nucleus ^{67}Ni to be at least 1 MeV lower than the centroid of the neighboring even-even ^{68}Ni. A similar result had been found in the Sn region, since the

centroid of the PDR for the odd nucleus ^{131}Sn was found to be lower than that of its even-even neighbor, ^{132}Sn [K$^+$07].

Although many self-consistent microscopic theoretical models have been developed to describe collective multipole excitations in nuclear systems, such as the random phase approximation (RPA) model, these all are able to deal only with even-even nuclei, i.e., nuclei with an even number of protons and neutrons. Self-consistent theoretical tools able to describe also odd nuclei, although not available so far, are then needed.

This thesis is intended to give a first theoretical model able to describe microscopically the multipole excitations in odd nuclei. In particular, because of its implications for the density dependence of the symmetry energy, our goal is to provide a consistent explanation for the experimentally observed shift in the pygmy dipole strength. Our interest is also associated with testing the model predictions for the collective or non-collective character of this resonance.

For simplicity, we restrict to odd nuclei near doubly-magic closed-shell configurations in order to neglect the effect of nuclear deformations and pairing correlations. The simplest possible picture of such an odd nucleus is that of an even-even core plus an odd-nucleon, which can be either a particle or a hole. If the core and the odd-nucleon were completely independent, the excitation spectrum would be just the sum of the vibrational spectrum of the core plus the single-particle excitation spectrum of the odd-nucleon. In a realistic picture, nonetheless, the core and the odd-nucleon are not independent. The following problem has to be dealt with: how the excitation energies and the wave functions of the even-even core (i.e. of the phonons) and the odd-particle (or hole) are mutually affected. For this reason, the interaction between the even-even core and the odd-nucleon is treated in the framework of microscopic particle-vibration coupling. In order to get the excitation spectrum of the odd nucleus, instead of separating explicitly the collective from the single-nucleon excitations, we consider states obtained by linear combinations of the two modes. The model is then applied to dipole response in ^{67}Ni and ^{69}Ni, and the results are compared to experimental findings.

In Chapter 1 the general properties of the equation of state of nuclear matter are exposed, focusing, in particular, to its isospin-asymmetric part and on the implications on exotic nuclei and neutron stars. In Chapter 2, we review the main properties of nuclear giant resonances, focusing in particular on the relationship between collective modes and density dependence of the symmetry energy. Besides, a microscopic original analysis of the pygmy dipole resonance in ^{68}Ni is reported. In Chapter 3, fundamental microscopic nuclear theories are exposed: the Hartree-Fock method with effective Skyrme interaction (SHF), the random phase approximation and the particle-vibration coupling theory (PVC). Our model, named *odd-particle-vibration model* (OPVC), is discussed in Chapter 4. Finally, in Chapter 5, the results of the calculations for ^{67}Ni and ^{69}Ni are presented. In Appendix A we report a brief resume of angular momentum theory and, in Appendix B, we expose the details of the calculation of the transition matrix element in the OPVC model.

Chapter 1

Equation of state of nuclear matter

Besides the many radioactive beam facilities that already exist in the world, a number of next-generation installations are being constructed or planned. At these facilities, nuclear reactions involving nuclei in which the number of neutrons exceeds that of protons can be studied, thus providing a great opportunity to study both the structure of rare isotopes and the properties of isospin-asymmetric nuclear matter. This has stimulated much interest and a lot of activity in a new research direction in nuclear physics, namely *isospin physics*. Complementary to the nuclear structure studies in this field are, thus, reaction studies with radioactive beams, and expecially heavy-ion reactions induced by neutron-rich beams at intermediate energies.

The ultimate goal of isospin physics is to determine the isospin dependence of the in-medium nuclear effective interaction, the *equation of state* (EOS) of *isospin-asymmetric nuclear matter* and, in particular, the density dependence of the *nuclear symmetry energy*. The latter has been identified as one of the most outstanding problems in nuclear physics nowadays.

Knowledge of the nuclear symmetry energy is essential for understanding not only many problems in nuclear physics, such as the dynamics of heavy-ion collisions induced by radioactive beams and the structure of exotic nuclei (their masses, neutron and proton density distributions, mean radii, collective excitations), but also a number of important issues in astrophysics, such as the mass-radius relation of neutron stars and the cooling of proto-neutron stars.

The trend of the symmetry energy as a function of the density is poorly known, expecially at supra-normal densities, that is, at densities beyond the saturation value. This is in constrast to our knowledge of the symmetric part of the nuclear EOS. As an example, through the efforts of both the nuclear structure and the heavy-ion reaction community for over three decades, the *incompressibility of symmetric nuclear matter* at its *saturation density*, $\rho_0 = 0.16$ fm^{-3}, has been determined to be $K_\infty = 240 \pm 20$ MeV from nuclear giant monopole resonances [Col08]. The EOS of symmetric nuclear matter around the saturation density has been constrained by measurements of collective flows and of subthreshold kaon production in relativistic nucleus-nucleus collisions, while bigger uncertainties remain at higher densities.

1.1 Equation of state of isospin-asymmetric nuclear matter

1.1.1 Microscopic and phenomenological many-body approaches

Theoretical studies of the EOS of isospin-asymmetric nuclear matter go back to the late 1960s. Since them, various approaches involving different physical approximations and numerical techniques have been developed to deal with the many-body problem of isospin-asymmetric nuclear matter [LCK08]. In this work we will mainly deal with microscopic effective models, which are based on effective density-dependent nuclear forces or effective interaction Lagrangians. In these approaches, a number of parameters are adjusted to fit the properties of many finite nuclei and nuclear matter. This type of models mainly includes the *relativistic mean field* (RMF) and the

non-relativistic *Hartree-Fock* theories. These approaches allow the most precise description of the properties of finite nuclei and nuclear matter. In particular, the non-relativistic Hartree-Fock with Skyrme forces, i.e., the Skyrme-Hartree-Fock method (see Section 3.1), and the RMF model constitute two main methods in the self-consistent mean-field approach to nuclear structure studies.

The RMF model has been very successful in describing many nuclear phenomena. For example, it provides a novel saturation mechanism for nuclear matter, an explanation of strong spin-orbit interaction in finite nuclei, a natural energy dependence of the nucleon optical potential, and so on. The RMF approach is based on effective interaction Lagrangians with the nucleons interacting via exchanges of mesons. In this approach, a number of parameters are adjusted to fit the properties of many nuclei and thus allow the most precise description of the properties of finite nuclei. Because this approach contains parameters that are fixed by nuclear properties around the saturation density, it thus usually gives an excellent description of the nuclear properties around or below the saturation density.

The non-relativistic Hartree-Fock approach has a very long history. In particular, those with Skyrme or Gogny forces have been very successful in describing the ground state and low-energy excitation properties of finite nuclei and nuclear matter. As a self-consistent mean-field, the SHF method is based on effective energy-density functionals formulated in terms of effective density-dependent nucleon-nucleon interactions with parameters of the functional adjusted to fit experimental data.

1.1.2 The nuclear equation of state and its isospin dependence

In the following, we review some typical results for the nuclear matter EOS and its isospin dependence from microscopic effective approaches. We shall point out the most obvious qualitative differences among the model predictions.

Fig. 1.1 shows typical predictions for the EOS, i.e., the energy per nucleon versus density, of asymmetric nuclear matter from the non-relativistic SHF model using the parameter set SIII and the RMF model using the parameter set TM1 [LCK08]. Isospin-asymmetry is indicated for each curve by the ratio ρ_p/ρ_n of the proton density (ρ_p) to that of neutrons (ρ_n).

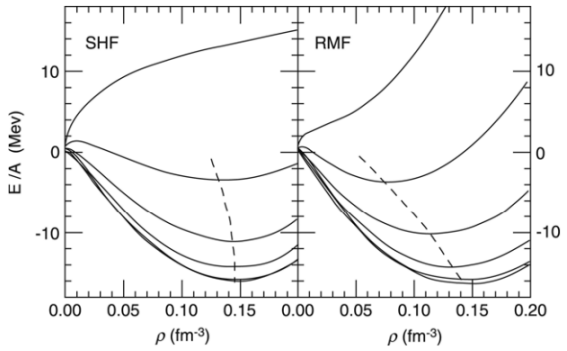

Figure 1.1
The equation of state of asymmetric nuclear matter from the Skyrme-Hartree-Fock (left panel) and relativistic mean field (right panel) model calculations [LCK08]. The solid curves correspond to proton-to-neutron ratios of 0, 0.2, 0.4, 0.6, 0.8 and 1 (from top to bottom). The dashed lines interpolate the minimums of the solid curves.

A common prediction from these studies is that the asymmetric nuclear matter is less stiff and bound at saturation. The minimum in the equation of state disappears before the pure neutron matter limit is reached, and the compressibility at saturation thus decreases as nuclear matter becomes more neutron-rich. Also, the saturation density is generally reduced with increasing neutron-to-proton ratio or isospin-asymmetry. For the phenomenological SHF and RMF approaches, although they give correct saturation properties for symmetric nuclear matter, their predictions for the EOS of asymmetric nuclear matter, such as the saturation density, are quantitatively different. In the SHF model the saturation density depends weaky on isospin-asymmetry,

while in the RMF model the dependence is much stronger. These different behaviors, which are related directly to the slope parameter of the symmetry energy and the incompressibility of symmetric nuclear matter, result in significant differences in the predicted nucleon density profiles and neutron skin thickness in radioactive nuclei.

1.1.3 The nuclear symmetry energy and its empirical parabolic law

For asymmetric nuclear matter, various theoretical studies have shown that the energy per nucleon can be well approximated by

$$E(\rho,\alpha) = E(\rho,\alpha=0) + E_{\rm sym}(\rho)\alpha^2 + O(\alpha^4), \tag{1.1}$$

in terms of baryon density $\rho = \rho_n + \rho_p$, isospin-asymmetry $\alpha = (\rho_n - \rho_p)/\rho$, energy per nucleon in symmetric nuclear matter $E(\rho,\alpha=0)$ and bulk nuclear symmetry energy

$$E_{\rm sym}(\rho) = \frac{1}{2}\frac{\partial^2 E(\rho,\alpha)}{\partial\alpha^2}\bigg|_{\alpha=0} \tag{1.2}$$

In Eq.(1.1) there are no odd-order α terms due to the exchange symmetry between protons and neutrons in nuclear matter (the charge symmetry of nuclear forces). Higher order terms in α are generally negligible for most purposes. Eq.(1.1) is known as the *empirical parabolic law* and it is considered to be valid only at small isospin-asymmetries. However, many relativistic and non-relativistic calculations have shown that it is actually valid up to $\alpha = 1$, at least for densities up to values of interest.

The saturation density ρ_0 is defined in correspondence to the minimum of the energy per particle in symmetric nuclear matter. The curvature of $E(\rho,\alpha=0)$ around this minimum is simply related to the nuclear matter incompressibility,

$$K_\infty = 9\rho_0^2\frac{\partial^2 E(\rho,\alpha=0)}{\partial\rho^2}\bigg|_{\rho=\rho_0}. \tag{1.3}$$

Using the empirical parabolic law, one can easily extract the symmetry energy $E_{\rm sym}(\rho)$ from microscopic calculations. In Fig. 1.2 the density dependence of the nuclear symmetry energy from several SHF and RMF calculations is shown [LCK08].

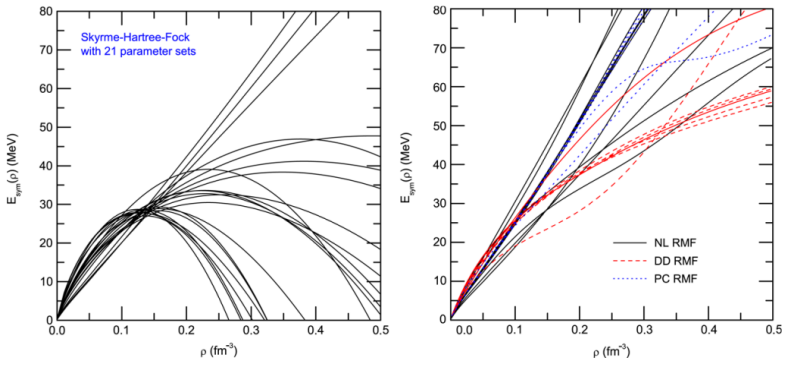

Figure 1.2
Left window: density dependence of the nuclear symmetry energy $E_{\rm sym}(\rho)$ from SHF with 21 sets of Skyrme interaction parameters [LCK08]. Right window: same as left panel from RMF model from several parameter sets in the nonlinear RMF model (solid curves), in the density dependent RMF model (dashed curves) and in the point coupling RMF model (dotted curves) [LCK08].

According to Eq.(1.1), the bulk symmetry energy $E_{\rm sym}(\rho)$ can be evaluated approximately from the two extreme cases of pure neutron matter and symmetric nuclear matter via

$$E_{\rm sym}(\rho) \simeq E(\rho,1) - E(\rho,0), \tag{1.4}$$

which implies that the symmetry energy $E_{\rm sym}(\rho)$ is an estimate of the energy cost to convert a proton into a neutron in symmetric nuclear matter at the fixed density ρ. Furthermore, around the symmetric nuclear matter saturation density ρ_0, the nuclear symmetry energy can be expanded to second order in the density as

$$E_{\rm sym}(\rho) = E_{\rm sym}(\rho_0) + \frac{L}{3}\left(\frac{\rho-\rho_0}{\rho_0}\right) + \frac{K_{\rm sym}}{18}\left(\frac{\rho-\rho_0}{\rho_0}\right)^2, \tag{1.5}$$

where L and $K_{\rm sym}$ characterize the density dependence of the nuclear symmetry energy around normal nuclear matter density, and thus provide important information on the behavior of the nuclear symmetry energy at both high and low densities.

The symmetry energy at normal nuclear matter density from various theoretical models is usually tuned to reproduce the empirical liquid-drop mass value, which has a value around 30 MeV. For example, in the non-relativistic SHF approach, the predicted values for $E_{\rm sym}(\rho_0)$ are between 26 and 35 MeV depending on the nuclear interactions used in the calculation, while the RMF theory usually gives higher values of $E_{\rm sym}(\rho_0)$, in the range from 30 to 44 MeV.

The *neutron skin thickness* ΔR of a nucleus is defined as the difference between the root-mean-square radii of neutrons, $\langle r_n^2\rangle^{1/2}$, and of protons, $\langle r_p^2\rangle^{1/2}$, i.e.,

$$\Delta R \equiv \langle r_n^2\rangle^{1/2} - \langle r_p^2\rangle^{1/2}. \tag{1.6}$$

S. Typel and B.A. Brown [TB01] noted that the thickness of the neutron skin is linearly correlated with $P(0.1)$, that is, the pressure of neutron-rich matter at the density 0.1 fm^{-3}. Besides, it has been shown that ΔR is sensitive to the slope parameter L at the normal nuclear matter density [CRV$^+$02]. In fact, for the pressure P at the saturation density,

$$P(\rho_0) = \rho^2\frac{\partial E(\rho,\alpha)}{\partial\rho}\bigg|_{\rho_0} = \rho_0^2\frac{\partial E(\rho,\alpha=0)}{\partial\rho}\bigg|_{\rho_0} + \rho_0^2\frac{\partial E_{\rm sym}(\rho)}{\partial\rho}\bigg|_{\rho_0}\alpha^2 = 0 + \rho_0^2\frac{L}{3\rho_0}\alpha^2 = \frac{L\rho_0}{3}\alpha^2, \tag{1.7}$$

and thus, if ΔR is correlated with P, it must be correlated with L, as well. As an example, we show in Fig. 1.3 the correlations between the neutron skin thickness of ^{208}Pb with L, $K_{\rm sym}$ and $E_{\rm sym}(\rho_0)$ calculated using the SHF model with 21 Skyrme interactions [LCK08]. As it is seen from this figure, there exist an approximate linear correlation between ΔR and L, while the correlations of ΔR with $K_{\rm sym}$ and $E_{\rm sym}(\rho_0)$ are less strong and even exhibit some irregular behavior.

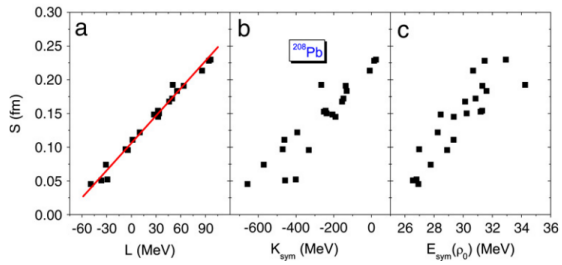

Figure 1.3
Neutron skin thickness (here indicated as S) of ^{208}Pb as a function of (a) L, (b) $K_{\rm sym}$ and (c) $E_{\rm sym}(\rho_0)$ for 21 sets of Skyrme interaction parameters. The line in panel (a) represents a linear fit [LCK08].

The extracted L value from isospin diffusion data (see below) allows to extract, from the linear fit of Fig. 1.3, a neutron skin thickness $\Delta R = 0.22 \pm 0.04$ fm for ^{208}Pb. The experimental data for ΔR in ^{208}Pb have large uncertainties, since it ranges from 0.10 to 0.28 fm [K$^+$04].

The proposed *parity radius experiment* (PREX) at the Jefferson Laboratory aims to measure the neutron radius in ^{208}Pb via parity violating electron scattering. Parity violation is sensitive to the neutron density because the Z^0 boson couples primarily to neutrons [HPS$^+$01]. The result of this purely electroweak experiment could be both accurate and model independent. In contrast, all previous measurements of bulk neutron densities used hadron probes that suffer from controversial uncertainties in the reaction mechanism. PREX should provide a unique observational constraint (within 0.05 fm) on the thickness of the neutron skin in a heavy nucleus.

1.2 Isospin effects in heavy-ion reactions as probes of the nuclear symmetry energy

Heavy-ion reactions provide a unique opportunity to investigate the EOS of isospin-asymmetric nuclear matter. For a wider review of these topics, one can consult [LCK08] and references therein.

To extract information on the EOS of neutron-rich matter, expecially the density dependence of the nuclear symmetry energy, from heavy-ion reactions induced by neutron-rich beams, one needs reliable theoretical tools. For this purpose, it has been expecially useful to have transport models that include explicitly the isospin degrees of freedom and thus the isospin-dependent physical quantities, such as the isovector potential and the isospin-dependent in-medium nucleon-nucleon cross section and Pauli blocking. Significant progress has been made during the last two decades in developing semi-classical transport models for nuclear reactions. The application of these models have enabled us to learn a great deal of interesting physics from heavy-ion reactions, expecially the EOS of nuclear matter.

Also, identification of experimental observables that are sensitive to the density dependence of the nuclear symmetry energy is required to extract the properties of isospin-asymmetric nuclear matter from heavy-ion reactions induced by neutron-rich nuclei. Since the symmetry potential for neutrons and protons have opposite signs and are generally weaker than the nuclear isoscalar potential at the same density, most isospin sensitive observables are usually based on differences or ratios of isospin multiplets of baryons, mirror nuclei and mesons, such as the neutron-to-proton ratio of emitted nucleons, the neutron-proton differential flow, the neutron-proton correlation function, the π^-/π^+, Σ^-/Σ^+ and K^0/K^+ ratios, etc.

Among many exciting results, it is of particular interest to mention the recent isospin diffusion experiments at the National Superconducting Cyclotron Laboratory (NSCL) at Michigan State University and the associated theoretical analysis that have led to a relatively stringent constraint on the nuclear symmetry energy at subnormal densities. These results mostly agree with recently obtained data from the isoscaling analysis of isotope ratios in intermediate-energy heavy-ion collisions. These different but complementary studies have provided so far the best phenomenological constraints on the symmetry energy at sub-normal densities.

The most important achievements in isospin physics obtained by the heavy-ion reaction community include: [LCK08]

- a symmetry energy of $E_{\rm sym}(\rho) \simeq 31.6(\rho/\rho_0)^\gamma$ with γ=0.69-1.05 was extracted for densities between $0.1\rho_0$ and $1.2\rho_0$;
- the slope parameter of the symmetry energy at normal density was found to be $L = 88 \pm 25$ MeV;
- at extremely low densities, below $0.05\rho_0$, nuclear clustering was found to be important.

Unfortunately, essentially no experimental information about the symmetry energy at higher densities is available at present. Nevertheless, high energy radioactive beam facilities under contruction at the CRS (China), FAIR (Germany), RIKEN (Japan) and SPIRAL2/GANIL (France) give us the great hope that the high density behavior of the symmetry energy can be studied experimentally in the near future.

1.3 Giant resonances as probes of the nuclear symmetry energy

Giant resonances, i.e., nuclear collective modes in which the nucleus vibrates as a whole, have recently been proved to be a fundamental tool to constrain several parameters of the equation of state of nuclear matter. This topic will be discussed in Chapter 2, where fundamental properties of GRs will be widely exposed.

1.4 Astrophysical implications of the EOS of neutron-rich matter

Understanding the EOS of neutron-rich matter, expecially the density dependence of the nuclear symmetry energy, is important not only for nuclear physics, but also for many critical issues in astrophysics, such as the mechanism of supernova explosions and the properties of neutron stars. For a wider review of these topics, one can consult [SPL$^+$05] and references therein.

Various studies have indicated that the symmetry energy mainly affects the chemical composition of neutron stars. Other properties, such as the cooling mechanism of proto-neutron stars, the possibility of kaon condensation in the cores of neutron stars, lepton profiles and neutrino flux, which all depend on the chemical composition of stars, are therefore also affected. For example, the prompt shock invoked to understand the explosion mechanism of a type II supernova requires a relatively soft EOS. The presence of protons in neutron stars affects not only the stiffness of its EOS, including whether a kaon condensation through the process $e^- \rightarrow K^- + \nu_e$ can be formed, but also its cooling mechanism. If the proton concentration is larger than a critical value of about 15%, the direct URCA process ($n \rightarrow p + e^- + \overline{\nu}_e$, $p + e^- \rightarrow n + \nu_e$) becomes possible and would then enhance the emission of neutrinos, making it a more important process in the cooling of neutron stars [SPL$^+$05].

Besides those properties related to the proton fraction, there are also properties of the neutron stars that are directly related to the magnitude and density slope of the symmetry energy [LP00]. Among these properties, the most known example is probably the mass-radius relation of a neutron star. While many neutron star properties depend on both isospin symmetric and asymmetric parts of the equation of state, the mass-radius relation is primarily determined by the slope L of the symmetry energy in the density range of 1 to $2\rho_0$ [HP01]. Since there exist a strong correlation between ΔR and L, one expects the neutron skin thickness to be a unique tool to investigate the properties of neutron stars. In addition, the transition density and pressure from the liquid core to the solid crust and the fractional moment of inertia of the neutron star crust are also directly affected by the symmetry energy.

Chapter 2

Giant resonances

A powerful method to study the properties of a system is to subject it to a weak external perturbation and to examine its response. The atomic nucleus, subject to the absorpion of a photon (electromagnetic perturbation) or to the inelastic scattering of a particle (hadronic perturbation), can respond, in the energy range approximately below 30 MeV, both through the excitation of relatively simple states involving only one or a few particles, or exhibiting broad resonances, which are known as *giant resonances* [BBB98, HW01].

A giant resonance, which corresponds to a *collective motion* involving many if not all the particles in the nucleus, can be viewed as a high-frequency, damped, (nearly) harmonic density or shape vibration around the equilibrium ground state configuration. The restoring forces for these resonances are directly related to macroscopic properties of the nucleus and they currently provide the most reliable information on the bulk properties of nuclear matter such as compression modulus and symmetry energy (see Chapter 1). Moreover, the investigation of the strength distribution gives access to the study of the nuclear deformations in the ground state as well as to the shape evolution of nuclei as a function of spin and temperature of the system.

Like any other resonance, a nuclear giant resonance is described by its *energy* E_R, its *width* Γ_R, its *strength* S_R and its *sum rules*. The fact that all nuclear resonances have a width of the order of 2-5 MeV implies that, within 10^{-23}s, that is, after few periods of vibration, the resonance is completely damped owing to energy dissipation in favour of other more complex system configurations or even to the emission of one nucleon or, less probably, a γ ray.

The nuclear random phase approximation (RPA) (see Section 3.2) is the simplest theory able to predict nicely the main features of giant resonances. This is done depicting the collective motion of the nucleons as a coherent superposition of particle-hole excitations.

2.1 Classification of giant resonances

Giant resonances can be classified according to their multipolarity L, spin S and isospin T quantum numbers. If protons and neutrons oscillate in phase, the vibration is called isoscalar, i.e., without variations in isospin ($\Delta T = 0$), whereas, if they oscillate out of phase, the vibration is called isovector ($\Delta T = 1$). As a rule, for the same multipole mode, the isovector one will be at a higher excitation energy than the isoscalar one since extra energy is required to separate the neutron and proton distributions. In $\Delta S = 1$ modes (magnetic modes), nucleons with spin up ($\uparrow$) vibrate against nucleons with spin down ($\downarrow$), while, if $\Delta S = 0$ (electric modes), spin vibrations are absent. Finally, giant resonances are classified depending on their angular momentum ΔL and parity. Of particular interest for this work will be $\Delta S = 0$, $\Delta T = 1$ modes, i.e., electric isovector (IV) vibrations in which protons and neutrons oscillate out of phase.

2.2 Decay of giant resonances

Since most giant resonances are located above the particle-decay threshold, they will mainly decay by particle emission, that is, neutrons and protons, and in light nuclei also by α particles. In a heavy nucleus, charged-particle decay is strongly suppressed because of the Coulomb barrier, so that, for these nuclei, particle decay occurs mainly by neutrons. Even γ-decay, although much hindered, is possible.

The study of the decay properties of the giant resonances is very interesting because it gives us insight into the mechanism responsible for the strong damping and allows us to check very stringently our microscopic descriptions of collective phenomena.

The total width of a giant resonance can be written as a sum of four components

$$\Gamma = \Delta\Gamma + \Gamma^{\uparrow} + \Gamma_{\gamma} + \Gamma^{\downarrow}. \tag{2.1}$$

Here $\Delta\Gamma$, the Landau damping, describes the effect of the coupling of the correlated particle-hole excitations with uncorrelated particle-hole configurations in the same excitation energy range, causing a fragmentation of the correlated wave function. $\Gamma^{\uparrow}$ is the escape width due to the coupling of the correlated 1p-1h state to the continuum, i.e., the width the resonance acquires by emission of particles; these processes take place on a very short time scale, typically of the order of 10^{-22} s. The width Γ_{γ} is correlated to the photon emission and in general it is only few percent of the total width, being of the order of the keV or smaller. At last, $\Gamma^{\downarrow}$ is the spreading width associated with the mixing of the correlated particle-hole state with more complex and numerous 2p-2h configurations. These 2p-2h states act as doorway states for the decay into 3p-3h and subsequently more complicated states till, finally, a completely equilibated system is reached. At each intermediate level, particle decay can occur; a typical time scale for this process is of the order of 10^{-19} s [HW01].

2.3 Multipole fields

The vibrational states of the nucleus are excited under the action of an external field, which can be electromagnetic or hadronic. The electromagnetic excitation operator, which can be obtained as a limit of the spherical expansion of the photon plane wave, reads

$$F^{(\mathrm{EM})}_{LM} = e i^L \sum_{i=1}^{Z} r_i^L Y_{LM}(\hat{r_i}) \tag{2.2}$$

where the reasons for inserting the i^L terms are treated in Appendix A.2.4. In the case of hadron inelastic scattering, one arrives at similar excitation operators starting, e.g., from the distorted wave Born approximation (DWBA) obtaining the following isoscalar (IS) and isovector (IV) operators, being $\tau_z = -1$ for protons and $\tau_z = +1$ for neutrons:

$$F^{(\mathrm{IS})}_{LM} = i^L \sum_{i=1}^{A} r_i^L Y_{LM}(\hat{r_i}), \tag{2.3}$$

$$F^{(\mathrm{IV})}_{LM} = i^L \sum_{i=1}^{A} r_i^L Y_{LM}(\hat{r_i})\tau_z(i). \tag{2.4}$$

2.3.1 Dipole operators

The electric dipole interaction of a spatially constant electromagnetic field $\mathcal{E}$ with the nucleons can be written as [BBB98]

$$H = e\mathcal{E}\sum_{p} z_p = e\mathcal{E}\big[\frac{N}{A}\sum_{p} z_p - \frac{Z}{A}\sum_{n} z_n + Z\bar{z}\big] \tag{2.5}$$

where p stands for protons, n for neutrons and $\overline{z} = \frac{\sum_i z_i}{A}$ denotes the position of the center-of-mass of the nucleus. The term $e\mathcal{E}Z\overline{z}$ corresponds to the interaction of the entire nucleus with the electric field, whereas the term $e\mathcal{E}\big[\frac{N}{A}\sum_p z_p - \frac{Z}{A}\sum_n z_n\big]$ gives the dipole E1 photo-absorption due to internal motion inside the nucleus. That is, each proton acts as if it had an effective charge $e\frac{N}{A}$, and each neutron as if it had an effective charge $-e\frac{Z}{A}$. It is now evident that we can get rid of the contribution of the center-of-mass motion by using the modified electromagnetic dipole operator

$$F_{1M}^{(\mathrm{EM})} = i^L \frac{e}{2} \sum_{i=1}^{A} \big[\frac{N-Z}{A} - \tau_z(i)\big] r_i Y_{1M}(\hat{r_i}). \tag{2.6}$$

In the dipole case, the lowest order term of the isoscalar operator does not produce a physical excitation: in fact, the operator (2.3) with $L = 1$ induces simply a translation of the whole system. This mode should in principle lie at zero energy and should be decoupled from the physical excitations within RPA, as this theory restores the symmetries broken at the HF level (see Section 3.1). In practice, numerical implementations are not able to realize exactly this symmetry restoration, resulting in the fact that a part of the *spurious state* in contained in one RPA state whose energy is close to, but not identical to zero. This means that the spurious state is not exactly orthogonal to the other RPA states. To avoid the undesired effects of these overlaps between the spurious state and the physical states, one way is to employ a modified isoscalar dipole operator. This modified operator reads

$$F_{1M}^{(\mathrm{IS})} = i^L \sum_{i=1}^{A} (r_i^3 - \eta r_i) Y_{1M}(\hat{r_i}) \tag{2.7}$$

with $\eta = 5\langle r^2\rangle/3$.

In the case of isovector dipole, the dipole motion associated with the displacement of the neutron and proton center-of-mass can be subtracted from the operator (2.4) as we did for the electromagnetic operator, obtaining

$$F_{1M}^{(\mathrm{IV})} = \frac{i^L}{2} \sum_{i=1}^{A} \big[\frac{N-Z}{A} - \tau_z(i)\big] r_i Y_{1M}(\hat{r_i}). \tag{2.8}$$

2.4 Sum rules

Intuitively, it is clear that the strength of a collective resonance will depend on the basic properties of the system, such as the number of particles participating in the response and the size of the system. This implies that the total transition strength should be limited by a sum rule which depends only on ground state properties.

In general, a sum rule is related to a Hermitian one-body operator F by

$$m_k = \sum_n (E_n - E_0)^k |\langle n|F|0\rangle|^2 \tag{2.9}$$

and it gives the k-th moment of the distribution of the excitation strength produced by the operator F. Here, n labels the complete set of eigenstates of the exact Hamiltonian H of energies E_n, being $|0\rangle$ the ground state of the system of energy E_0.

Among all moments m_k, the most important is the the energy-weighted sum rule (EWSR) m_1, for which it can be shown that

$$m_1 = \sum_n (E_n - E_0)|\langle n|F|0\rangle|^2 = \frac{1}{2}\langle 0|\big[F,\big[H,F\big]\big]|0\rangle. \tag{2.10}$$

It has been demonstrated by D.J. Thouless [Tho61] that Eq.(2.10) remains valid if the left hand side is evaluated with RPA wave functions and energies and the right hand side is calculated using the HF ground state wave function.

For the isoscalar operator (2.3), Eq.(2.10) gives the result

$$m_1 = \frac{\hbar^2}{2m} A \frac{L(2L+1)^2}{4\pi} \int d^3r \rho(r) r^{2L-2} = \frac{\hbar^2}{2m} A \frac{L(2L+1)^2}{4\pi} \langle r^{2L-2} \rangle. \tag{2.11}$$

If F is the isoscalar dipole operator referred to the nucleus center-of-mass, Eq.(2.7), the EWSR (2.10) becomes

$$m_1 = \frac{\hbar^2}{2m} \frac{A}{4\pi} (33\langle r^4 \rangle - 25\langle r^2 \rangle^2). \tag{2.12}$$

Instead, if F is the isovector dipole operator referred to the nucleus center-of-mass, Eq.(2.8), one obtains the *Thomas-Reiche-Kuhn sum rule*

$$m_1 = \frac{9}{4\pi} \frac{\hbar^2}{2m} \frac{NZ}{A} (1+\kappa) \simeq 60 \frac{NZ}{A} (1+\kappa) \text{ MeVmb}, \tag{2.13}$$

where κ is the so-called *dipole enhancement factor* connected with the momentum-dependent part of the nuclear force [BBB98].

2.5 The isoscalar giant monopole resonance

The isoscalar giant monopole resonance (ISGMR), also called the *breathing* or *compressional* mode, in a macroscopic picture corresponds to a radial oscillation of the nucleus as whole. It was first discovered in 1977 by means of inelastic α scattering. In nuclei with $A \geq 90$ the ISGMR has a concentrated strength distribution which can be well described by a Gaussian with a tail at the high-energy side in some nuclei. The centroid energy of the Gaussian is approximately $80A^{-1/3}$ MeV, while the width increases from about 2.5 MeV in the Pb region to about 4 MeV for $A = 90$ [HW01].

It is possible to relate the ISGMR energy E_{ISGMR} in a given nucleus to the finite nucleus incompressibility K_A through the relation

$$K_A = \frac{m\langle r^2 \rangle_0}{\hbar^2} E_{\text{ISGMR}}, \tag{2.14}$$

where m is the nucleon mass and $\langle r^2 \rangle_0$ is the ground state expectation value of r^2. Here the centroid E_{ISGMR} is calculated as

$$E_{-1} = \sqrt{\frac{m_1}{m_{-1}}}. \tag{2.15}$$

This relation between K_A and E_{ISGMR} allows to extract also the value of the nuclear matter incompressibility K_∞, which is constrained in the interval 240 ± 20 MeV In fact, K_∞ and K_A are connected by a relation analogous to the semi-empirical mass formula [SKC06].

2.6 The isovector giant dipole resonance

The isovector giant dipole resonance (IVGDR) was first observed in 1947 in photo-absorption and photo-fission experiments. For most non-deformed nuclei with $A > 50$ the measured total absorption cross section in the energy range 10-20 MeV can be very well fitted by a Lorentzian curve

$$\sigma(E) = \frac{\sigma_p}{1 + (E^2 - E_p^2)^2 / E^2 \Gamma^2} \tag{2.16}$$

where subscript p refers to the peak cross section. The systematics show that that the resonance energy decreases gradually with increasing mass number A, and it is well reproduced by the law $E_p = 80A^{-1/3}$ MeV; the width Γ of the resonance is strongly influenced by the shell structure of the nucleus, since its values range from about 4-5 MeV for closed-shell nuclei up to 8 MeV for nuclei between closed shells. For axially symmetric deformed nuclei, the cross section is split into

two parts, corresponding to an IVGDR vibration along or perpendicular to the symmetry axis [HW01].

Moreover, in the last decades, the main properties of the IVGDR build on excited states have also been measured, exploring regions of excitation energies between 10 and 500 MeV and spins up to $60\hbar$ through both fusion reactions and inelastic scattering. These experiments have demonstrated that there is no significant shift of the centroid energy with either temperature or angular momentum, whereas the width increases both with excitation energy and spin, the latter becoming important only above $35\hbar$ [SB06].

The energy of the IVGDR is strongly connected with the symmetry energy $E_{\rm sym}(\rho)$. In fact, a strong correlation is found between the centroid (calculated as $E_{-1} \equiv \sqrt{\frac{m_1}{m_{-1}}}$) and the quantity $f(0.1)$ defined as

$$f(0.1) \equiv \sqrt{E_{\rm sym}(0.1)(1+\kappa)} \tag{2.17}$$

where $E_{\rm sym}(0.1)$ is the symmetry energy evaluated at $\rho = 0.1$ fm^{-3} and κ is the dipole enhancement factor. This correlation has been used to extract a constraint on $E_{\rm sym}(0.1)$ which, introducing an acceptable range for κ, is found to lie in the interval 24.1 ± 0.8 MeV [TCV08].

2.7 The pygmy dipole resonance

Exotic modes of collective excitation represent unique structure phenomena in nuclei with a pronounced asymmetry in the number of protons and neutrons. A representative example is the pygmy dipole resonance (PDR), a low-energy mode energetically below the IVGDR, which has recently been found to be quite common in neutron-rich nuclei, such as ^{68}Ni [W$^+$09], ^{132}Sn [A$^+$05] and ^{208}Pb [R$^+$02]. This mode is thought to correspond to a resonant oscillation of the weakly bound neutron skin against the isospin saturated proton-neutron core [Pie06]. Consequently, one expects an increase of the PDR strength approaching isotopes with extreme neutron-to-proton ratios.

A large debate concerning the pygmy dipole resonance and its possible correlations with the symmetry energy and the parameters of the equation of state has gained great importance in the last few years.

One of the most debated issues is the collective character itself of the PDR. If the collective picture holds, it is possible to think of the pygmy dipole resonance to be a good constraint for the symmetry energy. In this case, infact, since the PDR can be roughly thought as a vibration of the external neutron crust against the core, we can expect its properties to be closely related to the neutron skin [Pie06, K$^+$07]. If the picture of a neutron-rich nucleus as an isospin-symmetric core plus some excess neutrons holds, and the two subsystems are, to some extent, separated in space, then the matrix elements of the residual interaction between them are small. The dipole response separate into two peaks. The EWSR in the lowest one is proportional to the number of excess neutrons and, as the latter scales as the neutron skin, it should scale with L as well.

In particular, in [C$^+$10], a strong correlation has been found between the EWSR exhausted by the pygmy dipole resonance in ^{68}Ni and ^{132}Sn and the parameter L in SHF and RMF models (in Fig. 2.1 the case of ^{68}Ni). This has allowed, via the experimental value of the EWSR, to constrain the values of L in the range 64.6 ± 15.7 MeV, compatible with the result coming from heavy-ion collision reactions (see Section 1.2). Besides, the linear correlation between L and ΔR, has allowed to constrain the neutron skin thickness of ^{68}Ni and ^{208}Pb, to, respectively, 0.200±0.015 fm and 0.194±0.024 fm. The latter result is compatible with that reported in Section 1.1.3 and coming from heavy-ion reactions.

A much different conclusion is drawn in [RN10], where it is claimed the correlation between the properties of the PDR (centroid and ESWR) and the symmetry energy to be poor. The reason would be the unreal collective character of the PDR, whose strength would be caused only by shell effects around the Fermi surface acting on a single particle-hole pair.

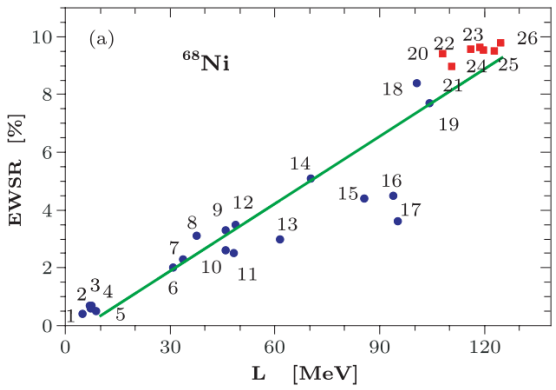

Figure 2.1
Correlation between L and the percentage of TRK sum rule exhausted by the PDR in ^{68}Ni. Dots and squares correspond, respectively, to different sets employed in SHF and RMF calculations. The straight line corresponds to the result of a linear fit [C$^+$10].

2.7.1 Low-energy dipole response in ^{68}Ni

We present here a brief microscopic theoretical analysis of the low-energy dipole response in ^{68}Ni [PBR$^+$11]. It has to be noticed that we will anticipate the use of microscopic nuclear structure theories, such as Skyrme-Hartree-Fock and RPA, which will be widely discussed in Chapter 3.

Method

We solve fully self-consistently the Skyrme-Hartree-Fock (HF) plus random phase approximation (RPA) equations [CCG$^+$11] in a discrete radial mesh (for further details on the calculation see Chapter 5). Our first and foremost interest is to analyze the microscopic structure of the PDR and its model dependence. For this reason, we have selected three different interactions of common use in nuclear structure calculations and that predict very different isovector properties: SGII (L=37.6 MeV, m^*/m=0.79), SkI3 (L=100.5 MeV, m^*/m=0.57) and SLy5 (L=48.3 MeV, m^*/m=0.70).

The strength function

The RPA strength function of ^{68}Ni for dipole excitation is depicted in Fig. 2.2(a) as a function of the energy for the three interactions under investigation. The arrow indicates the experimental value [W$^+$09]; in the inset, the PDR region is enlarged. Although its magnitude varies with the model, all interactions predict a low-energy peak: the smaller is the effective mass, the closer the peak in the PDR region appears to the giant dipole one. In addition, the larger the value of L, the higher the PDR peak lies, in qualitative agreement with [C$^+$10]. To estimate if different states are contributing coherently to the PDR, we display in Fig. 2.2(b) the reduced transition probability $B^{\mathrm{IV}}(E1)$ in the low-energy region in single-particle or Weisskopf units, which roughly indicate the number of particles involved in the excitation. In fact, Weisskopf units is a useful scale of the reduced transition probability for electric single-particle transition [BM69], defined by

$$B_W(E\lambda) = \frac{1.2^{2\lambda}}{4\pi}\left(\frac{3}{\lambda+3}\right)^2 A^{2\lambda/3} e^2 \mathrm{fm}^{2\lambda}. \tag{2.18}$$

As one can see from the figure, not all interactions predict RPA states with $B^{\mathrm{IV}}(E1)$ as large as to be considered collective states, i.e., involving a high number of particles.

The isoscalar character of the pygmy dipole strength

We display in Fig. 2.3 the contribution to the strength function of those RPA excited states, calculated by means of SkI3 force in ^{68}Ni, which are at least 70% isoscalar, i.e., in which the

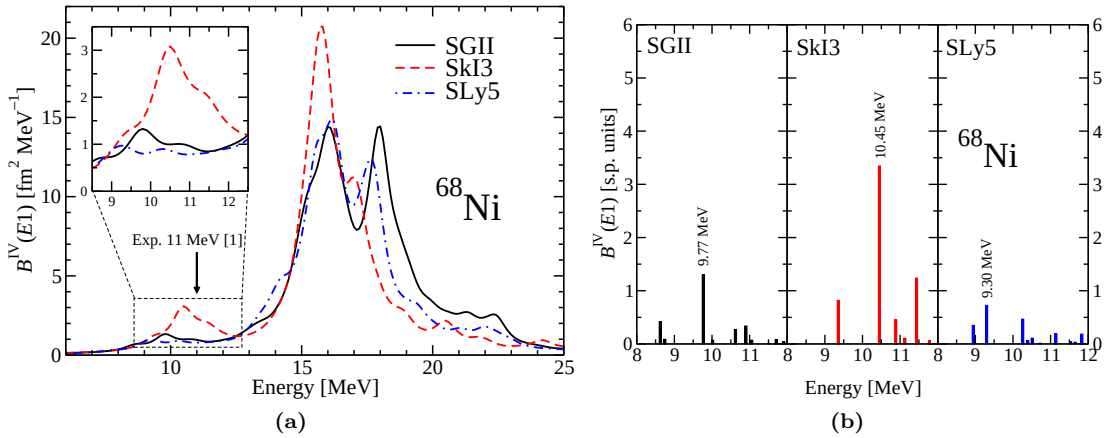

Figure 2.2
In panel (a) the strength function of ^{68}Ni for dipole excitation is depicted for SGII, SkI3 and SLy5 interactions. The low-energy B$^{\mathrm{IV}}$(E1) response in single-particle units in shown in panel (b).

transition densities of neutrons and protons are in phase in at least the 70% of the selected radial range (see Section 3.2).

We evaluate the isoscalar character of the dipole response by analyzing the neutron and proton transition densities along three regions: between 0 and R (left panel), 0 and $R/2$ (middle panel) and $R/2$ and R, where $R = 1.2A^{1/3}$ fm is the nuclear radius. For all the interactions, the PDR is essentially isoscalar, in agreement with [PNV^{+}09, E^{+}10]. Besides, the dynamics in the outermost region of the studied nucleus is governed by neutrons, which are very sensitive, in this region, to the L parameter as it is well known from studies of the neutron skin thickness ΔR. The slope L of the symmetry energy, in fact, directly affects the pressure of neutron rich matter and so, as a consequence, the thickness of the neutron-rich crust around the isospin-symmetric core.

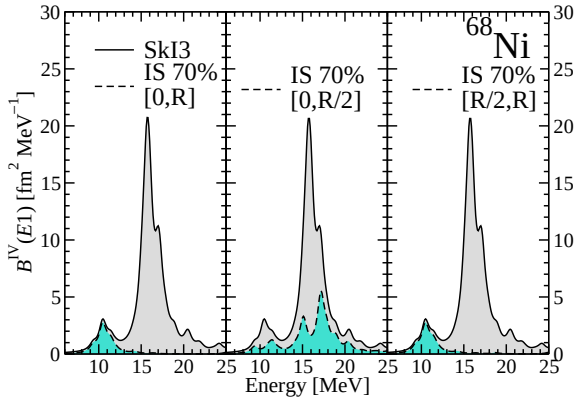

Figure 2.3
We display the contribution to the strength function of those RPA states which are at least 70% isoscalar for the case of SkI3 in ^{68}Ni along three regions: between 0 and R (left panel), 0 and $R/2$ (middle panel) and $R/2$ and R (right panel).

The transition densities

The neutron and proton (Fig. 2.4(a)) and isoscalar and isovector (Fig. 2.4(b)) transition densities as a function of the radial coordinate of the states displaying largest $B^{\mathrm{IV}}(E1)$ are depicted for all interactions for ^{68}Ni. The position of the proton and neutron r.m.s radii are also depicted. Qualitatively, the isoscalar character of the surface of the nucleus is confirmed although we see some model dependence along the radial axis.

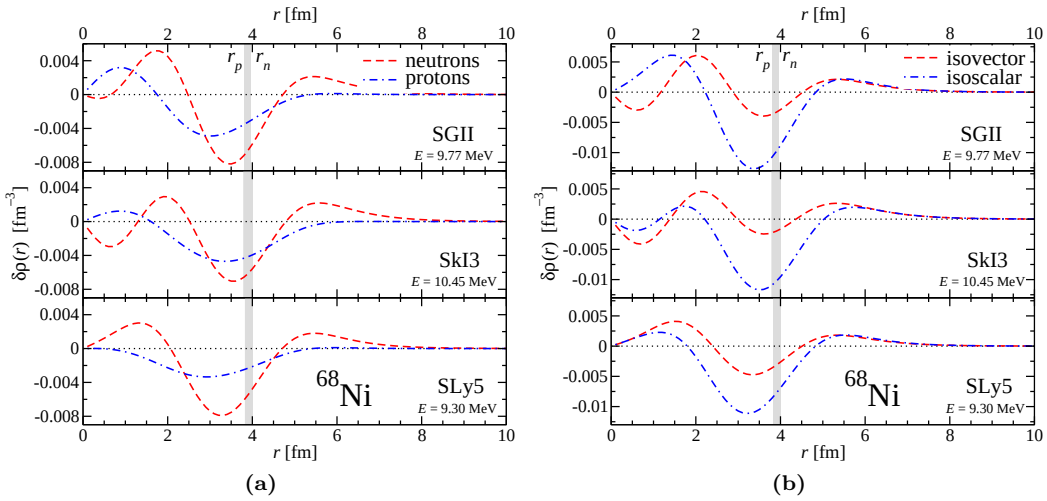

Figure 2.4
The neutron and proton (panel (a)) and isoscalar and isovector (panel (b)) transition densities as a function of the radial coordinate of the states displying largest $B^{\mathrm{IV}}(E1)$ are depicted for all interactions for ^{68}Ni

Conclusions

The smaller the effective mass and the larger the value of L, the closer to the giant dipole peak and the larger in strength we find the peak in the PDR region. Although some differences appear, the isoscalar character of the PDR is qualitatively supported by all models and it is basically due to the outermost neutrons. The collective character of the PDR is not supported by all models. This indicates that further microscopic studies on the PDR are needed.

Chapter 3

Microscopic nuclear structure theories

3.1 Hartree-Fock equations with Skyrme interaction

The Skyrme interaction is an effective density-dependent nucleon-nucleon force which has been widely employed in the past decades by the nuclear-physics community within the non-relativistic Hartree-Fock framework. Hartree-Fock calculations with this interaction have been performed over a wide range of the periodic table, providing results compatible to the experimental values for total binding energies, nuclear radii, deformations and single-particle level ordering. For a wider review one can consult [BHR03].

3.1.1 The Skyrme interaction

The Skyrme interaction is a zero-range density-dependent interaction between two nucleons. Originally proposed by T.H.R. Skyrme [Sky59], it has been improved and developed in the last years. At now, its most widely used form is,

$$\begin{aligned} V_{\text{eff}}(\mathbf{r}_1,\mathbf{r}_2) = {} & t_0(1+x_0P_\sigma)\delta(\mathbf{r}) + \frac{1}{2}t_1(1+x_1P_\sigma)[\mathbf{P'}^2\delta(\mathbf{r}) + \delta(\mathbf{r})\mathbf{P}^2] \\ & + t_2(1+x_2P_\sigma)\mathbf{P'}\cdot\delta(\mathbf{r})\mathbf{P} + \frac{1}{6}t_3(1+x_3P_\sigma)\rho^\alpha(\mathbf{R})\delta(\mathbf{r}) \\ & + iW_0(\boldsymbol{\sigma}_1+\boldsymbol{\sigma}_2)\cdot[\mathbf{P'}\times\delta(\mathbf{r})\mathbf{P}] \end{aligned} \tag{3.1}$$

where $\mathbf{r}_i$ and σ_i are the space and spin variables of the two nucleons, $\mathbf{r} = \mathbf{r}_1 - \mathbf{r}_2$, $\mathbf{R} = \frac{1}{2}(\mathbf{r}_1 + \mathbf{r}_2)$, $\mathbf{P} = \frac{1}{2i}(\nabla_1 - \nabla_2)$, $\mathbf{P'}$ is the Hermitian conjugate of $\mathbf{P}$ (acting on the left) and $P_\sigma = \frac{1}{2}(1 + \boldsymbol{\sigma}_1\cdot\boldsymbol{\sigma}_2)$ is the spin-exchange operator [C$^+$97]. Here, $\rho = \rho_n + \rho_p$ is the total nucleon density, and we will use the notation ρ_q to distinguish the neutron ($q = 0$) an proton ($q = 1$) densities. In Eq.(3.1), t_0 and t_3 are velocity-independent terms, whereas t_1 and t_2 are velocity-dependent terms; W_0 term is a two-body spin-orbit force. In the original form given by T.H.R. Skyrme there was no explicit density-dependent term but a three-body contact term with a strength parameter t_3,

$$v^{(3)}(\mathbf{r}_1,\mathbf{r}_2,\mathbf{r}_3) = t_3\delta(\mathbf{r}_1-\mathbf{r}_2)\delta(\mathbf{r}_2-\mathbf{r}_3)\delta(\mathbf{r}_3-\mathbf{r}_1). \tag{3.2}$$

In the Hartree-Fock approximation, the contribution of this three-body contact term is the same as that given by the t_3 term of Eq.(3.1) when $x_3 = 1$ and $\alpha = 1$. Such term provides a simple phenomenological representation of many-body effects, and describes the way in which the interaction between two nucleons is influenced by the presence of others.

Given the effective potential V_{eff}, the total Hamiltonian of the system becomes $H = T + V_{\text{eff}}$ where T is the kinetic term. The parameters t_0, t_1, t_2, t_3, x_0, x_1, x_2, x_3 and α are free parameters which can be obtained by fitting, on a restricted number of nuclei, both experimental data, like binding energies and r.m.s. radii, and theoretical properties of pure neutron matter, such as the

saturation density ρ_0, the incompressibility K_∞ and the symmetry energy at saturation density, $E_{\rm sym}(\rho_0)$.

3.1.2 Skyrme energy density functional

In the Hartree-Fock approximation, one supposes that the ground state of a nucleus is represented by a Slater determinant ϕ of single particle states ϕ_i,

$$\phi(x_1, x_2, \cdots, x_A) = \frac{1}{\sqrt{A!}}\det|\phi_i(x_j)|, \tag{3.3}$$

where x denotes the set of $\mathbf{r}$, σ and q coordinates. The expectation value of the total energy is

$$E = \langle\phi|(T + V_{\rm eff})|\phi\rangle = \int \mathcal{E}(\mathbf{r})d^3r. \tag{3.4}$$

For the Skyrme interaction, assuming that the subspace of occupied single-particle states is invariant under time reversal, the energy density functional $\mathcal{E}(\mathbf{r})$ is an algebraic function of the nucleon densities ρ_n and ρ_p, the kinetic energy τ_n and τ_p and spin densities $\mathbf{J}_n$ and $\mathbf{J}_p$. This quantities depend in turn on the single-particle states ϕ_i,

$$\rho_q(\mathbf{r}) = \sum_{i,\sigma} |\phi_i(\mathbf{r}, \sigma, q)|^2 \tag{3.5}$$

$$\tau_q(\mathbf{r}) = \sum_{i,\sigma} |\nabla\phi_i(\mathbf{r}, \sigma, q)|^2 \tag{3.6}$$

$$\mathbf{J}_q(\mathbf{r}) = -i \sum_{i,\sigma,\sigma'} \phi_i^*(\mathbf{r}, \sigma, q)[\nabla\phi_i(\mathbf{r}, \sigma', q) \times \langle\sigma|\boldsymbol{\sigma}|\sigma'\rangle], \tag{3.7}$$

and the sums are taken over all occupied single-particle states; besides $\tau = \tau_n + \tau_p$ and $\mathbf{J} = \mathbf{J}_n + \mathbf{J}_p$. In particular (we drop the dependence on $\mathbf{r}$ for simplicity),

$$\mathcal{E} = K + \mathcal{E}_0 + \mathcal{E}_3 + \mathcal{E}_{\rm eff} + \mathcal{E}_{\rm fin} + \mathcal{E}_{\rm so} + \mathcal{E}_{\rm sg} + \mathcal{E}_{\rm coul} \tag{3.8}$$

where K is the kinetic energy term, $\mathcal{E}_0$ is a zero-range term, $\mathcal{E}_3$ is the density-dependent term, $\mathcal{E}_{\rm eff}$ is an effective mass term, $\mathcal{E}_{\rm fin}$ is a finite range term, $\mathcal{E}_{\rm so}$ is a spin-orbit term, $\mathcal{E}_{\rm sg}$ is a term due to the tensor coupling with spin and gradient and $\mathcal{E}_{\rm coul}$ is a Coulomb term. Their expressions are [C+97]

$$\begin{aligned}
K &= \frac{\hbar^2}{2m_p}\tau_p + \frac{\hbar^2}{2m_n}\tau_n \\
\mathcal{E}_0 &= \frac{1}{4}t_0[(2 + x_0)\rho^2 - (2x_0 + 1)(\rho_p^2 + \rho_n^2)] \\
\mathcal{E}_3 &= \frac{1}{24}t_3\rho^\alpha[(2 + x_3)\rho^2 - (2x_3 + 1)(\rho_p^2 + \rho_n^2)] \\
\mathcal{E}_{\rm eff} &= \frac{1}{8}[t_1(2 + x_1) + t_2(2 + x_2)]\tau\rho \\
&\quad + \frac{1}{8}[t_2(2x_2 + 1) - t_1(2x_1 + 1)](\tau_p\rho_p + \tau_n\rho_n) \\
\mathcal{E}_{\rm fin} &= \frac{1}{32}[3t_1(2 + x_1) - t_2(2 + x_2)](\nabla\rho)^2 \\
&\quad - \frac{1}{32}[3t_1(2x_1 + 1) + t_2(2x_2 + 1)][(\nabla\rho_p)^2 + (\nabla\rho_n)^2] \\
\mathcal{E}_{\rm so} &= \frac{1}{2}W_0[\mathbf{J}\cdot\nabla\rho + \mathbf{J}_p\cdot\nabla\rho_p + \mathbf{J}_n\cdot\nabla\rho_n] \\
\mathcal{E}_{\rm sg} &= -\frac{1}{16}(t_1x_1 + t_2x_2)\mathbf{J}^2 + \frac{1}{16}(t_1 - t_2)[\mathbf{J}_p^2 + \mathbf{J}_n^2].
\end{aligned} \tag{3.9}$$

The Coulomb potential requires an approximation for the exchange term contributions in order to keep it local, since the Coulomb force has non-zero range; a local density approximation called the Slater approximation [Sla51] is then used to obtain

$$\mathcal{E}_{\rm coul}(\mathbf{r}) = \frac{e^2\rho_p(\mathbf{r})}{2}\int \frac{\rho_p(\mathbf{r}')}{|\mathbf{r}-\mathbf{r}'|}d^3r' - \frac{3e^2}{4}\left(\frac{3}{\pi}\right)^{1/3}\rho_p(\mathbf{r})^{4/3}. \tag{3.10}$$

3.1.3 Skyrme-Hartree-Fock equations

The Hartree-Fock equations for the Skyrme interaction are obtained by writing that the total energy E is stationary with respect to variations of the single-particle states ϕ_i, with the subsidiary condition that the ϕ_i are normalized [VB72]

$$\delta\left(E - \sum_i \epsilon_i \int |\phi_i(\mathbf{r})|^2 d^3r\right) = 0. \tag{3.11}$$

From Eq.(3.4) and (3.8),

$$\delta E = \sum_q \int d^3r \left[\frac{\hbar^2}{2m_q^*(\mathbf{r})}\delta\tau_q(\mathbf{r}) + U_q(\mathbf{r})\delta\rho_q(\mathbf{r}) + \mathbf{W}_q(\mathbf{r})\cdot\delta\mathbf{J}_q(\mathbf{r})\right] \tag{3.12}$$

where the coefficients of the variation are, dropping again the dependence on $\mathbf{r}$,

$$\frac{\hbar^2}{2m_q^*} = \frac{\delta\mathcal{E}}{\delta\tau_q} = \frac{\hbar^2}{2m_q} + \frac{1}{8}[t_1(2+x_1) + t_2(2+x_2)]\rho + \frac{1}{8}[t_2(2x_2+1) - t_1(2x_1+1)]\rho_q \tag{3.13}$$

$$\begin{aligned} U_q = \frac{\delta\mathcal{E}}{\delta\rho_q} &= \frac{1}{2}t_0[(2+x_0)\rho - (2x_0+1)\rho_q^2] \\ &+ \frac{1}{24}t_3\alpha\rho^{\alpha-1}[(2+x_3)\rho^2 - (2x_3+1)(\rho_p^2+\rho_n^2)] \\ &+ \frac{1}{12}t_3\rho^\alpha[(2+x_3)\rho - (2x_3+1)\rho_q] \\ &+ \frac{1}{8}[t_1(2+x_1) + t_2(2+x_2)]\tau + \frac{1}{8}[t_2(2x_2+1) - t_1(2x_1+1)]\tau_q \\ &- \frac{1}{16}[3t_1(2+x_1) - t_2(2+x_2)]\nabla^2\rho + \frac{1}{16}[3t_1(2x_1+1) + t_2(2x_2+1)]\nabla^2\rho_q \\ &- \frac{1}{2}W_0[\nabla\cdot\mathbf{J} + \nabla\cdot\mathbf{J}_q] + \frac{\delta\mathcal{E}_{\rm coul}}{\delta\rho_q} \end{aligned} \tag{3.14}$$

$$\mathbf{W}_q = \frac{\delta\mathcal{E}}{\delta\mathbf{J}_q} = \frac{1}{2}W_0[\nabla\rho + \nabla\rho_q] - \frac{1}{8}(t_1x_1 + t_2x_2)\mathbf{J} + \frac{1}{8}(t_1 - t_2)\mathbf{J}_q. \tag{3.15}$$

Inserting Eq.(3.12) in Eq.(3.11), one concludes that the single-particle wave functions ϕ_i have to satisfy the following set of equations

$$\left[-\nabla\cdot\frac{\hbar^2}{2m_q^*(\mathbf{r})}\nabla + U_q(\mathbf{r}) + \mathbf{W}_q(\mathbf{r})\cdot(-i)(\nabla\times\boldsymbol{\sigma})\right]\phi_i(\mathbf{r},\sigma,q) = \epsilon_i\phi_i(\mathbf{r},\sigma,q). \tag{3.16}$$

These equations, which are known as the *Skyrme-Hartree-Fock* (SHF) *equations*, although highly non linear, involve only local potentials, and therefore can be solved in coordinate space. This is a major difference with HF equations corresponding to finite range interactions which give rise to fully non-local potentials. Note that the eigenvalues ϵ_i are just the Lagrange multipliers introduced in Eq.(3.11); they are often called for convenience single-particle energies.

Looking at Eq.(3.16), we recognize the form of a typical Schrödinger equation. We can easily identify $m_q^*(\mathbf{r})$ as an effective mass, $U_q(\mathbf{r})$ as a central potential and $\mathbf{W}_q(\mathbf{r})$ as a spin-orbit potential.

Since $m_q^*(\mathbf{r})$, $U_q(\mathbf{r})$ and $\mathbf{W}_q(\mathbf{r})$ can be expressed in terms of the local densities ρ_q, τ_q and $\mathbf{J}_q$, they are known when all the occupied single-particle states are known. It is thus possible to implement a self-consistent calculation which, starting from an ensemble of trial wave functions (for example eigenfunctions of a standard Woods-Saxon potential), solves iteratively Eq.(3.16) building up the potentials with the solutions ϕ_i of the previous step until convergence. Once obtained the converged solutions for occupied states, one can employ the potentials and calculate wave function and single-particle energies for the unoccupied states as well. Single-particle unoccupied states lying in the continuum can be calculated either with completely or with a discretizing procedure using box boundary conditions.

It is important to notice that the kinetic energy part of the of the total energy E is not simply $\sum_i^A \mathbf{p}_i^2/2m$ because the kinetic energy of the center-of-mass should be subtracted:

$$\begin{aligned} T &= \sum_i^A \frac{\mathbf{p}_i^2}{2m} - \frac{(\sum_i^A \mathbf{p}_i)^2}{2mA} \\ &= \frac{1}{2m}(1-\frac{1}{A})\sum_i^A \mathbf{p}_i^2 - \frac{1}{2mA}\sum_{i\neq j}^A \mathbf{p}_i\cdot\mathbf{p}_j \end{aligned} \tag{3.17}$$

The first term in the second line is again a one-body kinetic term with a corrected mass $m' = m(1-\frac{1}{A})$; this takes care of a large part of the total center-of-mass correction on the total energy. The second term is a two-body correction much more difficult to incorporate and it is usually dropped.

In the case of spherical symmetry, the Skyrme-Hartree-Fock equations simplify greatly into a set of one-dimensional differential equations in the radial coordinate r. Infact, in this case, the single-particle wave functions can be written as (see Section A.3.1)

$$\phi_i(\mathbf{r},\sigma,\tau) = \frac{u_\alpha(r)}{r}[Y_l(\hat{r})\chi_{\frac{1}{2}}(\sigma)]_{(l\frac{1}{2})jm}\chi_q(\tau) \tag{3.18}$$

where the indexes i and α stands now for the sets of quantum numbers $i \equiv q,n,l,j,m$ and $\alpha \equiv q,n,l,j$, whereas χ_q is the two-component iso-spinor. One can thus easily deduce the SHF radial equations which read

$$\begin{aligned} &\frac{\hbar^2}{2m_q^*(r)}\left[-u''_\alpha(r) + \frac{l(l+1)}{r^2}u_\alpha(r)\right] - \frac{d}{dr}\left(\frac{\hbar^2}{2m_q^*(r)}\right)u'_\alpha(r) \\ &\quad + \left\{U_q(\mathbf{r}) + \frac{1}{r}\frac{d}{dr}\left(\frac{\hbar^2}{2m_q^*(r)}\right) + \left[j(j+1) - l(l+1) - \frac{3}{4}\right]\frac{W_q(r)}{r}\right\}u_\alpha(r) = \epsilon_\alpha u_\alpha(r) \end{aligned} \tag{3.19}$$

where $W_q(r)$ is defined reducing the spin orbit term $\mathbf{W}_q(\mathbf{r})\cdot(-i)(\nabla\times\boldsymbol{\sigma})$ to the usual form $\frac{1}{r}W_q(r)\mathbf{l}\cdot\boldsymbol{\sigma}$.

3.2 Particle-hole theories

The basic properties of the ground states of many nuclei can be well explained in the quite simple framework of independent particle models such as the Hartree-Fock approximation. Besides, analysis of the spectra of nuclear excitations reveals a series of nuclear excited states which can be very adequately explained as single-particle independent excitations. But there are also many excited states with features that cannot be understood in terms of shell model excitations: these modes can only be explained if we suppose that coherent participation by many nucleons takes place in the nucleus, resulting in a collective excitation of the system as a whole. Giant resonances (see Chapter 2) are a major example of such collective states. The *Tamm-Dancoff*, the *random phase* and *quasi-particle random phase* models, which will be presented in this Section, depict collective excited states as given by coherent superpositions of single (quasi)particle-hole (ph-) excitations (see Section A.2.5). For a wider explanation of these topics refer to [RS80] or [Row70].

3.2.1 Tamm-Dancoff approximation

The simplest microscopic treatment of nuclear excitations is the Tamm-Dancoff approximation (TDA). It is based on the ansatz of the Hartree-Fock approximation for the ground state and on the diagonalization of the Hamiltonian in a finite space of excited ph-configurations.

The Hamiltonian is given in the HF representation by

$$H = H_0 + V_{\rm res} \tag{3.20}$$

where, apart from an unimportant constant,

$$H_0 = \sum_\nu \epsilon_\nu a_\nu^\dagger a_\nu \tag{3.21}$$

$$V_{\rm res} = \frac{1}{4} \sum_{\mu\nu\rho\sigma} \overline{v}_{\mu\nu\rho\sigma} : a_\mu^\dagger a_\nu^\dagger a_\sigma a_\rho :. \tag{3.22}$$

Here H_0 is a one-body term which accounts for the independent-particle motion (HF Hamiltonian), whereas $\overline{v}_{\mu\nu\rho\sigma}$ is the matrix element of the two-body residual interaction $V_{\rm res}$ between antisymmetrized two-particle states, i.e. the part of the effective interaction wich is not taken into account in the Hartree-Fock mean field. Besides :...: is the normal ordered product.

The HF separation (3.20) was made in such a manner that the ground state $|HF\rangle$ of H_0 should be a good approximation of the ground state of H, but there is no reason why excited states of H_0 should resemble eigenstates of H. In particular, the lowest excited states of H_0, namely the particle-hole excitations

$$|m(i)^{-1}\rangle \equiv a_m^\dagger b_i^\dagger |HF\rangle \equiv a_m^\dagger a_{\widetilde{i}} |HF\rangle \tag{3.23}$$

are directly coupled to one another by the residual interaction. Note that we use here, for brevity, the convention that indices m, n are reserved for particles and i, j for holes; furthermore, we use the definition that creating a hole in a certain state is equivalent to destroy a particle in the time-reversal of that state and that create (destroy) a particle in the initial state is equivalent to destroy (create) a particle in the final state (see Appendix A.2.5). Thus

$$\begin{aligned}
\langle m(i)^{-1}|V_{\rm res}|n(j)^{-1}\rangle &= \frac{1}{4} \sum_{\mu\nu\rho\sigma} \overline{v}_{\mu\nu\rho\sigma} \langle HF| a_{\widetilde{i}}^\dagger a_m : a_\mu^\dagger a_\nu^\dagger a_\sigma a_\rho : a_n^\dagger a_{\widetilde{j}} |HF\rangle \\
&= \frac{1}{4} (\overline{v}_{m\widetilde{j}\widetilde{i}n} - \overline{v}_{\widetilde{j}m\widetilde{i}n} - \overline{v}_{m\widetilde{j}n\widetilde{i}} + \overline{v}_{\widetilde{j}mn\widetilde{i}}) \\
&= \overline{v}_{m\widetilde{j}\widetilde{i}n}
\end{aligned} \tag{3.24}$$

Since $\overline{v}$ is taken to be antisymmetrized, $\overline{v}_{m\widetilde{j}\widetilde{i}n}$ contains both direct and exchange matrix elements,

$$\overline{v}_{m\widetilde{j}\widetilde{i}n} = v_{m\widetilde{j}\widetilde{i}n} - v_{m\widetilde{j}n\widetilde{i}}. \tag{3.25}$$

These terms are displayed in Fig. 3.1 with Feynman graphs.

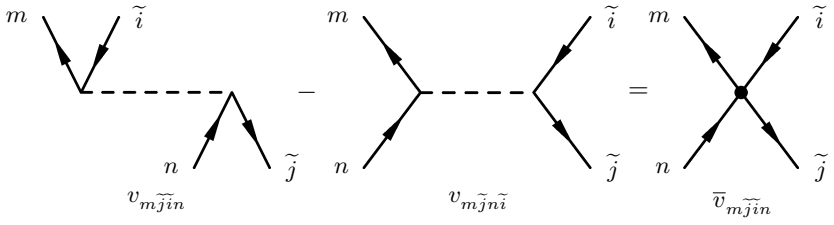

Figure 3.1
Graphical representation of the matrix element $\overline{v}_{m\widetilde{j}\widetilde{i}n}$ with the direct term $v_{m\widetilde{j}\widetilde{i}n}$ and the exchange term $v_{m\widetilde{j}n\widetilde{i}}$.

The matrix elements of the full Hamiltonian, between particle-hole states, are

$$\langle m(i)^{-1}|H|n(j)^{-1}\rangle = \delta_{mn}\delta_{ij}(E_0 + \epsilon_{mi}) + \overline{v}_{m\widetilde{j}\widetilde{i}n} \tag{3.26}$$

where E_0 is the ground state energy and $\epsilon_{mi} = \epsilon_m - \epsilon_i$ is the unperturbed particle-hole excitation energy.

If we assume that the eigenstates $|\nu\rangle$ of H can be expanded in terms of a finite set of particle-hole states,

$$|\nu\rangle = \sum_{nj} X^{\nu}_{nj} |n(j)^{-1}\rangle \tag{3.27}$$

we obtain the secular equation

$$\sum_{nj} \langle m(i)^{-1}|H|n(j)^{-1}\rangle X^{\nu}_{nj} = E_\nu X^{\nu}_{mi}. \tag{3.28}$$

Expanding Eq.(3.28) we get

$$\sum_{nj} (\delta_{mn}\delta_{ij}\epsilon_{mi} + \overline{v}_{m\widetilde{j}i\widetilde{n}}) X^{\nu}_{nj} = \Omega_\nu X^{\nu}_{mi} \tag{3.29}$$

where $\Omega_\nu = E_\nu - E_0$ is the excitation energy. Defining $A_{minj} = \delta_{mn}\delta_{ij}\epsilon_{mi} + \overline{v}_{m\widetilde{j}i\widetilde{n}}$, the secular equation becomes

$$\sum_{nj} A_{minj} X^{\nu}_{nj} = \Omega_\nu X^{\nu}_{mi}. \tag{3.30}$$

A diagonalization of the matrix A_{minj} thus permits to find the coefficients X^{ν}_{nj} and so to determine the nuclear excited states $|\nu\rangle$ via Eq.(3.27).

If one has a good quantum number, such as angular momentum, one should naturally exploit it to reduce the dimensions of the matrix to be diagonalized. Instead of Eq.(3.27), one should therefore use the expansion (see Appendix A.1.1)

$$|\nu, JM\rangle = \sum_{j_n j_j} X^{\nu J}_{nj} |n(j)^{-1}, JM\rangle, \tag{3.31}$$

where

$$|n(j)^{-1}, JM\rangle = \sum_{m_n m_j} \langle j_n m_n j_j m_j | JM\rangle a^{\dagger}_{j_n m_n} a_{\widetilde{j_j m_j}} |HF\rangle. \tag{3.32}$$

But, for time-reversal properties (see Appendix A.2.5)

$$a_{\widetilde{j_j m_j}} = (-1)^{j_j + m_j} a_{j_j - m_j} \tag{3.33}$$

and so we get

$$\begin{aligned} |n(j)^{-1}, JM\rangle &= \sum_{m_n m_j} (-1)^{j_j+m_j} \langle j_n m_n j_j m_j | JM\rangle a^{\dagger}_{j_n m_n} a_{j_j - m_j} |HF\rangle \\ &= \sum_{m_n m_j} (-1)^{j_j - m_j} \langle j_n m_n j_j - m_j | JM\rangle a^{\dagger}_{j_n m_n} a_{j_j m_j} |HF\rangle. \end{aligned} \tag{3.34}$$

The secular equation then becomes

$$\sum_{nj} (\delta_{mn}\delta_{ij}\epsilon_{mi} + \langle m(i)^{-1}, J|V_{\rm res}|n(j)^{-1}, J\rangle) X^{\nu J}_{nj} = \Omega_\nu X^{\nu J}_{mi} \tag{3.35}$$

where now

$$\begin{aligned} \langle m(i)^{-1}, J|V_{\rm res}|n(j)^{-1}, J\rangle &= \overline{v}_{m\widetilde{j}i\widetilde{n}} \\ &= \sum_{\text{all } m} (-1)^{j_j - m_j + j_i - m_i} \langle j_m m_m j_i - m_i | JM\rangle \langle j_n m_n j_j - m_j | JM\rangle \\ &\quad \times \langle j_m m_m, j_i m_i | V_{\rm res} | j_n m_n, j_j m_j\rangle. \end{aligned} \tag{3.36}$$

Defining

$$A^J_{minj} = \delta_{mn}\delta_{ij}\epsilon_{mi} + \langle m(i)^{-1}, J|V_{\rm res}|n(j)^{-1}, J\rangle, \tag{3.37}$$

the secular equation (3.35) takes the simple form

$$\sum_{nj} A^J_{minj} X^{\nu J}_{nj} = \Omega_\nu X^{\nu J}_{mi}. \tag{3.38}$$

3.2.2 The random phase approximation

In the TDA method, the ground state is purely the HF ground state and thus remains unchanged, neglecting the effects of the residual interaction in the ground state. One way out is a generalization of the TDA method in which we take, instead of the HF ground state, one in which a certain class of correlations has been summed. For example, if the excited states are described as vibrational excitations, the ground state correlations may be associated with the vibrational zero-point motion.

Historical development of the RPA began with the theory of D. Bohm and D. Pines (1953) for the plasma oscillations of an electron gas. In their theory, the parameters of the electromagnetic field, representing the interaction between the electrons, were quantized and treated as the collective coordinates of the plasma oscillations. The term random phase approximation referred to the neglect of the coupling between plasma vibrations of different momenta [BP53].

We start with a set of exact eigenstates of the Hamiltonian H,

$$H|\nu\rangle = E_\nu|\nu\rangle. \tag{3.39}$$

It is possible to define operators $\Gamma^\dagger_\nu$ and Γ_ν in such a way that

$$\Gamma^\dagger_\nu|0\rangle = |\nu\rangle \tag{3.40}$$

$$\Gamma_\nu|0\rangle = 0, \tag{3.41}$$

where $|0\rangle$ is the exact ground state of H. From the eigenvalue equation (3.39) we get the equation of motion

$$\left[H, \Gamma^\dagger_\nu\right]|0\rangle = (E_\nu - E_0)\Gamma^\dagger_\nu|0\rangle. \tag{3.42}$$

Multiplying from the left with an arbitrary state of the form $\langle 0|\delta\Gamma$, we get

$$\langle 0|\left[\delta\Gamma, \left[H, \Gamma^\dagger_\nu\right]\right]|0\rangle = (E_\nu - E_0)\langle 0|\left[\delta\Gamma, \Gamma^\dagger_\nu\right]|0\rangle. \tag{3.43}$$

At first we re-derive the TDA equations by approximating the exact ground state $|0\rangle$ by the HF ground state $|HF\rangle$ and the operator $\Gamma^\dagger_\nu$ by the collective ph-operator

$$\Gamma^\dagger_\nu = \sum_{nj} X^\nu_{nj} a^\dagger_n a_j \tag{3.44}$$

omitting, for simplicity, the superscripts for time-reversal conjugation. If now we take $\delta\Gamma = a^\dagger_i a_m$, Eq.(3.43) becomes

$$\sum_{nj}\langle HF|\left[a^\dagger_i a_m, \left[H, a^\dagger_n a_j\right]\right]|HF\rangle X^\nu_{nj} = \Omega_\nu X^\nu_{mi}. \tag{3.45}$$

This is exactly equivalent to the TDA equation (3.35) we derived earlier.

The above procedure has the advantage that it can be generalized in a straightforward way. If we think of the ground state containing p-h correlations, we can not only create a ph-pair, but also destroy one. So we can generalize the form of the operator $\Gamma^\dagger_\nu$ as

$$\Gamma^\dagger_\nu = \sum_{nj} X^\nu_{nj} a^\dagger_n a_j - \sum_{nj} Y^\nu_{nj} a^\dagger_j a_n. \tag{3.46}$$

The RPA ground state $|RPA\rangle$ is defined as $\Gamma_\nu|RPA\rangle = 0$. Let now $\delta\Gamma$ assume the form $a_m^\dagger a_i$ or $a_i^\dagger a_m$: therefore, from Eq.(3.43), we get the two sets of equations

$$\langle RPA|\left[a_i^\dagger a_m, \left[H, \Gamma_\nu^\dagger\right]\right]|RPA\rangle = \Omega_\nu \langle RPA|\left[a_i^\dagger a_m, \Gamma_\nu^\dagger\right]|RPA\rangle \tag{3.47}$$

$$\langle RPA|\left[a_m^\dagger a_i, \left[H, \Gamma_\nu^\dagger\right]\right]|RPA\rangle = \Omega_\nu \langle RPA|\left[a_m^\dagger a_i, \Gamma_\nu^\dagger\right]|RPA\rangle \tag{3.48}$$

where Ω_ν is the excitation energy of the state $|\nu\rangle$ in RPA approximation. These equation contain expectation values which are very complicated to calculate, because we do not know the exact form of the ground state $|RPA\rangle$.

We content ourselves with an approximation usually known as the *quasi-boson approximation*. If we assume that the correlated ground state does not differ very much from the HF ground state, we can calculate all expectation values in the HF approximation, for example

$$\begin{aligned}\langle RPA|\left[a_i^\dagger a_m, a_n^\dagger a_j\right]|RPA\rangle &\simeq \langle HF|\left[a_i^\dagger a_m, a_n^\dagger a_j\right]|HF\rangle \\ &= \delta_{ij}\delta_{mn}.\end{aligned} \tag{3.49}$$

Within the quasi-boson approximation, the amplitudes X_{mi}^ν and Y_{mi}^ν have a very direct meaning: their absolute squares give the probability of finding the components $a_m^\dagger a_i|0\rangle$ and $a_i^\dagger a_m|0\rangle$ in the excited state $|\nu\rangle$:

$$\langle 0|a_i^\dagger a_m|\nu\rangle \simeq \langle HF|\left[a_i^\dagger a_m, \Gamma_\nu^\dagger\right]|HF\rangle = X_{mi}^\nu \tag{3.50}$$

$$\langle 0|a_m^\dagger a_i|\nu\rangle \simeq \langle HF|\left[a_m^\dagger a_i, \Gamma_\nu^\dagger\right]|HF\rangle = Y_{mi}^\nu. \tag{3.51}$$

Equations (3.47) and (3.48) can now be written in the compact form

$$\begin{pmatrix} A & B \\ -B^* & -A^* \end{pmatrix}\begin{pmatrix} X^\nu \\ Y^\nu \end{pmatrix} = \Omega_\nu \begin{pmatrix} X^\nu \\ Y^\nu \end{pmatrix} \tag{3.52}$$

where the sub-matrices A and B are defined as

$$\begin{aligned} A_{minj} &= \langle HF|\left[a_i^\dagger a_m, \left[H, a_n^\dagger a_j\right]\right]|HF\rangle \\ &= \delta_{mn}\delta_{ij}\epsilon_{mi} + \langle m(i)^{-1}|V_{\text{res}}|n(j)^{-1}\rangle \\ &= \delta_{mn}\delta_{ij}\epsilon_{mi} + \overline{v}_{mjin} \end{aligned} \tag{3.53}$$

$$\begin{aligned} B_{minj} &= -\langle HF|\left[a_i^\dagger a_m, \left[H, a_j^\dagger a_n\right]\right]|HF\rangle \\ &= \langle m(i)^{-1}, n(j)^{-1}|V_{\text{res}}|HF\rangle \\ &= \overline{v}_{mnij} \end{aligned} \tag{3.54}$$

Here $\overline{v}_{m\overline{j}\overline{i}n}$ has the same form of Eq.(3.25), whereas

$$\overline{v}_{mnij} = v_{mnij} - v_{mnji}. \tag{3.55}$$

These terms are displayed, respectively, in Fig. 3.2(a) and 3.2(b).

Once again, diagonalizing the matrix

$$\begin{pmatrix} A & B \\ -B^* & -A^* \end{pmatrix}$$

we get full knowledge of the excited states of the system via Eq.(3.46).

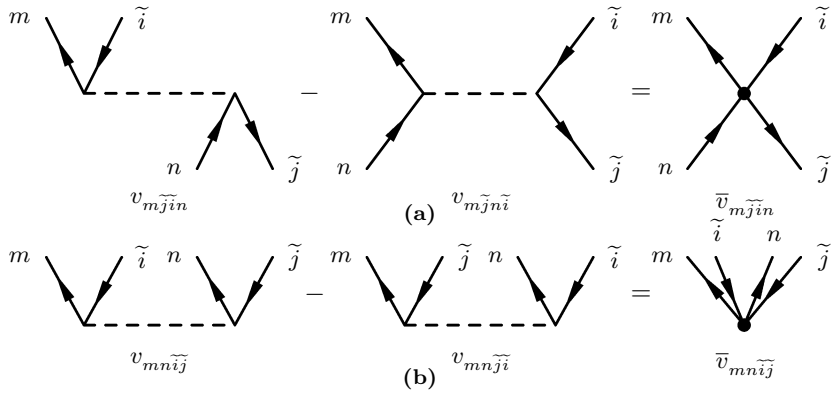

Figure 3.2
Graphical representation of (A) the matrix element $\overline{v}_{m\widetilde{j}\widetilde{i}n}$ with the direct term $v_{m\widetilde{j}\widetilde{i}n}$ and the exchange term $v_{m\widetilde{j}n\widetilde{i}}$ and (B) the matrix element $\overline{v}_{mn\widetilde{i}\widetilde{j}}$ with the direct term $v_{mn\widetilde{i}\widetilde{j}}$ and the exchange term $v_{mn\widetilde{j}\widetilde{i}}$.

If we have good quantum numbers, such as angular momentum, we can work, as we did in the TDA case, with an angular momentum coupled representation. Thus, instead of (3.46), we make the expansion

$$\Gamma^\dagger_\nu(JM) = \sum_{nj} X^{\nu J}_{nj} A^\dagger_{nj}(JM) - \sum_{nj} Y^{\nu J}_{nj} A_{nj}(\widetilde{JM}). \tag{3.56}$$

where $A^\dagger_{nj}(JM)$ and $A_{nj}(\widetilde{JM})$ are the coupled ph-creation and destruction operators,

$$\begin{aligned} A^\dagger_{nj}(JM) &= \sum_{m_n m_j} \langle j_n m_n j_j m_j | JM\rangle a^\dagger_{j_n m_n} a_{\widetilde{j_j m_j}} \\ &= \sum_{m_n m_j} (-1)^{j_j - m_j} \langle j_n m_n j_j - m_j | JM\rangle a^\dagger_{j_n m_n} a_{j_j m_j} \end{aligned} \tag{3.57}$$

$$\begin{aligned} A_{nj}(\widetilde{JM}) &= (-1)^{J+M} A_{nj}(J-M) \\ &= \sum_{m_n m_j} (-1)^{J+M+j_j-m_j} \langle j_n m_n j_j - m_j | J - M\rangle a^\dagger_{j_j m_j} a_{j_n m_n}. \end{aligned} \tag{3.58}$$

The submatrices A and B then become

$$A^J_{minj} = \delta_{mn}\delta_{ij}\epsilon_{mi} + \langle m(i)^{-1} J | V_{\rm res} | n(j)^{-1} J\rangle = \delta_{mn}\delta_{ij}\epsilon_{mi} + \overline{v}_{mjin} \tag{3.59}$$

$$B^J_{minj} = \langle m(i)^{-1} J, n(j)^{-1} J | V_{\rm res} | HF\rangle = \overline{v}_{mnij} \tag{3.60}$$

and now the matrix elements of the two-body residual interaction can be evaluated as in Eq.(3.36).

In the RPA approximation, the reduced transition probability, Eq.(A.38), of going from the ground state, $|0\rangle$, to an excited state $|\nu\rangle$, becomes

$$B(T_\lambda; 0 \to \nu) = \left| \sum_{mi} \big(X^\nu_{mi} + Y^\nu_{mi}\big) \langle m || T_\lambda || i\rangle \right|^2. \tag{3.61}$$

Besides, we define the transition density of the excited state ν, $\delta\rho_\nu(r)$, as

$$\delta\rho_\nu(r) = \frac{1}{\sqrt{2\lambda+1}} \sum_{mi} \big(X^\nu_{mi} + Y^\nu_{mi}\big) \langle m || Y_\lambda || i\rangle \frac{u_m(r) u_i(r)}{r^2}, \tag{3.62}$$

where we have used Eq.(A.55) for the single-particle wave function. Thus the reduced transition probability becomes

$$B(T_\lambda; 0 \to \nu) = (2\lambda+1) \left| \int r^{\lambda+2} \delta\rho_\nu(r) dr \right|^2. \tag{3.63}$$

3.2.3 The quasi-particle random phase approximation

TDA and RPA can, in principle, be applied to all even-even nuclei; in practice, however, their usefulness is restricted to doubly-closed shell nuclei. The reason is that, away from closed shells, pairing correlations become so important that they cannot be neglected in a realistic analysis of the nuclear states. For superconducting nuclei, the RPA generalizes to the QRPA (quasi-particle RPA) in the framework of standard BCS theory [Row70, RS80]. In this theory the Hamiltonian is expressed in the Hartree-Fock-Bogolyubov representation

$$H = H_0 + V_{\rm res} \tag{3.64}$$

We define the quasi-particle creation and destruction operators $\alpha^\dagger_\nu$ and α_ν as

$$\begin{aligned} \alpha^\dagger_\nu &= u_\nu a^\dagger_\nu - v_\nu a_{\overline{\nu}} \\ \alpha_\nu &= u_\nu a_\nu - v_\nu a^\dagger_{\overline{\nu}}, \end{aligned} \tag{3.65}$$

where the normalization condition $u^2_\nu + v^2_\nu = 1$ holds; u_ν and v_ν have a direct physical interpretation: the single-particle state ν is unoccupied with probability amplitude u^2_ν and occupied with probability amplitude v^2_ν. Then

$$H_0 = \sum_\nu \epsilon_\nu \alpha^\dagger_\nu \alpha_\nu \tag{3.66}$$

$$V_{\rm res} = \frac{1}{4} \sum_{\mu\nu\rho\sigma} \overline{v}_{\mu\nu\rho\sigma} : a^\dagger_\mu a^\dagger_\nu a_\sigma a_\rho : \tag{3.67}$$

and the normal ordering is now with respect to the quasi-particle vacuum $|QRPA\rangle$.

Making the expansion

$$\Gamma^\dagger_\nu = \sum_{\alpha\beta} X^\nu_{\alpha\beta} \alpha^\dagger_\alpha \alpha^\dagger_\beta - \sum_{\alpha\beta} Y^\nu_{\alpha\beta} \alpha_\alpha \alpha_\beta \tag{3.68}$$

we obtain a matrix equation identical to (3.52) but with

$$\begin{aligned} A_{\alpha\beta\gamma\delta} = &+ (E_\alpha + E_\beta)\delta_{\alpha\gamma}\delta_{\beta\delta} \\ &+ \langle \alpha\beta | V_{\rm res} | \gamma\delta \rangle (u_\alpha u_\beta u_\gamma u_\delta + v_\alpha v_\beta v_\gamma v_\delta) \\ &+ \langle \alpha(\beta)^{-1} | V_{\rm res} | \gamma(\delta)^{-1} \rangle (u_\alpha v_\beta u_\gamma v_\delta + v_\alpha u_\beta v_\gamma u_\delta) \\ &- \langle \alpha(\beta)^{-1} | V_{\rm res} | \delta(\gamma)^{-1} \rangle (u_\alpha v_\beta v_\gamma u_\delta + v_\alpha u_\beta u_\gamma u_\delta) \end{aligned} \tag{3.69}$$

$$\begin{aligned} B_{\alpha\beta\gamma\delta} = &- \langle \alpha\beta | V_{\rm res} | \gamma\delta \rangle (u_\alpha u_\beta v_\gamma v_\delta + v_\alpha v_\beta u_\gamma u_\delta) \\ &+ \langle \alpha(\beta)^{-1}, \gamma(\delta)^{-1} | V_{\rm res} | QRPA \rangle (u_\alpha v_\beta u_\gamma v_\delta + v_\alpha u_\beta v_\gamma u_\delta) \\ &- \langle \alpha(\beta)^{-1}, \delta(\gamma)^{-1} | V_{\rm res} | QRPA \rangle (u_\alpha v_\beta u_\gamma v_\delta + v_\alpha u_\beta v_\gamma u_\delta) \end{aligned} \tag{3.70}$$

where E_α and E_β are the quasi-particle energies and the particle-hole matrix elements are

$$\begin{aligned} \langle \alpha(\beta)^{-1} | V_{\rm res} | \gamma(\delta)^{-1} \rangle &= \langle \alpha\delta | V_{\rm res} | \beta\gamma \rangle = \overline{v}_{\alpha\delta\beta\gamma} \\ \langle \alpha(\beta)^{-1}, \gamma(\delta)^{-1} | V_{\rm res} | QRPA \rangle &= \langle \alpha\gamma | V_{\rm res} | \beta\delta \rangle = \overline{v}_{\alpha\gamma\beta\delta}. \end{aligned} \tag{3.71}$$

It is evident that, from Eq.(3.69) and Eq.(3.70), we can obtain the RPA expression for A_{minj} and B_{minj} (Eq.(3.53) and Eq.(3.54)) in the limit

$$\begin{aligned} v_m = v_n = u_i = u_j = 0 \\ u_m = u_n = v_i = v_j = 1. \end{aligned}$$

3.3 Particle-vibration coupling

The variation in the average nuclear potential associated with the collective vibrations provides a coupling between the vibrational degrees of freedom and those of the individual particles. In this Section, we consider the various effects arising from this coupling, such as renormalization of the properties of the particles and of the vibrational quanta. The original theory, developed in [BM75], has been widely employed in the last decades (e.g. [BBB$^+$77, Ham74, CSB10]). An alternative but equivalent formulation, based on the Green's function method, have been also successfully developed [RW73, LR06]. For a wider review, one can consult [MBB$^+$85].

3.3.1 Coupling matrix elements

From a macroscopic point of view, the presence of collective vibrations induces shape oscillations in the nucleus; this modes are, consequently, associated with variations in the total particle density and in the nuclear average potential.

The leading-order particle-vibration coupling Hamiltonian is linear in the vibrational amplitude α and can be written in the form

$$H_{\text{int}} = k\alpha F(x) \tag{3.72}$$

where $F(x)$ is a one-particle operator describing the dependence of the potential on the nucleonic variables x, and k is the coupling constant which characterizes the relationship between the potential and the density. Here F depends not only on the space-variables but also on the spin- or isospin-variables, corresponding to various degrees of freedom of the nucleons. In the following we confine ourselves to the shape oscillations as examples of possible vibrations. For a shape oscillation of multipole order λ, $R(\vartheta,\phi)$, which expresses the shape of the nucleus, will take the form

$$R(\vartheta,\phi) = R_0\big(1 + \sum_\mu Y^*_{\lambda\mu}(\vartheta,\phi)\alpha_{\lambda\mu}\big). \tag{3.73}$$

where R_0 is the mean nuclear radius. The variation δU in the average nuclear potential U induced by the density oscillation will consequently be

$$\delta U = -R_0\frac{dU(r)}{dr}\sum_\mu Y^*_{\lambda\mu}(\vartheta,\phi)\alpha_{\lambda\mu}. \tag{3.74}$$

The Hamiltonian of the coupled system will thus be of the form

$$H = H_{\text{sp}} + H_{\text{coll}} + V \tag{3.75}$$

where $H_{\text{sp}} = \sum_i \epsilon_i a_i^\dagger a_i$ is a single-particle Hamiltonian, $H_{\text{coll}} = \sum_\lambda \Omega_\lambda \Gamma^\dagger_\lambda \Gamma_\lambda$ is the collective vibration Hamiltonian and V is the coupling Hamiltonian which must, so far, coincide with δU.

To first order in deformation, thus, the coupling Hamiltonian is

$$V = -k_\lambda(r)\sum_\mu Y^*_{\lambda\mu}(\vartheta,\phi)\alpha_{\lambda\mu} = (-1)^{\lambda+1}(2\lambda+1)^{1/2}k_\lambda(r)(Y_\lambda\alpha_\lambda)_{\lambda\lambda(00)} \tag{3.76}$$

where we have defined

$$k_\lambda(r) = R_0\frac{dU(r)}{dr}. \tag{3.77}$$

and made use of the definition of coupling between two angular momenta (see Appendix A.1.1).

The matrix element of the coupling (3.76) for the scattering of a particle with the excitation of a quantum, is given by [BM75]

$$\begin{aligned}\gamma^\lambda_{ij} &\equiv \langle j, \lambda_{j\lambda(im_i)}|V|im_i\rangle \\ &= (-1)^{i+j}(2i+1)^{-1/2}(2\lambda+1)^{-1/2}\langle j||k_\lambda Y_\lambda||i\rangle\langle\lambda||\alpha_\lambda||0\rangle \\ &= -\mathrm{i}^{l_i+\lambda-l_j}\left(\frac{2\lambda+1}{4\pi}\right)^{1/2}\langle i\frac{1}{2}\lambda 0|j\frac{1}{2}\rangle\left(\frac{\Omega_\lambda}{2C_\lambda}\right)^{1/2}\langle j|k_\lambda(r)|i\rangle\end{aligned} \tag{3.78}$$

with the parity selection rule that requires $l_i+\lambda-l_j$ to be even; here Ω_λ is the energy of the phonon of vibration. For states near the Fermi level, $\langle j_2|k_\lambda(r)|j_1\rangle$ equals approximately the depth of the mean field potential, which is about 50 MeV [BM69]. Besides C_λ is the restoring force parameter, which is simply related to the reduced transition probability, $B(E\lambda)$, by the relation

$$B(E\lambda; 0 \to \lambda) = (2\lambda+1)\left(\frac{3}{4\pi}ZeR^\lambda\right)^2 \frac{\Omega_\lambda}{2C_\lambda}. \tag{3.79}$$

For processes involving the creation of a particle-hole pair, it is possible to obtain the matrix elements [BM75]

$$\langle i^{-1}, j_{(i^{-1}j)\lambda\mu}|V|\lambda\mu\rangle = -\left(\frac{2i+1}{2\lambda+1}\right)^{1/2}\gamma_{ij}^\lambda \tag{3.80}$$

$$\langle i^{-1}, j, \lambda_{(i^{-1}j\lambda)00}|V|0\rangle = -(2i+1)^{1/2}\gamma_{ij}^\lambda. \tag{3.81}$$

The enhancement of these matrix elements by a factor $(2i+1)^{1/2}$, as compared with the matrix element γ_{ij}^λ, expresses the fact that each of the $(2i+1)$ particles in the filled shell can be excited by the interaction with the vibrational field. The basic first order matrix elements are illustrated by the Feynman graphs in Fig. 3.3.

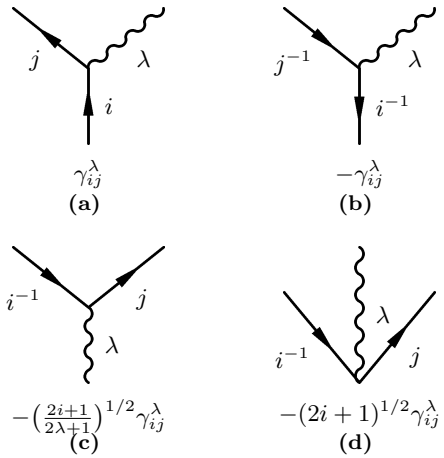

Figure 3.3
Diagrams illustrating first-order coupling between particle and vibration. Diagram (a) and (b) represent, respectively, the scattering of a particle and a hole with the excitation of a quantum; diagram (c) represents the absorbtion of a vibration involving production of a particle-hole pair, whereas diagram (d) illustrates the virtual excitation of the vacuum with emission of a phonon and of a particle-hole pair.

Wigner-Eckhart theorem (see Appendix A.2.2) allows us to define the reduced matrix element $\langle i||\gamma^\lambda||j\rangle$ of γ_{ij}^λ for the coupling between a particle and a vibration,

$$\gamma_{ij}^\lambda = \frac{1}{\sqrt{2i+1}}\langle im_i 00|im_i\rangle\langle i||\gamma^\lambda||j\rangle = \frac{1}{\sqrt{2j_1+1}}\langle i||\gamma^\lambda||j\rangle \tag{3.82}$$

where we have defined $\langle i||\gamma^\lambda||j\rangle \equiv \langle j, \lambda||V||i\rangle$.

3.3.2 Evaluation of PVC vertex with Skyrme interaction

In the case of coupling with density modes, the basic vertex $\langle i||\gamma^{nL}||j\rangle$ can be calculated starting from the representation of the phonon nL in RPA approximation

$$|nLM\rangle = \Gamma_n^\dagger(LM)|RPA\rangle, \tag{3.83}$$

$$\Gamma_n^\dagger(LM) = \sum_{ph} X_{ph}^{nL} A_{ph}^\dagger(LM) - \sum_{ph} Y_{ph}^{nL} A_{ph}(\widetilde{LM}). \tag{3.84}$$

If the residual interaction $V_{\rm res}$, which accounts for the difference between the Hartree-Fock mean field and the two-body effective interaction, is used at the vertex, one obtains, for the reduced matrix element [CSB10],

$$\langle i||\gamma^{nL}||j\rangle = \sqrt{2L+1}\sum_{ph} X_{ph}^{nL} V_L(ihjp) + (-)^{L+j_h-j_p} Y_{ph}^{nL} V_L(ipjh) \tag{3.85}$$

where V_L is the particle-hole coupled matrix element of the residual interaction,

$$\begin{aligned} V_L(ihjp) = \sum_{\text{all } m} (-)^{j_j-m_j+j_h-m_h} &\langle j_i m_i j_j - m_j|LM\rangle\langle j_p m_p j_h - m_h|LM\rangle \\ &\times \langle j_i m_i, j_h m_h|V_{\rm res}|j_j m_j, j_p m_p\rangle. \end{aligned} \tag{3.86}$$

If we neglect the possibility of having particle-hole pairs made up with two nucleons having different charge, we can label the residual interaction by $V_{\rm res}^{qq'}$, where q and q' denote the charge states of two pairs ph and $p'h'$. Since the Skyrme interaction depends actually on density, the following general expression holds

$$V_{\rm res}^{qq'} = \frac{\delta^2\mathcal{E}}{\delta\rho_q\delta\rho_{q'}} \tag{3.87}$$

where $\mathcal{E}$ is the HF energy functional. Thus, residual interaction receives contributions from t_0 and t_3 parts of the force (central, velocity-independent), from t_1 and t_2 parts (velocity-dependent) and from W_0 and V_c parts (spin-orbit and Coulomb terms, respectively).

If we consider the simple case in which we have only t_0 and t_3 terms of the Skyrme interaction [CCG+11],

$$V_{\rm res}^{qq'} = v_0^{qq'}(r)\delta(\mathbf{r}_1 - \mathbf{r}_2) \tag{3.88}$$

and the detailed expression for the function $v_0^{qq'}(r)$ is, if $q = q'$,

$$\begin{aligned} v_0^{qq'}(r) = &\frac{1}{2}t_0(2+x_0) + \frac{1}{16}t_3(\alpha+1)(\alpha+2)\rho^\alpha(r) + \frac{1}{12}t_3(x_3+\frac{1}{2})\rho^\alpha(r) \\ &+ \frac{1}{48}t_3\alpha(1-\alpha)(1+2x_3)\rho^{\alpha-2}(r)\rho_-^2(r) - \frac{1}{12}t_3(2x_3+1)\alpha\rho^{\alpha-1}(r)\rho_-(r) \end{aligned} \tag{3.89}$$

and, if $q \neq q'$,

$$\begin{aligned} v_0^{qq'}(r) = &\frac{1}{2}t_0(1-x_0) + \frac{1}{16}t_3(\alpha+1)(\alpha+2)\rho^\alpha(r) - \frac{1}{12}t_3(x_3+\frac{1}{2})\rho^\alpha(r) \\ &+ \frac{1}{48}t_3\alpha(1-\alpha)(1+2x_3)\rho^{\alpha-2}(r)\rho_-^2(r) \end{aligned} \tag{3.90}$$

where ρ_- stands for $\rho_n - \rho_p$.

In this case the coupled matrix elements reduce to

$$V_L(ihjp) = \frac{i^{-l_i-l_h+l_j+l_p}}{2L+1}\langle i||Y_L||j\rangle\langle p||Y_L||h\rangle \int \frac{dr}{r^2} v_0^{qq'}(r)u_i(r)u_j(r)u_p(r)u_h(r) \tag{3.91}$$

$$V_L(ipjh) = (-1)^{L+j_p-j_h} V_L(ihjp) \tag{3.92}$$

where the radial part u of the single-particle wave function has been introduced. In this simplified case,

$$\langle i||\gamma^{nL}||j\rangle = \sqrt{2L+1}\sum_{ph}(X_{ph}^{nL} + Y_{ph}^{nL})V_L(ihjp). \tag{3.93}$$

3.3.3 Effective moments

Because of the large transition moments associated with the vibrational excitations, the particle-vibration coupling gives rise to important modifications in the effective one-particle moments. As a result of the coupling, the single-particle states are clothed in a cloud of quanta; to first order in the coupling, the dressed (or renormalized) single-particle state $\tilde{i}$ is given, in perturbation theory, by

$$|\tilde{i}\rangle = |i\rangle - \sum_j \frac{\gamma^\lambda_{ij}}{\epsilon_{ji} + \Omega_\lambda}|j,\lambda\rangle \tag{3.94}$$

where ϵ_{ji} is the single-particle excitation energy (which is equal to $\epsilon_j - \epsilon_i$ in the absence of pair correlations). If we consider the matrix elements of the field operator F between the dressed single-particle states, the inclusion of the vibrational moment gives a simple renormalization of the transition moment

$$\widetilde{\langle i_2|F|i_1\rangle} \equiv \langle \tilde{i}_2|F|\tilde{i}_1\rangle = (1+\chi_F)\langle i_2|F|i_1\rangle \tag{3.95}$$

with the coefficient χ_F given by

$$\chi_F = -2k\alpha_0^2 \frac{\Omega_\lambda}{\Omega_\lambda^2 - \epsilon_{ji}^2} \tag{3.96}$$

being α_0 the zero-point amplitude of the vibrational motion and k the coupling constant defined in Eq.(3.72). The renormalization of single-particle moments is illustrated by the diagrams in Fig. 3.4.

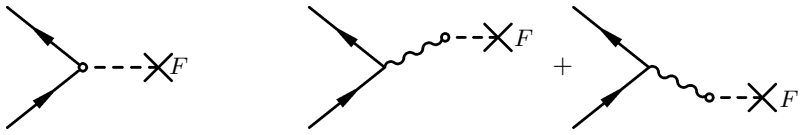

bare moment polarization effect

Figure 3.4
Diagrams illustrating the renormalization of single-particle moment resulting from particle-vibration coupling.

The ratio χ_F between the induced moment and that of the single-particle is referred to as the *polarizability coefficient*. The simple form (3.96) applies to moments that are proportional to the field coupling; more generally, the polarizability coefficient involves the ratio between the one-particle matrix elements of the field coupling and of the moment and may thus depend explicitly on the one-particle states involved.

3.3.4 Self-energies

The particle-vibration coupling acting in second order also gives rise to energy shifts in states involving a single particle (or hole) or a single quantum, as well as a contribution to the energy of the closed-shell configuration. The corresponding diagrams are shown in Fig. 3.5.

The energy shift of the closed-shell configuration associated with the virtual excitation of a particle-hole pair $(i^{-1}j)$ and a quantum λ (Fig. 3.5(a)) can be obtained from the matrix element (3.81),

$$\delta E_0(ij\lambda) = -\frac{(2i+1)(\gamma^\lambda_{ij})^2}{\epsilon_j - \epsilon_i + \Omega_\lambda}. \tag{3.97}$$

It is now clear that the total self-energy for a closed-shell configuration is obtained summing over all particle-hole pairs and quanta:

$$\delta E_0 = \sum_{i<F, j>F, \lambda} \delta E_0(ij\lambda) \tag{3.98}$$

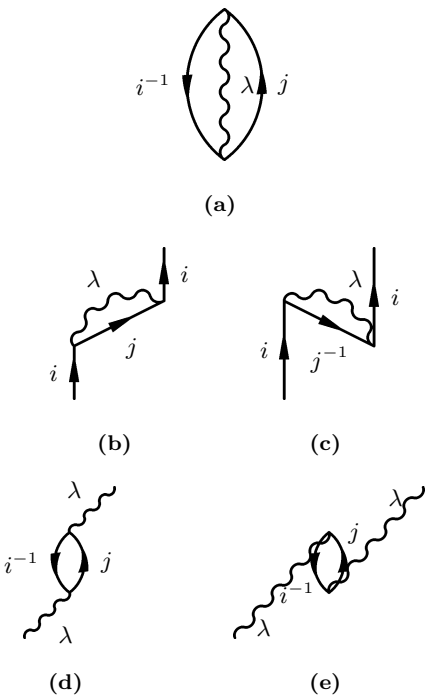

Figure 3.5
Self-energy terms. Diagram (a) represents the vacuum self-energy, while (b) and (c) represent, respectively, the self-energy for a single particle in the case there is a particle or a hole in the intermediate state. Diagrams (d) and (e), instead, represent the self-energy for a phonon.

The self-energy of a single particle receives contributions corresponding to the two diagrams in Fig. 3.5(a) and (b), associated with the coupling to orbits j above and below the Fermi level,

$$\Sigma_i(j\lambda) = \begin{cases} \frac{(\gamma^\lambda_{ij})^2}{\epsilon_i - \epsilon_j - \Omega_\lambda} & \epsilon_j > \epsilon_F \\ -\frac{(\gamma^\lambda_{ij})^2}{\epsilon_j - \epsilon_i - \Omega_\lambda} & \epsilon_j < \epsilon_F \end{cases} \tag{3.99}$$

The total self-energy for a single-particle, defined as $\Sigma_i = \overline{\epsilon_i} - \epsilon_i$ where $\overline{\epsilon_i}$ is the energy of the dressed single-particle state, is thus

$$\Sigma_i = \sum_{\lambda, j>F} \frac{(\gamma^\lambda_{ij})^2}{\epsilon_i - \epsilon_j - \Omega_\lambda} - \sum_{\lambda, j<F} \frac{(\gamma^\lambda_{ij})^2}{\epsilon_j - \epsilon_i - \Omega_\lambda}. \tag{3.100}$$

The one particle self-energy decreases the energy of lowest particle states and increases that of the highest hole states, and thus acts to reduce the gap between occupied and unoccupied orbits.

The phonon self-energy is represented by the two diagrams in Fig. 3.5(d) and (e),

$$\delta\Omega_\lambda(ij) = -\frac{2i+1}{2\lambda+1}(\gamma^\lambda_{ij})^2 \left(\frac{1}{\epsilon_j - \epsilon_i - \Omega_\lambda} + \frac{1}{\epsilon_j - \epsilon_i + \Omega_\lambda} \right). \tag{3.101}$$

The total energy shift is thus

$$\delta\Omega_\lambda = \sum_{i<F, j>F} \delta\Omega_\lambda(ij) \tag{3.102}$$

and it represents the change in the phonon frequency arising from the coupling to all possible particle hole configurations $(i^{-1}j)$.

Chapter 4

Collective response in odd nuclei: the OPVC model

A doubly-magic even-even nucleus is spherically symmetric and, consequently, it has a simple vibrational spectrum. This is no more true for an odd-mass nucleus, since, in the most elementary interpretation, its ground state will be considered as the state obtained by adding a particle or a hole to the neighboring even-even nucleus in its lowest energy state. The consequence is that the symmetries of the doubly-magic even-even nucleus are broken in the neighboring odd nucleus. The collective excited states of the latter, though, cannot be reproduced by means of simple RPA calculations as in the even-even case (see Section 3.2).

If the *even-even core* and the *odd-particle* or *hole* were completely independent, the excitation spectrum of the odd system would be just the sum of the vibrational spectrum of the first plus the single-particle excitation spectrum of the latter. In a realistic picture, nonetheless, the core and the odd-particle (or hole) are not independent. One realistic approach developed for the description of the excitations of odd nuclei was the particle-vibration coupling model (see Section 3.3). The following problem is dealt with in this model: how are the excitation energies and the wave functions of the even-even core (i.e., of the phonons) and the odd-particle or hole mutually affected. One of the problems solved by the PVC is the so-called problem of the splitting of particle-vibration multiplets in odd nuclei. This problem arises since the coupling between the angular momentum j of the ground state of the odd nucleus and the spin L of the excitation of the core leads to a multiplet of states with spin ranging from $|L - j|$ to $L + j$. If there were no interaction between the odd nucleon and the core, these states would be degenerate with the same excitation energy as that of the corresponding states in the neighboring even-even nucleus. Experiments, however, show deviations from this simple model in regard to the position of the multiplet states.

It is possible to find in the literature several attempts to employ in a consistent way the particle-vibration coupling theory for the analysis of the excitations of odd nuclei. In [DD65], separating explicitly the collective from the quasi-particle excitations, a new set of QRPA equations is introduced which is claimed to predict the multiplet splitting. In [KLT01], a consistent generalization of RPA for odd nuclei is suggested, basing the derivation on the Green's function method and using the equation for the three-particle Green's function. A formula for the response function of the odd nucleus is derived as the sum of a core, a particle and a coupling contributions. This model gives the possibility to describe both the single-particle and collective parts of the excitation spectrum, together with the multiplet splitting for collective states.

Another approach to the odd nuclei problem was worked out within a self-consistent variant of the theory of finite Fermi systems [BFT95], which treats the degenerate ground state of an odd nucleus on the average. Essentially this model is equivalent to the RPA with changed occupation number of the valence level. This makes it possible to calculate the strength function for the transitions from the odd nucleus ground state into the continuum, but is does not produce any

multiplet splitting in view of averaged treatment of the ground state.

In this Chapter we will introduce an original consistent microscopic model for the collective response in odd nuclei. This model will be valid for nuclei near closed-shell configurations, i.e., odd nuclei obtained by adding a particle (or a hole) to closed-shell even-even cores. This hypothesis is fundamental because it reduces drastically the complexity of the problem. In fact, dealing with closed-shell configurations allows one not to consider the pairing correlations, since closed-shell nuclei are not superfluid. Besides, considering doubly-magic systems makes it possible to neglect the effects of nuclear deformations. In our model, too, we will deal with the interaction between the core and the odd-particle (hole) in the framework of particle-vibration coupling: for this reason, the model will be referred as *OPVC model* (odd-particle-vibration coupling). Our model will be basically different from [DD65] and [KLT01] since, instead of separating explicitly the collective from the (quasi)-particle excitations, we will consider them as states obtained by linear combinations of the two modes, as it is done in [KS63].

4.1 General features of the OPVC model

Let us consider the case in which an odd nucleus is formed by an even-even closed-shell core plus an odd-particle (or hole). In the following, we will use the abbreviation *odd-nucleon* meaning *odd-particle* or *hole*.

If the interaction between the core and the odd-nucleon is completely neglected, the Hamiltonian of the system is

$$H_0 = H^{\rm odd} + H^{\rm core}. \tag{4.1}$$

In the previous equation, $H^{\rm odd}$ is a single-particle Hamiltonian acting on the odd-nucleon,

$$H^{\rm odd} = \sum_{nljm} \epsilon_{nlj}\; d^\dagger_{nljm}\, d_{nljm}, \tag{4.2}$$

where $nljm$ is a generic odd-nucleon state and $d^\dagger_{n'l'j'm'}$ is a particle ($a^\dagger_{n'l'j'm'}$) creation operator in the case of odd nuclei consisting in an even-even closed-shell core plus a particle (*particle-plus-core nuclei*). Instead, $d^\dagger_{n'l'j'm'}$ is a hole ($b^\dagger_{n'l'j'm'}$) creation operator in the case of odd nuclei consisting in an even-even closed-shell core plus a hole (*hole-plus-core nuclei*). $H^{\rm core}$, instead, is a core Hamiltonian,

$$H^{\rm core} = \sum_{\xi LM} \Omega_{\xi L}\; \Gamma^\dagger_\xi(LM)\; \Gamma_\xi(LM), \tag{4.3}$$

where ξLM is a generic vibrational core state ξ of angular momentum LM and $\Gamma^\dagger_\xi(LM)$ is its creation operator.

The generic state $|\nu ljm\rangle$ of the odd nucleus, i.e., the generic eigenstate of H_0, will be, simply, either a *single-nucleon state*, i.e., a configuration in which the odd-nucleon is in a given quantum state and core vibrations are absent,

$$|\nu ljm\rangle = \left[d^\dagger_{nlj} \otimes \mathbb{I}\right]_{jm} |0\rangle \equiv |(nlj \otimes 0)ljm\rangle \tag{4.4}$$

or a *nucleus-plus-vibration state*, i.e., a configuration in which the odd-nucleon is in a given quantum state and core vibrates,

$$|\nu ljm\rangle = \left[d^\dagger_{n'l'j'} \otimes \Gamma^\dagger_\xi(L)\right]_{jm} |0\rangle \equiv |(n'l'j' \otimes \xi L)ljm\rangle. \tag{4.5}$$

States of the type (4.4) and (4.5) will be referred as *pure states*.

The states $|\nu ljm\rangle$, defined by Eqs.(4.4) and (4.5), are characterized by three quantum numbers: the orbital angular momentum l, the total angular momentum j and its projection on the z-axis, m. The total angular momentum and parity of the states, $\pi = (-1)^l$, are good quantum numbers if we request the system to be spherically symmetric.

In Eqs.(4.4) and (4.5), $|0\rangle = |0_{odd}\rangle \otimes |0_{core}\rangle$, where $|0_{odd}\rangle$ is the single-particle vacuum where the odd-nucleon can be added, whereas $|0_{core}\rangle$ is the exact ground state of the closed-shell core where multipole vibrations can be excited. $|0_{odd}\rangle$ can be well approximated by the Hartree-Fock single-particle vacuum $|HF_{odd}\rangle$ and $|0_{core}\rangle$ can be well-accounted for in RPA approximation, $|0_{core}\rangle \simeq |RPA_{core}\rangle$, being $|RPA_{core}\rangle$ the RPA ground state of the core.

From the previous equations, it is evident that $d^\dagger_{n'l'j'm'}$ and $\Gamma^\dagger_\xi(LM)$ are operators acting on different Hilbert subspaces, those, respectively, of the odd-nucleon and of the even core. In particular, $d^\dagger_{n'l'j'm'}$ acts on $|0_{odd}\rangle$, while $\mathbb{I}$ and $\Gamma^\dagger_\xi(LM)$ are operators acting on $|0_{core}\rangle$.

Using the definition of coupling of two angular momenta and the properties of Clebsch-Gordan coefficients (see Section A.1.1), one can write

$$\left[d^\dagger_{nlj} \otimes \mathbb{I}\right]_{jm} = \sum_{m'} \langle jm'00|jm\rangle d^\dagger_{nljm'} = d^\dagger_{nljm}. \tag{4.6}$$

Moreover, accounting for $\Gamma^\dagger_\xi(LM)$ in RPA approximation,

$$\left[d^\dagger_{n'l'j'} \otimes \Gamma^\dagger_\xi(L)\right]_{jm} = \sum_{m'M} \langle j'm'LM|jm\rangle d^\dagger_{n'l'j'm'} \Gamma^\dagger_\xi(LM) \tag{4.7}$$

$$\Gamma^\dagger_\xi(LM) = \sum_{ph} X^{\xi L}_{ph} A^\dagger_{ph}(LM) - \sum_{ph} Y^{\xi L}_{ph} A_{ph}(\widetilde{LM}) \tag{4.8}$$

$$A^\dagger_{ph}(LM) = \sum_{m_p m_h} (-1)^{j_h - m_h} \langle j_p m_p j_h - m_h|LM\rangle a^\dagger_{pm_p} a_{hm_h} \tag{4.9}$$

$$A_{ph}(\widetilde{LM}) = \sum_{m_p m_h} (-1)^{L+M+j_h-m_h} \langle j_p m_p j_h - m_h|L-M\rangle a^\dagger_{hm_h} a_{pm_p} \tag{4.10}$$

In the previous formulas, the short-hand notation $|im_i\rangle$ has been introduced to represent the quantum state $|n_i l_i j_i m_i\rangle$.

This picture would be quite successful in reproducing the exact eigenstates of odd nuclei if we could completely neglect the coupling between the core vibrations and the odd-nucleon. In general, the introduction of a coupling V between the core and the odd-nucleon will modify deeply the eigenstates of the system with respect to the simple expressions (4.4) and (4.5). In this case, the nuclear Hamiltonian will become

$$H = H_0 + V. \tag{4.11}$$

Nevertheless, since the interaction between the core and the odd-nucleon is thought to be weak, we expect perturbative theory to be a powerful tool to obtain a simple but realistic insight into the real eigenvectors of the system.

The main assumption of our OPVC model is that the net effect of the interaction between the odd-nucleon and the core is to linearly *mix* various pure states of the odd nucleus, resulting in a more general expression for the eigenstates of the coupled odd system [KS63]. This picture is fully compatible with first order perturbative theory, where the perturbed states are obtained as linear combinations of unperturbed states. In the following, we will refer to pure states also as *uncoupled states* or *naked* states, and to mixed states of the odd nucleus as *coupled* or *dressed* states.

With this in mind, we define the generic state of the odd nucleus to be, in the OPVC approximation,

$$|\nu ljm\rangle = c^\dagger_{\nu ljm}|0\rangle \tag{4.12}$$

where we suppose that

$$c^\dagger_{\nu ljm} = \sum_n \mathcal{A}^{\nu lj}_n \left[d^\dagger_{nlj} \otimes \mathbb{I}\right]_{jm} + \sum_{n'l'j'\xi L} \mathcal{B}^{\nu lj}_{n'l'j'\xi L} \left[d^\dagger_{n'l'j'} \otimes \Gamma^\dagger_\xi(L)\right]_{jm}. \tag{4.13}$$

In the previous formula, $\{\mathcal{A}_i\}$ and $\{\mathcal{B}_i\}$ are the coefficients of the state mixing referring, respectively, to pure single-nucleon and nucleon-plus-vibration states. For this coefficients, the following

normalization rule must hold

$$\sum_n \left(\mathcal{A}_n^{\nu lj}\right)^2 + \sum_{n'l'j'\xi L} \left(\mathcal{B}_{n'l'j'\xi L}^{\nu lj}\right)^2 = 1. \tag{4.14}$$

It is important to notice that, since angular momentum and parity are good quantum numbers of the system in spherical symmetry, there can be a mixing only between states with the same total angular momentum, j, and parity, π. Since in the second term of the r.h.s. of Eq.(4.13) the parity is $(-1)^{l'+L}$, the value of l' is automatically determined by L.

Before proceeding further, we define a notation which will be used in the following. The i-th single-particle (or hole) and phonon energies will be always indicated as ϵ_i and Ω_i, respectively. The energy of the pure (uncoupled) states will be indicated as E_i, where i is some index of the state, whereas the energy of the i-th mixed (coupled) state will be referred to as $\overline{E}_i$. Besides, as a short-hand notation, we will indicate as $\mathcal{C}_k^i$ the probability of the dressed state i to be found in the uncoupled state k, i.e., $(\mathcal{A}_k^i)^2$ or $(\mathcal{B}_k^i)^2$ depending on whether the pure state k is of the type (4.4) or (4.5).

4.2 Evaluation of the strength function for collective excitations

The main task of this work will be to derive a consistent formula for the strength function characterizing the collective excitations of the odd nucleus under the effect of a multipole external field.

The total strength function characterizing the excitations induced by a multipole field F_λ on the state $|\nu_1 l_1 j_1\rangle$, $S(E)$, is directly related to the reduced transition probability by Eq.(A.40),

$$S(E) = \sum_{\nu_2 l_2 j_2} B(F_\lambda; \nu_1 l_1 j_1 \rightarrow \nu_2 l_2 j_2)\delta(E - (\overline{E}_2 - \overline{E}_1)). \tag{4.15}$$

where

$$B(F_\lambda; \nu_1 l_1 j_1 \rightarrow \nu_2 l_2 j_2) = \frac{1}{2j_1+1}|\langle \nu_2 l_2 j_2||F_\lambda||\nu_1 l_1 j_1\rangle|^2. \tag{4.16}$$

The interest for the strength function stems in its close relationship with the experimental cross section, which allows direct comparison between theoretical models and experiments. For dipole transitions induced by photo-absorption reactions, e.g., this relation reads

$$\sigma_{E1}(E) = \frac{16\pi^3}{9}\frac{e^2}{\hbar c} E S(E). \tag{4.17}$$

The reduced matrix element $\langle \nu_2 l_2 j_2||F_\lambda||\nu_1 l_1 j_1\rangle$ is, as a consequence of the Wigner-Eckhart Theorem (see Appendix A.2.2), directly related to the non-reduced matrix element by the relation

$$\langle \nu_2 l_2 j_2||F_\lambda||\nu_1 l_1 j_1\rangle = \frac{1}{\sqrt{2j_2+1}} \sum_{m_1 m_2 \mu} \langle j_1 m_1 \lambda\mu | j_2 m_2\rangle \langle \nu_2 l_2 j_2 m_2 | F_{\lambda\mu} | \nu_1 l_1 j_1 m_1\rangle. \tag{4.18}$$

The matrix element $\langle \nu_2 l_2 j_2 m_2 | F_{\lambda\mu} | \nu_1 l_1 j_1 m_1\rangle$ is, in the OPVC model,

$$\langle \nu_2 l_2 j_2 m_2 | F_{\lambda\mu} | \nu_1 l_1 j_1 m_1\rangle = \langle 0 | c_{\nu_2 l_2 j_2 m_2} F_{\lambda\mu} c^\dagger_{\nu_1 l_1 j_1 m_1} | 0\rangle. \tag{4.19}$$

The evaluation of the reduced matrix element $\langle \nu_2 l_2 j_2||F_\lambda||\nu_1 l_1 j_1\rangle$ directly provides a general formula able to predict the complete multipole response of odd nuclei in the framework of our OPVC model.

The complete calculation of the transition matrix element is explicitly done in Appendix B; here we report the result, which is valid both in the case of particle-plus-core and hole-plus-core nuclei:

$$
\begin{aligned}
&\langle \nu_2 l_2 j_2 || F_\lambda || \nu_1 l_1 j_1 \rangle \\
&\quad \simeq \sum_{n_1 n_2} \mathcal{A}^{\nu_1 l_1 j_1}_{n_1} \mathcal{A}^{\nu_2 l_2 j_2}_{n_2} \langle n_2 l_2 j_2 || F_\lambda || n_1 l_1 j_1 \rangle \\
&\quad + \frac{\sqrt{2j_1+1}}{\sqrt{2\lambda+1}} \sum_{n_2 \xi} \mathcal{A}^{\nu_2 l_2 j_2}_{n_2} \mathcal{B}^{\nu_1 l_1 j_1}_{n_2 l_2 j_2 \xi \lambda} (-1)^{j_1+\lambda-j_2} \sum_{ph} \left\{ X^{\xi\lambda}_{ph} + Y^{\xi\lambda}_{ph} \right\} \langle p || F_\lambda || h \rangle \\
&\quad + \frac{\sqrt{2j_2+1}}{\sqrt{2\lambda+1}} \sum_{n_1 \xi} \mathcal{B}^{\nu_2 l_2 j_2}_{n_1 l_1 j_1 \xi \lambda} \mathcal{A}^{\nu_1 l_1 j_1}_{n_1} \sum_{ph} \left\{ X^{\xi\lambda}_{ph} + Y^{\xi\lambda}_{ph} \right\} \langle p || F_\lambda || h \rangle \\
&\quad + \sqrt{2j_1+1}\sqrt{2j_2+1} \sum_{n'_1 l'_1 j'_1} \sum_{n'_2 l'_2 j'_2} \sum_{\xi L} \mathcal{B}^{\nu_1 l_1 j_1}_{n'_1 l'_1 j'_1 \xi L} \mathcal{B}^{\nu_2 l_2 j_2}_{n'_2 l'_2 j'_2 \xi L} \\
&\qquad \times (-)^{j_1+\lambda+j'_2+L} \begin{Bmatrix} j'_2 & j'_1 & \lambda \\ j_1 & j_2 & L \end{Bmatrix} \langle n'_2 l'_2 j'_2 || F_\lambda || n'_1 l'_1 j'_1 \rangle \\
&\quad + \sqrt{2j_1+1}\sqrt{2j_2+1} \sum_{n' l' j'} \sum_{\xi_1 L_1} \sum_{\xi_2 L_2} \mathcal{B}^{\nu_1 l_1 j_1}_{n' l' j' \xi_1 L_1} \mathcal{B}^{\nu_2 l_2 j_2}_{n' l' j' \xi_2 L_2} \\
&\qquad \times \sqrt{2L_1+1}\sqrt{2L_2+1} (-)^{j_2+\lambda+j'} \\
&\qquad \times \begin{Bmatrix} L_1 & \lambda & L_2 \\ j_2 & j' & j_1 \end{Bmatrix} \sum_{p_1 p_2 h_1 h_2} (X^{\xi_1 L_1}_{p_1 h_1} X^{\xi_2 L_2}_{p_2 h_2} + Y^{\xi_1 L_1}_{p_1 h_1} Y^{\xi_2 L_2}_{p_2 h_2}) \\
&\qquad \times \Bigg((-)^{j_{p_1}+j_{h_1}} \delta_{h_1 h_2} \begin{Bmatrix} L_1 & \lambda & L_2 \\ j_{p_2} & j_{h_1} & j_{p_1} \end{Bmatrix} \langle p_1 || F_\lambda || p_2 \rangle \\
&\qquad + (-)^{j_{p_1}+j_{h_2}+L_1+L_2} \delta_{p_1 p_2} \begin{Bmatrix} L_1 & \lambda & L_2 \\ j_{h_2} & j_{p_1} & j_{h_1} \end{Bmatrix} \langle h_1 || F_\lambda || h_2 \rangle \Bigg).
\end{aligned} \tag{4.20}
$$

The transition process represented by the reduced matrix element (4.20) is depicted in terms of Feynman graphs in Figs. from 4.1 to 4.7. In particular, Fig. 4.1 represents the total transition process as a sum of six terms, each coming from a different contribution to the total transition matrix element. These terms are represented in Figs. from 4.2 to 4.7. In these graphs, the thick black arrows stand for dressed (mixed) states of the odd nucleus, whereas the shaded boxes represent projectors of the dressed states upon pure odd nucleus states. The thin lines and the wavy lines stand, on the contrary, for odd-nucleon states and phonon states of the even-even core, respectively. The thin arrows stand, finally, for particle or hole states in the even-even core.

As we said in the introduction to this Chapter, one of the main tasks in the analysis of the response of an odd nucleus is the correct interpretation of the multiplet splitting. This aspect is automatically taken into account in our model, since the expression (4.20) accounts for transition to a state of definite angular momentum and parity. This allows to separate the multipole strength function in contributions coming from transitions to different J^π subspaces, i.e., to split the components of the multiplet.

4.3 The zero-coupling limit

From Eq.(4.20), one can obtain an expression for the reduced transition probability in the zero-coupling limit, i.e. in the case that the exact eigenstates of the odd nucleus are the pure states (4.4) and (4.5).

As one can easily see, the pure single-nucleon states (4.4) can be obtained as a limit of the general expression (4.13) for the dressed states just setting all the $\{\mathcal{B}_i\}$ and all the $\{\mathcal{A}_i\}$ but one equal to zero. The normalization condition (4.14) implies the remaining coefficient $\mathcal{A}$ to be equal to 1. On the contrary, the particle-plus-vibration states (4.5) can be obtained from Eq.(4.13) just setting all the $\{\mathcal{A}_i\}$ and all the $\{\mathcal{B}_i\}$ but one equal to zero. The normalization condition (4.14) implies the remaining coefficient $\mathcal{B}$ to be equal to 1, as well.

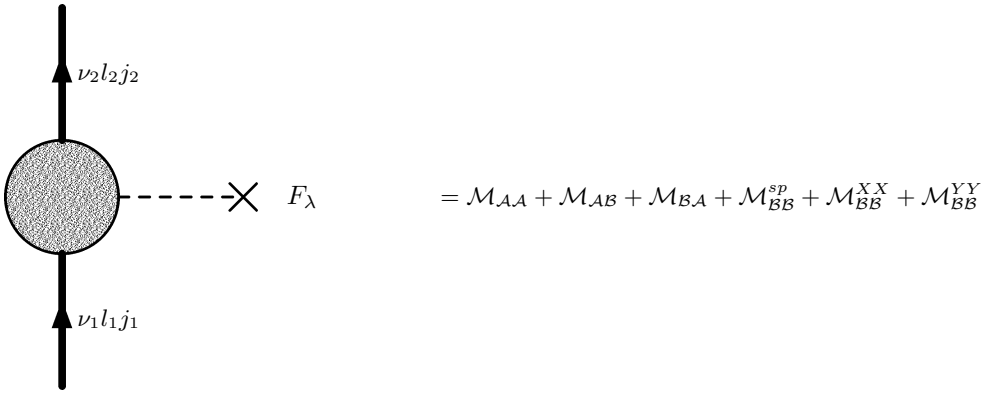

Figure 4.1
Feynman graph representation of the reduced transition matrix element, Eq.(4.20), as a sum of different contribution depicted in Figs. from (4.2) to (4.7).

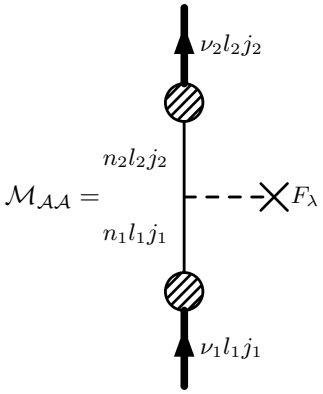

Figure 4.2
Feynman graph $\mathcal{G}_{\mathcal{AA}}$ corresponding to the $\mathcal{M}_{\mathcal{AA}}$ term (see Appendix B) of the reduced matrix element of the transition, Eq.(4.20). The corresponding process is the transition from a single-nucleon state to a single-nucleon state; in this case the external field F interacts only with the odd-nucleon modifying its single-particle state.

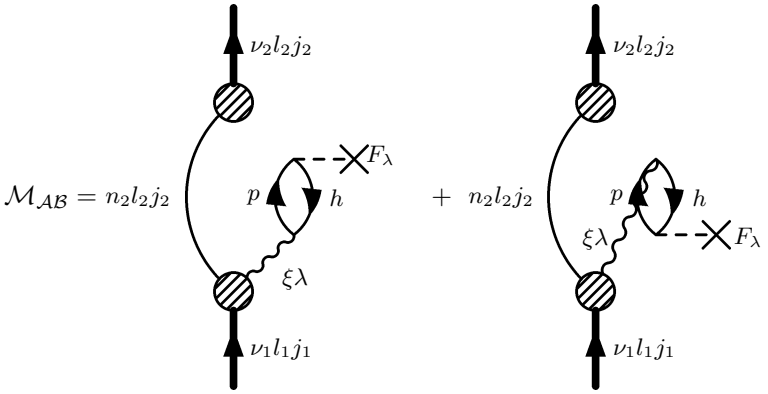

Figure 4.3
Feynman graph corresponding to the $\mathcal{M}_{\mathcal{AB}}$ term (see Appendix B) of the reduced matrix element of the transition, Eq.(4.20). The corresponding process is the transitions from a nucleon-plus-vibration state to a single-nucleon state; in this case the field F annihilates the vibration without affecting the odd-nucleon.

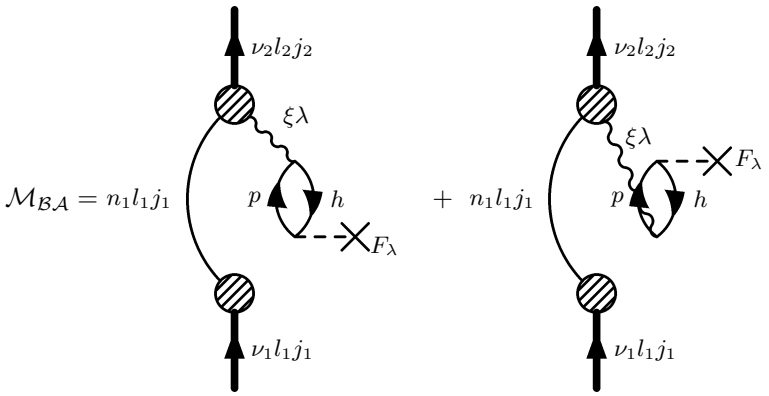

Figure 4.4
Feynman graph corresponding to the $\mathcal{M}_{\mathcal{BA}}$ term (see Appendix B) of the reduced matrix element of the transition, Eq.(4.20). The corresponding process is the transition from a single-nucleon state to a nucleon-plus-vibration state; the field F interacts with the core inducing a vibration without affecting the odd-nucleon.

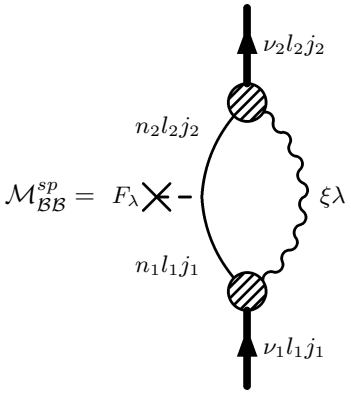

Figure 4.5
Feynman graph corresponding to the $\mathcal{M}^{sp}_{\mathcal{BB}}$ term (see Appendix B) of the reduced matrix element of the transition, Eq.(4.20). The corresponding process is the transition from a nucleon-plus-vibration state to a nucleon-plus-vibration state. In this case, the external field F interacts only with the odd-nucleon, leaving the core vibration untouched.

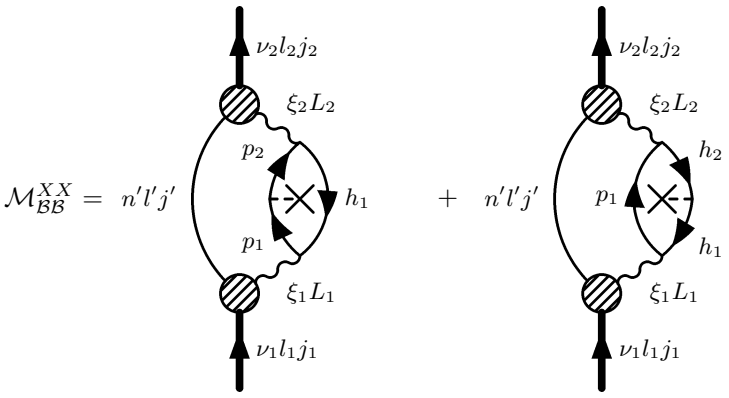

Figure 4.6
Feynman graph corresponding to the $\mathcal{M}^{XX}_{\mathcal{BA}}$ term (see Appendix B) of the reduced matrix element of the transition, Eq.(4.20). The corresponding process is the transition from a nucleon-plus-vibration state to a nucleon-plus-vibration state. In this case, the field F interacts with the vibration modifying the oscillatory mode.

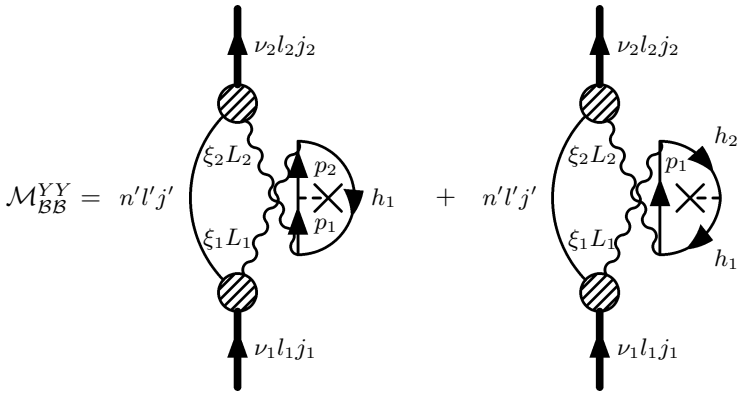

Figure 4.7
Feynman graph corresponding to the $\mathcal{M}^{YY}_{\mathcal{BA}}$ term (see Appendix B) of the reduced matrix element of the transition, Eq.(4.20). The corresponding process is the transition from a nucleon-plus-vibration state to a nucleon-plus-vibration state. In this case, the field F interacts with the vibration modifying the oscillatory mode.

In the zero-coupling case, one expects the ground state of the odd nucleus to be simply a pure single-nucleon state, $|gs\rangle = |(n_0 l_0 j_0 \otimes 0) l_0 j_0 m_0\rangle$, in which, in the case of particle-plus-core odd nuclei, the odd-particle is created in lowest possible energy level, whereas, in the case of hole-plus-core odd nuclei, the odd-hole is created in the highest possible energy level.

If we restrict to transitions from the ground state of the odd nucleus, we obtain two expressions for the reduced matrix element of the transition, depending on wheter the final pure state is single-nucleon or not. In the first case, from Eq.(4.20), if the final state is some $|f_1\rangle = |(n_f l_f j_f \otimes 0) l_f j_f m_f\rangle$, we obtain

$$\langle f_1||F_\lambda||gs\rangle = \langle (n_f l_f j_f \otimes 0) l_f j_f||F_\lambda||(n_0 l_0 j_0 \otimes 0) l_0 j_0\rangle \simeq \langle n_f l_f j_f||F_\lambda||n_0 l_0 j_0\rangle \tag{4.21}$$

and the corresponding reduced transition probability becomes

$$B(F_\lambda; gs \to f_1) = \frac{1}{2j_0+1}\langle f_1||F_\lambda||gs\rangle^2 \simeq \frac{1}{2j_0+1}|\langle n_f l_f j_f||F_\lambda||n_0 l_0 j_0\rangle|^2. \tag{4.22}$$

Instead, in the latter case, if the final state is some $|f_2\rangle = |(n'_f l'_f j'_f \otimes \xi L) l_f j_f m_f\rangle$, Eq.(4.20) implies that

$$\begin{aligned}\langle f_2||F_\lambda||gs\rangle &= \langle (n'_f l'_f j'_f \otimes \xi L) l_f j_f||F_\lambda||(n_0 l_0 j_0 \otimes 0) l_0 j_0\rangle \\ &\simeq \frac{\sqrt{2j_f+1}}{\sqrt{2\lambda+1}}\delta_{L\lambda}\delta_{0f'}\sum_{ph}\left\{X^{\xi\lambda}_{ph} + Y^{\xi\lambda}_{ph}\right\}\langle p||F_\lambda||h\rangle \\ &= \frac{\sqrt{2j_f+1}}{\sqrt{2\lambda+1}}\delta_{L\lambda}\delta_{0f'}\langle \xi\lambda||F_\lambda||RPA_{core}\rangle.\end{aligned} \tag{4.23}$$

The previous equation implies that we can restrict to states $|f_2\rangle = |(n_0 l_0 j_0 \otimes \xi\lambda) l_f j_f m_f\rangle$. The corresponding reduced transition probability is, in this case,

$$B(F_\lambda; gs \to f_2) \simeq \frac{2j_f+1}{(2j_0+1)(2\lambda+1)}|\langle \xi\lambda||F_\lambda||RPA_{core}\rangle|^2. \tag{4.24}$$

The total strength function associated with the transitions from the ground state of the odd nucleus is thus

$$\begin{aligned}S(E) \simeq &\sum_{n_f l_f j_f}\frac{1}{2j_0+1}|\langle n_f l_f j_f||F_\lambda||n_0 l_0 j_0\rangle|^2\delta(E-\epsilon_{f0}) \\ &+\sum_{j_f \xi}\frac{2j_f+1}{(2j_0+1)(2\lambda+1)}|\langle \xi\lambda||F_\lambda||RPA_{core}\rangle|^2\delta(E-\Omega_{\xi\lambda})\end{aligned} \tag{4.25}$$

where $\epsilon_{f0} = \epsilon_{n_f l_f j_f} - \epsilon_{n_0 l_0 j_0}$ and $\Omega_{\xi\lambda}$ is the energy of the ξ-th phonon of multipolarity λ.

Now, since $j_f = |j_0 - \lambda|, |j_0 - \lambda| + 1, \ldots, j_0 + \lambda$,

- if $j_0 > \lambda$,

$$\sum_{j_f}(2j_f+1) = 2(\sum_{j_f} j_f) + (2\lambda+1) = 2\frac{j_0 - \lambda + j_0 + \lambda}{2}(2\lambda+1) + (2\lambda+1) = (2\lambda+1)(2j_0+1) \tag{4.26}$$

- if $\lambda > j_0$,

$$\sum_{j_f}(2j_f+1) = 2(\sum_{j_f} j_f) + (2j_0+1) = 2\frac{\lambda - j_0 + \lambda + j_0}{2}(2j_0+1) + (2j_0+1) = (2\lambda+1)(2j_0+1) \tag{4.27}$$

and so Eq.(4.25) reduces to

$$S(E) \simeq \sum_{n_f l_f j_f} \frac{1}{2j_0+1} |\langle n_f l_f j_f || F_\lambda || n_0 l_0 j_0 \rangle|^2 \delta(E - \epsilon_{f0}) + \sum_{\xi} |\langle \xi\lambda || F_\lambda || RPA_{core} \rangle|^2 \delta(E - \Omega_{\xi\lambda}). \tag{4.28}$$

The meaning of this result is clear: in the zero-coupling limit, the excited states of the odd nucleus can be seen either as single-particle excitation of the odd-particle (or hole) or as collective excitations of the core; thus the resulting strength function must be simply the sum between the strength function associated with the single-particle excitations and the strength function associated with core transitions.

4.4 A many-body argument for the state mixing

Until now, we have introduced the interaction between the odd-nucleon and the core and its global effect on the system, but we have not specified yet its characteristics, which are, although, fundamental to obtain the correct values for the coefficients $\{\mathcal{A}_i\}$ and $\{\mathcal{B}_i\}$ of the superposition (4.13). In this Section, we will implement a many-body argument [LR06] to derive an alternative formulation of particle-vibration coupling theory. In such framework, we will derive, from a rigorous point of view, the coefficients $\{\mathcal{A}_i\}$ and $\{\mathcal{B}_i\}$ of the mixing between pure states of odd nuclei.

In the many-body theory, one defines the single-particle exact *Green's function* as

$$G_{\alpha\beta} = -i\langle 0 | T\{a_\alpha a_\beta^\dagger\} | 0 \rangle, \tag{4.29}$$

which describes the propagation of one particle in a nucleus with exact ground state $|0\rangle$. In Eq. (4.29), T is the time ordering operator and the indexes α,β, specifying single-particle creation and annihilation operators, include space, spin and time coordinates.

The equation of the one-nucleon motion, in the language of Green's functions, takes the form

$$[\omega - K - \Sigma(\omega)]G(\omega) = 1 \tag{4.30}$$

where $G(\omega)$ is the Fourier-transformed Green's function, K is the kinetic energy and $\Sigma(\omega)$ is the *self-energy*, also called *mass operator*. In general, the mass operator Σ can be written as the sum of an energy-independent and of an energy-dependent term,

$$\Sigma(\omega) = \Sigma^0 + \Sigma^e(\omega) \tag{4.31}$$

where the index e indicates the energy dependence. Eq.(4.30) takes now the form

$$[\omega - h - \Sigma^e(\omega)]G(\omega) = 1 \tag{4.32}$$

where h denotes now the single-particle Hamiltonian with an energy independent mean field, $h = K + \Sigma^0$, which can be described very well in mean-field theories, such as Hartree-Fock theory.

We introduce now the Hartree-Fock basis, $\{|\psi_k\rangle\}$, which diagonalizes the energy-independent hamiltonian h,

$$h|\psi_k\rangle = \epsilon_k|\psi_k\rangle \tag{4.33}$$

where $|\psi_k\rangle$ is characterized by the set of quantum numbers $k = \{t_k, n_k, j_k, l_k, m_k\}$ if we work with spherical symmetry. In this basis one can rewrite Eq.(4.32) as follows:

$$\sum_l \big[(\omega - \epsilon_k)\delta_{kl} - \Sigma^e_{kl}(\omega)\big] G_{lk'}(\omega) = \delta_{kk'} \tag{4.34}$$

where the letters k,k',l denote full sets of the spherical quantum numbers mentioned above.

In the next step we represent the exact single-particle Green's function entering Eq.(4.32) in the Lehmann expansion, which has the form

$$G_{kl}(\omega) = \sum_h \frac{\chi^{h0}_k \chi^{h0*}_l}{\omega - \epsilon_h - i\eta} + \sum_p \frac{\chi^{0p}_k \chi^{0p*}_l}{\omega - \epsilon_p + i\eta} \tag{4.35}$$

where $\eta \to 0^+$ and the matrix elements are defined as

$$\chi^{h0}_k = \langle N-1|a^\dagger_k|0\rangle, \tag{4.36}$$

$$\chi^{0p}_k = \langle 0|a^\dagger_k|N+1\rangle. \tag{4.37}$$

Here, $|0\rangle$ denotes the ground state of the subsystem of N particles in the even-even nucleus, whereas the states $|N-1\rangle$ and $|N+1\rangle$ correspond to the ground state and to excited states of the subsystems of $(N-1)$ and $(N+1)$ particles, respectively.

The most important origin in the energy dependence of Σ^e is given by the coupling to collective vibrations. In this framework, we can write Σ^e as a convolution of the particle-phonon coupling amplitude Γ and the exact single-particle Green's function:

$$\Sigma^e_{kl}(\omega) = \sum_{k'l'} \int_{-\infty}^{+\infty} \frac{d\omega'}{2\pi i} \Gamma_{kl'lk'}(\omega') G_{k'l'}(\omega + \omega'), \tag{4.38}$$

where the amplitude Γ has the following spectral expansion:

$$\Gamma_{kl'lk'}(\omega) = -\sum_\mu \left(\frac{\gamma^{\mu*}_{k'k}\gamma^\mu_{l'l}}{\omega - \Omega_\mu + i\eta} - \frac{\gamma^\mu_{kk'}\gamma^{\mu*}_{ll'}}{\omega + \Omega_\mu - i\eta} \right) \tag{4.39}$$

in terms of the phonon frequencies Ω_μ and of the phonon verteces γ^μ. The latter are determined by the relation

$$\gamma^\mu_{kl} = \langle k|\gamma^\mu|l\rangle = \sum_{k'l'} V_{kl'lk'} \delta\rho^\mu_{k'l'}, \tag{4.40}$$

where $V_{kl'lk'}$ denotes the matrix element of the residual interaction and $\delta\rho$ is the transition density. To a first degree of approximation, it is possible to assume that the coupling involves only unperturbed phonons. This implies that one can substitute, in Eq.(4.38), the exact Green's function G with the mean field Green's function, defined as $G^0(\omega) = (\omega - h)^{-1}$. Since the mean field Green's function is

$$G^0_{kl}(\omega) = \frac{\delta_{kl}}{\omega - \epsilon_k + i\sigma_k\eta}, \tag{4.41}$$

where $\sigma_k = +1$ if k is a particle state and $\sigma_k = -1$ if k is a hole state, the mass operator Σ^e takes the form:

$$\Sigma^e_{kl}(\omega) = \frac{\delta_{j_k j_l}\delta_{l_k l_l}}{2j_k + 1} \sum_{\mu,n} \frac{\langle k||\gamma^{\mu(\sigma_n)}||n\rangle \langle l||\gamma^{\mu(\sigma_n)}||n\rangle^*}{\omega - \epsilon_n - \sigma_n(\Omega_\mu - i\eta)}. \tag{4.42}$$

Here, we have used the notation

$$\langle k||\gamma^{\mu(\sigma_n)}||n\rangle = \delta_{\sigma_n,+1}\langle k||\gamma^\mu||n\rangle + \delta_{\sigma_n,-1}\langle n||\gamma^\mu||k\rangle^*. \tag{4.43}$$

As it was shown in [RW73], it is justified to use the diagonal approximation,

$$\Sigma^e_{kl}(\omega) = \delta_{kl}\Sigma^e_k(\omega) \tag{4.44}$$

with

$$\Sigma^e_k(\omega) = \frac{1}{2j_k+1}\sum_{\mu,n}\frac{|\langle k||\gamma^{\mu(\sigma_n)}||n\rangle|^2}{\omega-\epsilon_n-\sigma_n(\Omega_\mu - i\eta)}. \tag{4.45}$$

Thus, within the diagonal approximation of the mass operator, the exact Green's function G is also diagonal in the single-particle basis $\{|\psi_k\rangle\}$ and the Dyson equation forms, for each k, a nonlinear eigenvalue equation

$$[\omega - \epsilon_k - \Sigma^e_k(\omega)]G_k(\epsilon) = 1. \tag{4.46}$$

The poles of the Green's function $G_k(\omega)$ correspond to the zeros of the function

$$f(\omega) = \omega - \epsilon_k - \Sigma^e_k(\omega). \tag{4.47}$$

For each quantum number k there exist several solutions $\epsilon^{(\lambda)}_k$ characterized by the index λ. This means that, because of the coupling to the collective vibrations, the single-particle state k is fragmented. In the vicinity of the pole $\epsilon^{(\lambda)}_k$, the Green's function can be represented as follows:

$$G^{(\lambda)}_k(\omega) \simeq \frac{S^{(\lambda)}_k}{\omega - \epsilon^{(\lambda)}_k + i\sigma_k\eta}, \tag{4.48}$$

where the residuum, or *spectroscopic factor*, $S^{(\lambda)}_k$ has the meaning of the single-particle (hole) strength of the state λ with single-particle quantum numbers k. Differentiation of Eq.(4.46) with respect to ω provides the expression for the residuum:

$$S^{(\lambda)}_k = \left(1 - \frac{d\Sigma^e_k(\omega)}{d\omega}\bigg|_{\omega=\epsilon^{(\lambda)}_k}\right)^{-1}. \tag{4.49}$$

There are several ways to solve Eq.(4.46). Here we employ the method used in [RW73]: since the mass operator of the form (4.42) has a simple-pole structure, it is convenient to reduce Eq.(4.46) to a diagonalization problem of the following matrix:

$$\begin{pmatrix} \epsilon_k & \eta^\mu_{kn_1} & \eta^\mu_{kn_2} & \cdots \\ \eta^{\mu*}_{kn_1} & \sigma_{n_1}\Omega_\mu + \epsilon_{n_1} & 0 & 0 \\ \eta^{\mu*}_{kn_2} & 0 & \sigma_{n_2}\Omega_\mu + \epsilon_{n_2} & 0 \\ \vdots & 0 & 0 & \ddots \end{pmatrix} \tag{4.50}$$

where

$$\eta^\mu_{kn_i} = \frac{\langle k||\gamma^{\mu(\sigma_{n_i})}||n_i\rangle}{\sqrt{2j_k+1}}. \tag{4.51}$$

The eigenvalues of the matrix (4.50) are the desired poles $\epsilon^{(\lambda)}_k$ of the exact Green's function.

The many body argument just exposed allows a deep understanding of the exact single-particle Green's function, which differs from the mean field Green's function because of the coupling between single-particles and phonons due to the effect of residual interaction.

The analogies of this situation with the general properties of our OPVC model are evident: the underlying idea is that, in the odd nucleus, the vibrations in the even-even core interact, i.e., couple, to single-particle degrees of freedom of the odd-nucleon, modifying both the core collective and the single-particle properties. The complete solution of the problem, in odd nuclei, would come from a suitable generalization of the matrix (4.50) which is able to predict, after diagonalization, all

the properties of the odd nucleus eigenstates (4.13). The generalization we propose is the following

$$\begin{pmatrix} \epsilon_{k_1} & 0 & 0 & \eta^{\mu_1}_{k_1 n_1} & \eta^{\mu_2}_{k_1 n_2} & \cdots \\ 0 & \epsilon_{k_2} & 0 & \eta^{\mu_1}_{k_2 n_1} & \eta^{\mu_2}_{k_2 n_2} & \cdots \\ 0 & 0 & \ddots & \cdots & \cdots & \cdots \\ \eta^{\mu_1 *}_{k_1 n_1} & \eta^{\mu_1 *}_{k_2 n_1} & \vdots & \sigma_{n_1}\Omega_{\mu_1} + \epsilon_{n_1} & 0 & 0 \\ \eta^{\mu_2 *}_{k_1 n_2} & \eta^{\mu_2 *}_{k_2 n_2} & \vdots & 0 & \sigma_{n_2}\Omega_{\mu_2} + \epsilon_{n_2} & 0 \\ \vdots & \vdots & \vdots & 0 & 0 & \ddots \end{pmatrix}_{J^\pi} . \tag{4.52}$$

Since we set at zero-energy the vibration-free configuration of the even-even core, the energy of the odd nucleus pure states (4.4) will simply coincide with the single-particle energy of the odd-nucleon, whereas, in the case of the pure states (4.5) it will coincide with the sum of the odd-nucleon energy plus the phonon vibrational energy. In the matrix (4.52), thus, on the principal diagonal we find the energies of the pure states from which the odd nucleus dressed state originates after the mixing. We note that all the involved states must be coupled to the same angular momentum and parity, J^π. ϵ_{k_i} represents the energy of the i-th pure single-nucleon state entering the mix, while $\sigma_{n_i}\Omega_{\mu_i} + \epsilon_{n_i}$ represents the energy of the i-th pure nucleon-plus-vibration state. It is important to notice that, since the odd-nucleon, for a fixed odd nucleus, is always a particle or a hole, ϵ must be a single-particle or single-hole energy throught the all matrix (4.52). Off diagonal we find the residual interaction between pure states (4.4) and (4.5), which we suppose can be well-accounted for by expression (4.51). The assumption we make is that the interaction between pure states of the same type is negligible.

A full diagonalization of the matrix (4.52) allows us a complete insight into the mixed states (4.13) of the odd nucleus in the OPVC model. In fact, each eigenvector will be one of the final mixed states: the corresponding eigenvalue will be the energy of that state, whereas its coordinates will represent its amplitude on each pure state, i.e., its coefficients $\{\mathcal{A}_i\}$ and $\{\mathcal{B}_i\}$.

All the terms entering the OPVC matrix (4.52) can be evaluated by means of microscopic nuclear structure theories exposed in the previous Chapters. In particular, single-particle energies can be obtained with self-consistent Skyrme-Hartree-Fock calculations, while the phonon frequencies can be calculated in RPA approximation set up on the even-even closed-shell core. At last, the residual interaction coupling particles and phonons can be accounted for as the second derivative of the Skyrme energy functional (see Section 3.3.2). This represents a great element of novelty with respect to the classical formulation of particle-vibration coupling matrix which employed macroscopic PVC vertex and energies.

Chapter 5

Numerical results for the dipole response in ^{67}Ni and ^{69}Ni

In this Chapter, the OPVC model described in Chapter 4 will be applied to the calculation of the collective dipole response in two odd-mass neutron-rich nuclei, ^{67}Ni and ^{69}Ni. They are obtained by adding a hole and a particle, respectively, to the closed-shell core ^{68}Ni.

The interest in these two nuclei lies in some recent Coulomb-excitation experiments which provided experimental data about the features of the pygmy dipole resonance in ^{68}Ni and neighboring nuclei [W$^+$09]. In these experiments, the γ decay from Coulomb-excitation of ^{68}Ni at 600 MeV/nucleon on a Au target was measured using the RISING setup at the fragment separator of GSI (Darmstadt). The ^{68}Ni beam was produced by a fragmentation reaction of ^{86}Kr at 900 MeV/nucleon on a ^{9}Be target and selected by a fragment separator. The γ rays produced at the Au target were measured with HPGe detectors at forward angles and with BaF_2 scintillators at backward angles. In Fig. 5.1(a) the selected fragments are shown in an A/Q versus Z plot, being Q the charge of the fragment (which can differ from Z for incomplete-stripping reactions). The measured spectra, in the case of ^{68}Ni, show a peak centered at approximately 11 MeV, whose intensity can be explained in terms of an enhanced strength of the dipole response function in the low-energy region (Fig. 5.1(b)).

A preliminary analysis of the recorded experimental data has claimed the pygmy dipole centroid in ^{67}Ni to be at least 1 MeV lower than the centroid of the neighboring ^{68}Ni. A similar result was obtained in [K$^+$07] for the doubly-magic closed-shell nucleus ^{132}Sn and its neighboring hole-plus-core odd nucleus, ^{131}Sn, using a similar experimental setup. In Fig. 5.1(c) we report the dipole strength distribution in the low-energy region for the two nuclei. It is evident, from this figure, a down-shift of about 1-2 MeV of the response of ^{131}Sn with respect to that of ^{132}Sn.

It is then of great importance to provide a theoretical model able to predict and interpret experimental data on the pygmy dipole resonance in odd-mass nuclei, such as this experimentally observed shift in the centroid of neighboring nuclei. The interest is also associated with testing the model predictions for the collective or non-collective character of this resonance. In fact, the PDR can be be used as a constraint to the parameters of the equation of state of nuclear matter (see Chapter 2) only if it displays a certain degree of collectivity.

5.1 Equal filling approximation

The numerical analysis of odd nuclei is particularly complicated since the presence of the odd-particle (or hole) breaks the time-reversal and spherical symmetry of the even-even (closed-shell) core. This is particularly relevant since the Skyrme-Hartree-Fock equations, Eq.(3.16), are valid only in presence of time-reversal symmetry, and their radial equivalent, Eq.(3.19), can be used only

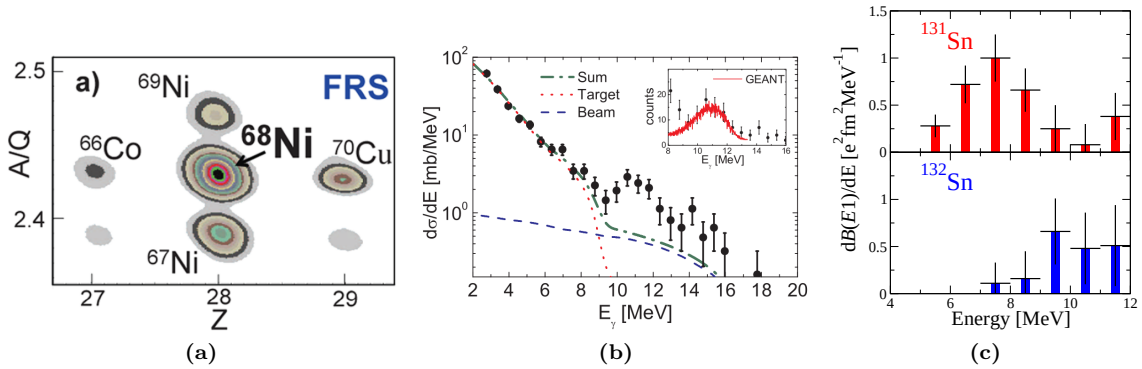

Figure 5.1
In panel (a), the fragments coming from a fragmentation reaction of ^{86}Kr at 900 MeV/nucleon on a ^{9}Be target are shown in a A/Q versus Z plot [W^{+}09]. In panel (b), the high-energy γ-ray spectrum measured with BaF_2 detectors and Doppler corrected with the velocity of the projectile. The lines are a statistical model calculations for the target (dotted line) and for the beam (dashed line) nuclei. In the inset, the continuus line superimposed to the measured data is the result of a GEANT simulation for γ-transitions at 11 MeV [W^{+}09]. In panel (c), the dipole strength distribution in the low-energy region for ^{131}Sn and ^{132}Sn [K^{+}07].

in case of spherical symmetry. Besides, our OPVC, described in Chapter 4, requests the system to be time-reversal and spherically symmetric, too.

To keep time reversal symmetry when dealing with odd-mass nuclei one is forced to adopt phenomenological approaches in which the unpaired nucleon is treated in an equal footing with its time-reversed companion. From a practical point of view, this phenomenological approach amounts to look at the unpaired nucleon as distributed, with equal probability, in a given orbital and in the time-reversed partner. In the case of preserving spherical symmetry, where the orbitals have the $2j+1$ degeneracy the unpaired nucleon is distributed among all possible angular momentum projections $m = -j, \ldots, j$ with equal probability $1/(2j+1)$. The above procedure is usually referred in the literature as the equal (or uniform) filling approximation (EFA) and has been used quite often in the description of odd nuclei at the mean-field level and with different interactions (e.g. [BQM07, BCH06]). This intuitive and reasonable procedure has recently been justified in terms of standard argument of quantum statistical mechanics [PR08].

In the following, we will widely use the EFA and the implications of the use of this approximation will be underlined.

5.2 Skyrme-Hartree-Fock calculation

We solve the radial Skyrme-Hartree-Fock equations in coordinate space for ^{67}Ni and ^{69}Ni, Eq.(3.19). We are allowed to do this since the EFA grants time-reversal and spherical symmetry. This gives us access to the wave functions and energies of all the single-particle states below the Fermi surface in the two nuclei. Once obtained the single-particle occupied states, the unoccupied states are then calculated too by using the resulting mean field. This is done discretizing the continuum by using box boundary conditions. The radial mesh extends up to 15 fm, i.e., $\simeq 3$ times the nuclear radius (given by $R = 1.2A^{1/3}\text{fm} \simeq 4.9\text{fm}$), whereas the radial step equals 0.1 fm. We employ two different Skyrme interactions, SkI3 and SLy5.

SkI3 [RF95] is one of the Skyrme interactions which better mimic the relativistic mean field (RMF) calculations. It was originally derived to provide a good explanation of the isotope shifts in the charge radius in Pb isotopes, which previous Skyrme interactions failed to predict. On the contrary, these shifts were correctly reproduced in standard RMF calculation. In [RF95] the reason for this different behavior was found in the different density dependence of the spin-orbit potential. A new family of spin-orbit-modified interaction, to which SkI3 belongs, was then proposed to reproduce RMF-like calculation in the Skyrme framework. The effective mass associated with

SkI3 interaction is m^*/m=0.58, whereas the value of the slope L of the symmetry energy at the saturation density is L=100.5 MeV.

SLy5 [C$^+$98] is a modern Skyrme interaction widely used for the description of exotic nuclei, i.e., nuclei far from the stability line. Its parameters have been fitted in order to reproduce the properties of pure neutron matter, such as its saturation point ρ_0, the incompressibility K_∞ and the simmetry energy at the saturation density $E_{\rm sym}(\rho_0)$. Besides, a good reproduction of the binding energies of doubly-magic nuclei (^{16}O, ^{40,48}Ca, ^{56}Ni, ^{132}Sn and ^{208}Pb) as well as their r.m.s. radii was requested. The effective mass associated with SLy5 interaction is m^*/m=0.70, whereas L=48.3 MeV.

The results are shown in Fig. 5.2 for SkI3 interaction; for SLy5 interaction we find the same level ordering and a compatible level spacing. In this pictorial representation, full dots stand for occupied single-particle states. As we can see from the picture, the odd-hole in the ground state of ^{67}Ni lies in the $2p_{1/2}$ orbital, whereas the odd-particle in ^{69}Ni lies in the $1g_{9/2}$ orbital.

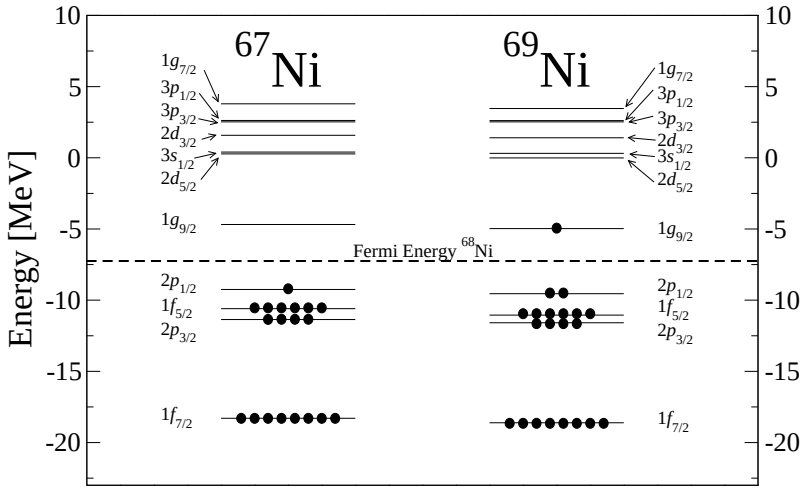

Figure 5.2
Results for single-particle levels in ^{67}Ni and ^{69}Ni obtained as solution of Skyrme-Hartree-Fock equations with SkI3 interaction. In the picture, full dots stand for occupied single-particle states.

5.3 RPA calculation for the even-even core

General aspects of the calculation

The single-particle levels calculated in the SHF approximation are then employed to build a basis of particle-hole configurations for dipole excitations, which can be used to solve RPA equations in their matrix formulation, Eq.(3.52). This allows us to obtain the complete isovector dipole vibrational spectrum of the core. Consistently with Chapter 4, the RPA response of the core is calculated supposing the odd-particle (hole) to be in the lowest (highest) possible energy level. In order to get the correct isovector dipole response, the modified dipole operator (2.8) is used. The maximum energy of the unoccupied single-particle states included in the RPA model space is set at 70 MeV, which equals approximately 10 shells over the Fermi surface. This parameter, together with the dimension of the radial mesh, has been chosen carefully so that the results of the excitation spectrum are stable enough, i.e., the total calculated EWSR does not change appreciably increasing the dimension of the box or the energy cutoff. We should also mention that, for self-consistency, the complete residual interaction has been accounted for as the second derivative of the Skyrme energy functional (see Section 3.3.2).

RPA-EFA equations for the core response

The introduction of the EFA directly affects the results for the RPA response of the even-even core introducing, in principle, important differences with respect to the response of ^{68}Ni alone. In fact, the presence of the odd-nucleon will modify the RPA response of the core, since, in the case of particle-plus-core nuclei, the odd level will be partially-occupied and so only partially accessible to particle states, whereas, in the case of hole-plus-core nuclei, the odd level will be partially-empty and so only partially accessible to hole states. We take care of this problems using, instead of RPA matrices, Eqs.(3.53) and (3.54), the QRPA matrices, Eqs.(3.69) and (3.70), in the zero-pairing limit. We refer to the consequently modified RPA equations as RPA-EFA equations.

Let us consider first the general case of a particle-plus-core nucleus. The probabilities of finding a single-particle state i occupied (v_i^2) or unoccupied (u_i^2) below the Fermi surface of the even-even core are, respectively, 1 and 0. In case of a single-particle state m above the Fermi surface, the probabilities are $v_m^2 = 0$ and $u_m^2 = 1$ unless the orbital m is the one in which the odd-particle lies, say p. In this case $u_m^2 = 2j_p/(2j_p+1)$ and $v_m^2 = 1/(2j_p+1)$ because of the EFA. The QRPA matrices A and B in the zero pairing limit then become

$$A_{minj} = \delta_{mn}\delta_{ij}(\epsilon_m - \epsilon_i) + \begin{cases} \overline{v}_{mjin} & \text{if} \quad m \neq p, n \neq p \\ \sqrt{\frac{2j_p}{2j_p+1}}\overline{v}_{mjin} & \text{if} \quad m = p, n \neq p \quad \text{or} \quad m \neq p, n = p \\ \frac{2j_p}{2j_p+1}\overline{v}_{mjin} & \text{if} \quad m = p, n = p \end{cases} \tag{5.1}$$

$$B_{minj} = \begin{cases} \overline{v}_{mnij} & \text{if} \quad m \neq p, n \neq p \\ \sqrt{\frac{2j_p}{2j_p+1}}\overline{v}_{mnij} & \text{if} \quad m = p, n \neq p \quad \text{or} \quad m \neq p, n = p \\ \frac{2j_p}{2j_p+1}\overline{v}_{mnij} & \text{if} \quad m = p, n = p \end{cases} \tag{5.2}$$

Consider now the case of an hole-plus-core odd nucleus. The probabilities of finding a single-particle state m occupied (v_m^2) or unoccupied (u_m^2) above the Fermi surface of the even-even core are, respectively, 0 and 1. In case of a single-particle state i below the Fermi surface, the probabilities are $v_i^2 = 1$ and $u_i^2 = 0$ unless the orbital i is the one in which the odd-hole lies, say h. In this case $v_i^2 = 2j_h/(2j_h+1)$ and $u_i^2 = 1/(2j_h+1)$ because of the EFA. The matrices A and B now become

$$A_{minj} = \delta_{mn}\delta_{ij}(\epsilon_m - \epsilon_i) + \begin{cases} \overline{v}_{mjin} & \text{if} \quad i \neq h, j \neq h \\ \sqrt{\frac{2j_h}{2j_h+1}}\overline{v}_{mjin} & \text{if} \quad i = h, j \neq h \quad \text{or} \quad i \neq h, j = h \\ \frac{2j_h}{2j_h+1}\overline{v}_{mjin} & \text{if} \quad i = h, j = h \end{cases} \tag{5.3}$$

$$B_{minj} = \begin{cases} \overline{v}_{mnij} & \text{if} \quad i \neq h, j \neq h \\ \sqrt{\frac{2j_h}{2j_h+1}}\overline{v}_{mnij} & \text{if} \quad i = h, j \neq h \quad \text{or} \quad i \neq h, j = h \\ \frac{2j_h}{2j_h+1}\overline{v}_{mnij} & \text{if} \quad i = h, j = h \end{cases} \tag{5.4}$$

These new matrices are referred to as RPA-EFA matrices.

Influence of the EFA on the core RPA results

In Fig. 5.3 we plot, with black continuus and red dashed lines, the RPA response of the core, respectively, with the use of RPA and RPA-EFA equations. This is done for the two nuclei under investigation, ^{69}Ni and ^{67}Ni, and for the two Skyrme interactions, SkI3 and SLy5. The remaining plots in the figure will be explained in the following.

As we can see from the figure, SkI3 interaction produces, in the RPA response of ^{68}Ni, a sharp peak increase in the dipole strength at low energy, well distinguished from the giant dipole resonance and its tail. The centroid of this resonance is found at about 10.5 MeV, in quantitative agreement with the recent experimental findings [W$^+$09]. On the contrary, the RPA response produced by the standard SLy5 interaction does not produce such an evident peak, but two bumps, the bigger centered at approximately 9.4 and the other at 10.5 MeV, which cannot be well distinguished from the tail of the GDR. Although its magnitude varies with the model, all interactions predict a low energy bump: the smaller is the effective mass, the closer the peak in the PDR region appear to the giant dipole one. In addition, the larger the value of L, the higher the PDR peaks appears, in qualitative agreement with [C$^+$10]. This fact is quite interesting because it suggests that the collectivity of the PDR is not supported by all models, but depend on the effective interaction employed.

The units of the strength functions represented in Fig. 5.3 is $[e^2\text{fm}^2\text{MeV}^{-1}]$ since we averaged the original RPA calculation with a 1 MeV width Lorentzian function. In fact, the total width for a collective mode, Γ, can be written as the sum of four terms (see Section 2.2). The first is the Landau width $\Delta\Gamma$, which can be accounted for by any type of RPA calculation. The $\Gamma^{\uparrow}$ and Γ_{γ} widths, instead, can be accounted for only by continuum RPA calculations, i.e., considering exactly the continuum over the Fermi surface without introducing discretizing box boundary condition. This is, though, a feature that our discrete calculation cannot provide. The last contribution comes from the spreading width $\Gamma^{\downarrow}$ which no RPA calculation is able to reproduce. Consequently, since our calculation is able to predict only a small part of the total width, we find useful to provide an artificial smoothing capable of reproducing a width closer to experimental findings.

As we can see from Fig. 5.3, the RPA-EFA strength is energetically up-shifted both in the case of ^{67}Ni and ^{69}Ni in the pygmy dipole resonance region ($\equiv$ 9-13 MeV of excitation energy). For simplicity we restrict our considerations to SkI3 interaction, for which the shift is $\simeq$ 150 keV in the case of ^{69}Ni and $\simeq$ 100 keV in the case of ^{67}Ni. In the case of SLy5, in fact, similar considerations may be held.

The reason for such shift can be qualitatively accounted for referring to the effect of residual interaction on single-particle states. We consider the neutron particle-hole pairs that contribute mostly to the PDR of the even-even core, that is, the pairs whose excitation energy is in the energy range of the PDR. Their excitation energies are listed in Tab. 5.1 together with the relative contribution of each pair to the total reduced transition probability of the PDR. The weighted energy of these particle-hole pairs equals 12.5 MeV; this means that, being the centroid of the pygmy dipole at about 10.5 MeV, the residual interaction down-shifts globally the single-particle excitation spectrum of 2 MeV. As one can notice, the residual interaction turns out to be attractive for the pygmy dipole resonance, in opposition to the case of the giant dipole resonance, which is up-shifted with respect to the unperturbed response.

single-particle transition	Energy	Weight
$2p_{1/2} \rightarrow 2d_{3/2}$	10.8 MeV	28.2%
$2p_{3/2} \rightarrow 2d_{5/2}$	11.4 MeV	11.7%
$2p_{3/2} \rightarrow 3s_{1/2}$	11.8 MeV	4.1%
$1f_{5/2} \rightarrow 2d_{3/2}$	12.3 MeV	3.5%
$1f_{7/2} \rightarrow 1g_{9/2}$	13.7 MeV	45.8%
$1f_{5/2} \rightarrow 1g_{7/2}$	14.4 MeV	6.5%

Table 5.1
For each particle-hole excitation contributing mostly to the PDR in ^{68}Ni even-even core, the energy and the relative contribution of each pair to the total reduced probability of the PDR are listed. The latter is evaluated via Eq.(3.61). The weighted energy of these particle-hole pairs equals 12.5 MeV.

Let us consider, first, the case of ^{69}Ni. In this case, the total contribution of the residual interaction in less than in the case of ^{68}Ni because of the EFA involving the $1g_{9/2}$ orbital. This means that, since the residual interaction is attractive, the spectrum of the even-even core of ^{69}Ni

will be up-shifted with respect to that of ^{68}Ni. The shift we expect is of the order of 1/10 (the part of the residual interaction we lose because of the EFA) times 45.8 % (the weight of the interested particle-hole pair) times 2 MeV. The result is approximately 100 keV, which, in such a qualitative argument, is compatible with the calculated value of 150 keV.

Consider now the case of ^{67}Ni. We expect again an up-shift, this time of the order of 1/2 times 28.2% times 2 MeV. The result is approximately 300 keV, higher but still of the order of the calculated value of 100 keV.

5.4 Calculation of the dipole response in ^{67}Ni and ^{69}Ni in the zero-coupling limit

General features of the zero-coupling limit results

We now calculate the spectrum of dipole excitations in ^{67}Ni and ^{69}Ni in the zero-coupling limit, Eq.(4.28). The core term in evaluated in RPA-EFA approximation (as in the previous Section), whereas the single-particle contribution is evaluated by means of Eq.(A.58) by using the single-particle states calculated within the SHF approximation. In Eq.(4.28), in the case of ^{69}Ni, the $n_0l_0j_0$ state is the particle state $1g_{9/2}$, whereas the $n_fl_fj_f$ states are all those particle states which fulfill selection rules of parity and angular momentum for 1^- excitations from $1g_{9/2}$, i.e., single-particle states with $J^\pi = \{\frac{7}{2}^-, \frac{9}{2}^-, \frac{11}{2}^-\}$. In the case of ^{67}Ni, $n_0l_0j_0$ is the hole state in $2p_{1/2}$ and the $n_fl_fj_f$ states are all those hole states allowed by selection rules, i.e., single-particle states with $J^\pi = \{\frac{1}{2}^+, \frac{3}{2}^+\}$.

The results for the complete dipole response in the uncoupled model are represented in Fig. 5.3 for ^{69}Ni and ^{67}Ni and for SkI3 and SLy5 interactions. The dashed-dotted green lines represent the strength function for the two odd nuclei in the zero-coupling limit, whereas the blue bars represent the single-particle contribution. The latter is measured is [e^2fm^2] since, for the sake of clarity, we do not provide here an articial width for single-particle excitations.

As we can see from Fig. 5.3, in the uncoupled dipole response of ^{69}Ni we observe an energy shift and a clear increase in the total strenght in the PDR region. The reason for the increment in the pygmy dipole region is that the single-particle excitations from $1g_{9/2}$ are intense and mainly located in that energy range. In the case of ^{67}Ni, the dipole response does not differ very much from that of ^{68}Ni, except for the shift in the PDR region and for a little decrease in intensity in the region on the PDR and of the IVGDR (mainly due to the EFA). The single-particle excitations do not contribute very much since their strength is small and they are located in the tail of the IVGDR. In the zero-coupling limit, as one can imagine, the collective dipole response of the analyzed odd nuclei, and in particular their strength function, do not show substantial modifications with respect to the same properties of closed-shell neighboring even-even nuclei. The main source of modification turns out to be the introduction of the equal filling approximation induced by the odd-nucleon, which causes an energy shift of the order of 150 keV and 100 keV, respectively, in the case of ^{69}Ni and ^{67}Ni both for the two Skyrme interactions under investigation. The contribution of the single-particle transitions, instead, appears to be almost negligible, expecially in the case of ^{67}Ni.

The visible single-particle excitations in Fig. 5.3 can be easily identified. In fact, in the case of ^{69}Ni, we expect the four most intense transitions to correspond to single-particle excitations from $1g_{9/2}$ orbital to the four closest particle states allowed by selection rules of angular momentum and parity for dipole transition. These states are $2f_{7/2}$, $1h_{11/2}$, $1h_{9/2}$ and $2h_{11/2}$, whose characteristics are listed in Tab. 5.2 for SkI3 and SLy5 interactions. Similarly, one can easily recognize the single-particle transitions in ^{67}Ni, corresponding to hole excitations from the $2p_{1/2}$ state to the closest possible destinations, $2s_{1/2}$ and $1d_{3/2}$, whose features are listed, too, in Tab. 5.2.

Analysis of the sum rules in the zero-coupling limit

The OPVC model does not predict, so far, any analytical expression for the exact energy weighted sum rule m_1 (see Section 2.4) of each contribution to the total strength function. Nonetheless, we

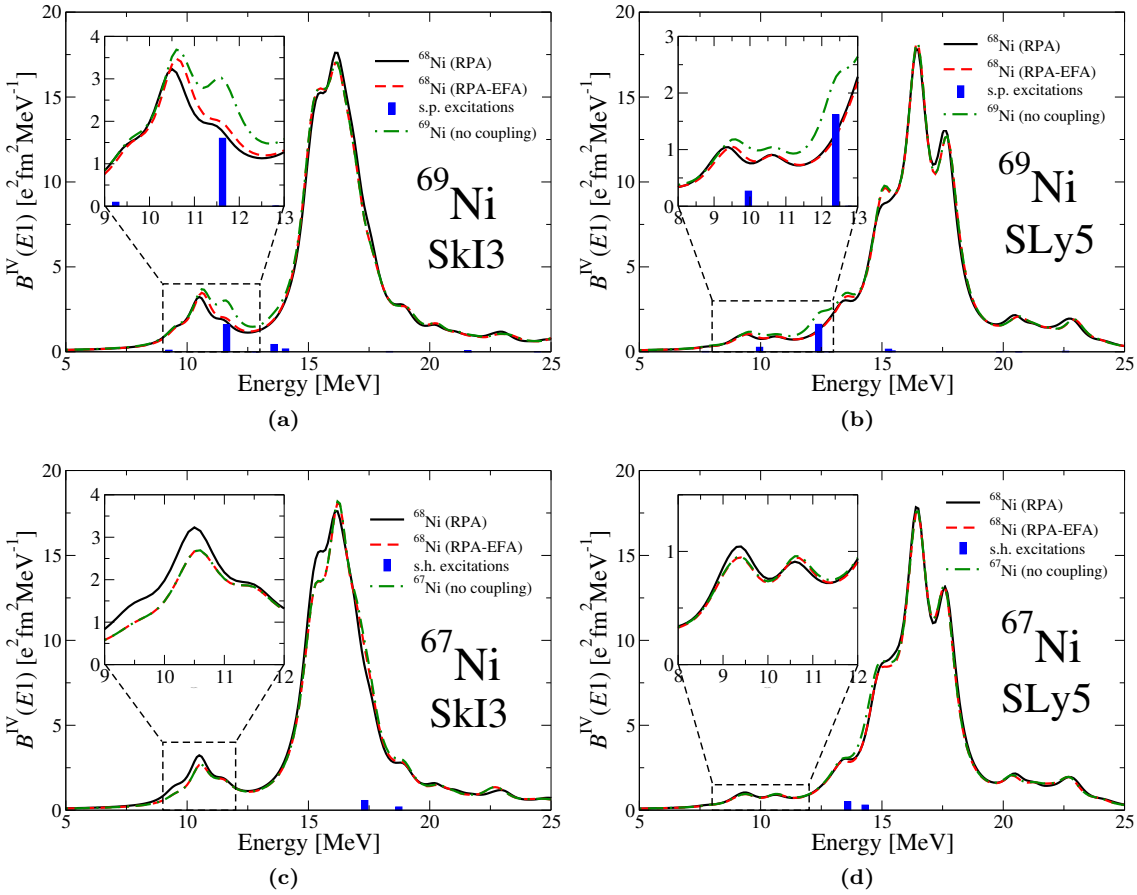

Figure 5.3
In panel (a) and (b) ((c) and (d)), respectively, the collective response for dipole excitation in the zero-coupling limit for ^{69}Ni (^{67}Ni) with SkI3 and SLy5 interactions (green dashed-dotted lines). Black continuus and red dashed lines represent the RPA response of the core, respectively, with the use of RPA and RPA-EFA equations. The blue bars represent, finally, the dipole single-particle excitations from the $1g_{9/2}$ orbital for ^{69}Ni and single-hole excitations from $2p_{1/2}$ for ^{67}Ni.

nucleus	single-particle transition	energy (SkI3, SLy5)
^{69}Ni	$1g_{9/2} \rightarrow 2f_{7/2}$	9.2, 9.9 MeV
^{69}Ni	$1g_{9/2} \rightarrow 1h_{11/2}$	11.6, 12.4 MeV
^{69}Ni	$1g_{9/2} \rightarrow 1h_{9/2}$	12.8, 15.3 MeV
^{69}Ni	$1g_{9/2} \rightarrow 2h_{11/2}$	13.6, 15.4 MeV
^{67}Ni	$2s_{1/2} \rightarrow 2p_{1/2}$	17.3, 13.6 MeV
^{67}Ni	$1d_{3/2} \rightarrow 2p_{1/2}$	18.7, 14.3 MeV

Table 5.2
Most important single-particle dipole transitions from the ground state of ^{69}Ni and ^{67}Ni for the two Skyrme interactions SkI3 and SLy5.

can evaluate each term and compare them, as an overall check of the calculation.

First of all, we evaluate the EWSR for the RPA contribution of the even-even core. In Tab. 5.3 (a) and (b) we list, for different interactions, m_1 coming from RPA (m_1^{RPA}) and RPA-EFA ($m_1^{\mathrm{RPA-EFA}}$) calculations of the core, respectively. In panel (a) the percentage of exhausted EWSR with respect to the double-commutator sum rule, Eq.(2.13), is indicated. In panel (b) the results are indicated for the two different nuclei since the RPA-EFA calculation is different for ^{69}Ni and ^{67}Ni, differently from the core RPA one. Besides, in panel (b), the percentual ratio between $m_1^{\mathrm{RPA-EFA}}$ and m_1^{RPA} is indicated.

m_1^{RPA}	^{68}Ni
SkI3	1135.7(97.7%)
SLy5	1142.9(98.0%)

(a)

$m_1^{\mathrm{RPA-EFA}}$	^{69}Ni	^{67}Ni
SkI3	1129.7 (99.5%)	1114.7 (98.2%)
SLy5	1135.2 (99.3%)	1108.4 (97.0%)

(b)

Table 5.3
In panels (a) and (b) we list, for different interactions, m_1 coming from RPA and RPA-EFA calculations of the core, respectively. In panel (a) the percentage of exhausted EWSR with respect to the DC sum rule, Eq.(2.13), is indicated. In panel (b) the results are indicated for the two different nuclei. Besides, in panel (b), the percentual ratio between $m_1^{\mathrm{RPA-EFA}}/m_1^{\mathrm{RPA}}$ is indicated. All m_1 are measured in [e^2fm^{2}MeV].

As one expects, $m_1^{\mathrm{RPA-EFA}}$ is always lower than m_1^{RPA} because of the partial screening of some levels, which naturally causes a slight reduction of the total intensity. Besides, as one can see from Tab. 5.3, this effect is bigger for ^{67}Ni than for ^{69}Ni.

Similarly, we evaluate the EWSR m_1^{odd} for the single-particle excitations of the odd-particle (or hole). The results are shown in Tab. 5.4 for the two nuclei and the two interactions under investigation. Between parenthesis, we indicate the corresponding value of $\hat{\alpha}$. The latter, defined as $\hat{\alpha} = A^{\mathrm{core}} \times m_1^{\mathrm{odd}}/m_1^{\mathrm{RPA-EFA}}$, gives an order of magnitude of the number of nucleons involved in single-particle transitions and so it should be close to 1.

m_1^{odd}	^{69}Ni	^{67}Ni
SkI3	31.8 (1.91)	13.5 (0.82)
SLy5	27.4 (1.64)	11.7 (0.72)

Table 5.4
EWSR m_1^{odd} for the single-particle excitations of the odd-particle (or hole). The results are shown for the two nuclei and the two interactions under investigation. Between parenthesis, we indicate the corresponding value of $\hat{\alpha}$. All m_1 are measured in [e^2fm^{2}MeV].

As we can see from Tab. 5.4, the value of $\hat{\alpha}$ is compatible with 1 although it is sistematically larger for ^{69}Ni and lower for ^{67}Ni.

Here we propose an empirical rule to check the accuracy of the single-particle calculation in the case of particle-plus-core nuclei. In this case, in fact, the single-particle excitations have fixed parent level (e.g. $1g_{9/2}$ in ^{69}Ni) and variable destination. In the case of hole-plus-core nuclei, instead, hole excitations from a fixed level are to be interpreted as single-particle excitations *to* that level, and so the parent level is variable. For fixed parent level, one can try to evaluate the expected value of m_1^{odd} by means of a specification of Eq.(2.11) to the dipole ($L = 1$) case,

$$m_1^{\mathrm{odd,DC}} = \frac{\hbar^2}{2m^*_{\mathrm{odd}}} \frac{9}{4\pi} \int d^3r \rho_{\mathrm{odd}}(r). \tag{5.5}$$

In the previous equation, A has been substituted with 1 since we are dealing with single-particle excitations. Besides, $\rho_{\mathrm{odd}}(r)$ has been defined as the density distribution of the parent orbital for single-particle transitions,

$$\rho_{\mathrm{odd}}(r) = \frac{2j_{\mathrm{odd}} + 1}{4\pi} u^2_{\mathrm{odd}}(r), \tag{5.6}$$

being $u_{\rm odd}$ the radial wave function of that orbital and $j_{\rm odd}$ its angular momentum. Finally, $m^*_{\rm odd}$ has been defined as the effective mass of the parent orbital,

$$m^*_{\rm odd} \equiv \int d^3r \rho_{\rm odd}(r) m^*(r) \tag{5.7}$$

where, in the integral, $m^*(r)$ is the effective mass defined by Eq.(3.13) in the framework of the Skyrme interaction.

Evaluating the integral in Eq.(5.7) we find that, for ^{69}Ni, $m^*_{\rm odd}/m = 0.75$ for SkI3 and $m^*_{\rm odd}/m = 0.80$ for SLy5. In Fig. 5.4 we plot $m^*(r)/m$ and $u^2_{\rm odd}(r)$ for the two interactions SkI3 and SLy5.

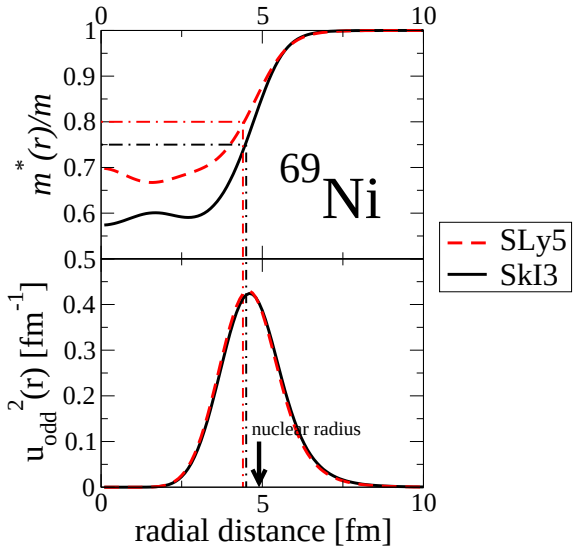

Figure 5.4
In the upper panel we plot $m^*(r)/m$ in ^{69}Ni for SkI3 and SLy5, whereas $u^2_{\rm odd}$ is represented in the lower panel. The dot-dashed line highlightens $m^*_{\rm odd}$ and the corresponding radial position on the wave function; the latter is compatible with the barycentre of the density distribution.

In ^{69}Ni, the calculated $m_1^{\rm odd}$ comes out to be 98% of $m_1^{\rm odd,DC}$ for SkI3 interaction and 96% for SLy5 interaction implying a good agreement between expectations and results. These results have been calculated including all the single-particle states up to 7 shells since we verified that the exhausted $m_1^{\rm odd}$ does not grow significantly increasing further the energetic range.

In Tab. 5.5 we report, finally, the total calculated $m_1^{\rm zc}$ for the two odd nuclei in the zero-coupling limit obtained as $m_1^{\rm odd} + m_1^{\rm RPA-EFA}$.

$m_1^{\rm zc}$	^{69}Ni	^{67}Ni
SkI3	1161.5	1128.2
SLy5	1162.6	1120.1

Table 5.5
Total calculated $m_1^{\rm zc}$ for the odd nuclei in the zero-coupling limit obtained as $m_1^{\rm odd} + m_1^{\rm RPA-EFA}$. All m_1 are measured in $[e^2{\rm fm}^2{\rm MeV}]$.

5.5 Calculation of the dipole response within the OPVC model

5.5.1 The OPVC matrices

In order to implement the OPVC model described in Chapter 4, the first necessary step is to set up the OPVC matrices, Eq.(4.52), and to diagonalize them so as to obtain the coefficients $\{\mathcal{A}_i\}$ and $\{\mathcal{B}_i\}$ describing the state mixing of the eigenstates of the odd nucleus, Eq.(4.13).

For each of the two nuclei under investigation, ^{69}Ni and ^{67}Ni, one has to build a matrix (4.52) in the subspace J^π corresponding to the ground state. These data can be found experimentally: in the case of ^{69}Ni and ^{67}Ni, the experimental ground states are $\frac{9}{2}^+$ and $\frac{1}{2}^-$, respectively [NNDC]. The first data is robust, while the latter is confirmed, or not proved wrong, by the β decay of ^{67}Cu. As one can easily see, both in the case of ^{69}Ni and ^{67}Ni, the subspace J^π of the experimental ground state corresponds to that of the ground state in the uncoupled representation, i.e., the vibration-free state in which the odd-particle (hole) is in the lowest (highest) possible energy level. In fact, this corresponds to the subspace $\frac{9}{2}^+$ for ^{69}Ni, since the lowest possible particle level is a $1g_{9/2}$ orbital, whereas it corresponds to the subspace $\frac{1}{2}^-$ for ^{67}Ni, since the highest possible hole level is a $2p_{1/2}$ orbital. This happens because the neighboring ^{68}Ni is a spherical closed-shell doubly-magic nucleus, thus preventing deep level mixing caused by nuclear deformations due to the odd-nucleon. The OPVC ground states of ^{69}Ni and ^{67}Ni are simply the eigenstates of this matrices corresponding, respectively, to the lowest and highest eigenvalue. The diagonalization of these matrices will thus provide the coefficients $\{\mathcal{A}_i\}$ and $\{\mathcal{B}_i\}$ describing completely the state $|\nu_1 l_1 j_1\rangle$ of Eq.(4.20).

Besides, one has to build a matrix for each subspace allowed by selection rules for dipole transitions from the ground state. The diagonalization of these matrices will provide the complete set of excited states of the odd nucleus, i.e., the states $|\nu_2 l_2 j_2\rangle$ of Eq.(4.20). The possible subspaces are three for ^{69}Ni $\left(\frac{7}{2}^-, \frac{9}{2}^-, \frac{11}{2}^-\right)$ and two for ^{67}Ni $\left(\frac{1}{2}^+, \frac{3}{2}^+\right)$.

In building the matrices, single-particle energies calculated by means of Skyrme-Hartree-Fock approximation (see Section 5.2) have been employed. Besides, the phonons of multipolarity 0^+, 1^-, 2^+, 3^- and 4^+ have been included, too. These phonons have been calculated in RPA-EFA approximation as in Section 5.3. The maximum energy of the unoccupied single-particle states included in the RPA model space is set at 70 MeV. This parameter, together with the dimension of the radial mesh, has been chosen carefully so that the results of the excitation spectrum are stable enough, i.e., the total calculated EWSR does not change appreciably increasing the dimension of the box or the energy cutoff. Not all the phonons of the selected multipolarities have been used in the calculation of the OPVC matrices. In fact, only those who exhausted at least 1% of the isoscalar or isovector non-energy-weighted sum rule m_0 were considered in order to exclude from the calculation non-collective excited states of the core. Besides, an energy cutoff of 50 MeV for the phonons was introduced.

In Fig. 5.5 we report the low-lying isoscalar response for quadrupole (2^+) and octupole (3^-) excitations in the even-even core of ^{69}Ni for SkI3 and SLy5 interactions. The main peaks are underlined and their characteristics are reported in Tab. 5.6. The same plot for the even-even core of ^{67}Ni is very similar and is not explicitly shown. We stress here the characteristics of low-lying vibrations since they will be important in the coupling between the odd-nucleon and the core. As one can see from Fig. 5.5, the quadrupole pattern is very similar for the two interactions; in the octupole case, instead, SkI3 shows two distinct peaks whereas SLy5 shows three peaks and a small bump.

5.5.2 Dipole response in ^{69}Ni

Diagonalization of OPVC matrix

After the diagonalization of the OPVC matrices, one is faced with a number of new states of the odd nucleus in the coupled representation.

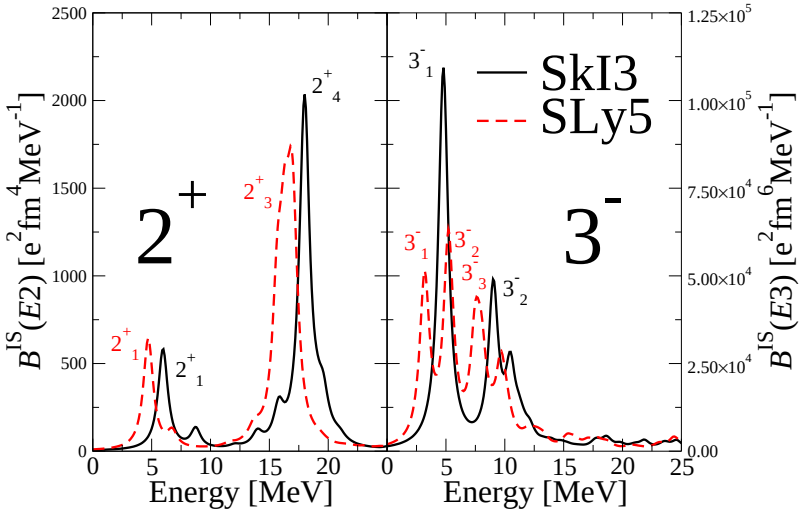

Figure 5.5
Low-lying response for quadrupole (2^+) and octupole (3^-) excitations in the even-even core of ^{69}Ni for SkI3 and SLy5 interactions.

SkI3			
ξ	Ω_ξ	$m_0^{\mathrm{IS}}\%$	$B(E\lambda)^{\mathrm{EM}}$
2_1^+	5.96	16.7	359.8
2_4^+	18.01	52.7	437.1
3_1^-	4.78	42.8	15862.0
3_2^-	9.02	17.7	5463.2

(a)

SLy5			
ξ	Ω_ξ	$m_0^{\mathrm{IS}}\%$	$B(E\lambda)^{\mathrm{EM}}$
2_1^+	4.71	16.6	363.1
2_3^+	16.31	21.2	186.6
3_1^-	5.22	21.6	9187.8
3_2^-	7.51	10.5	3770.5
3_3^-	9.67	7.6	5987.4

(b)

Table 5.6
Main characteristics of the low-lying response peaks for quadrupole (2^+) and octupole (3^-) excitations in the even-even core of ^{69}Ni for SkI3 and SLy5 interactions. For each state ξ, the energy Ω_ξ (in MeV) and the percentage of exhausted isoscalar (m_0^{IS}) sum rules is indicated. Besides, for each state ξ, the exhausted electromagnetic sum rule is indicated in units of $[e^2\mathrm{fm}^{2\lambda}]$. Energies are measured in MeV.

In Fig. 5.6, we plot, for SkI3 and SLy5 interactions, a comparison between pure and mixed states for ^{69}Ni above the Fermi surface. In the left column we plot single-nucleon levels coming from Skyrme-Hartree-Fock calculation, whereas, on the right column, we plot those dressed states i whose $\mathcal{C}_k^i$ (see Section 4.1) is bigger than 0.05, being k any single-nucleon state. In this latter case, the length of the lines is proportional to $\mathcal{C}_k^i$. The colors have been chosen so that states with the same orbital angular momentum have the same color.

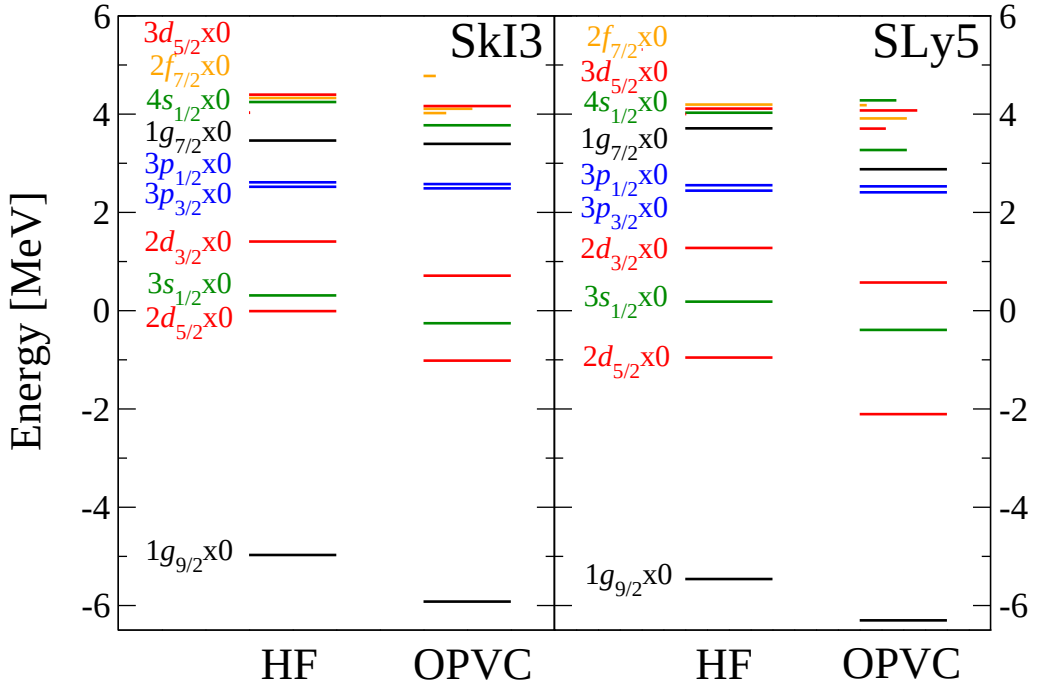

Figure 5.6
Comparison between pure and dressed levels for ^{69}Ni above the Fermi surface. In the left column we plot single-nucleon levels coming from SHF, whereas, on the right column, we plot those dressed states i whose $\mathcal{C}_k^i$ is bigger than 0.05, being k any single-nucleon state. In this latter case, the length of the lines is proportional to $\mathcal{C}_k^i$. The colors have been chosen so that states with the same orbital angular momentum have the same color.

Single-nucleon level shift

As we can see from Fig. 5.6, the coefficient $\mathcal{C}_k^i$ is very close to 1 for states near the Fermi surface, indicating a limited amount of mixture between a pure single-nucleon state and other pure states. It is easy, though, to identify the original pure state and the corresponding poorly dressed state, which will be called *dressed single-nucleon state*. Besides, some of these states, like $1g_{9/2} \otimes 0$, $2d_{5/2} \otimes 0$, $3s_{1/2} \otimes 0$, $2d_{3/2} \otimes 0$ and $1g_{7/2} \otimes 0$ (in SLy5) appear to be down-shifted of 0.5-1 MeV, while other seem not to be shifted appreciably, like $3p_{3/2} \otimes 0$ and $3p_{1/2} \otimes 0$.

This occurrence can be easily explained with a simple model involving a drastic reduction of the huge OPVC matrix. In fact, one expects, since the considered single-nucleon states are low in energy, not to be many possible pure states available for the coupling and close to them in energy. Since one would expect a strong mixing only between states somewhat close in energy, the dimension of the matrix can be reduced retaining but one single state for the mixing with the initial single-nucleon state. This picture is of course approximate, but it can give the order of magnitude of the energy shift caused by the coupling with different states. Let us consider, as an example, the case of $1g_{9/2} \otimes 0$, whose unperturbed energy is -4.971 MeV. The closer pure state available for a mixing is the state $1g_{9/2} \otimes 2_1^+$, whose energy is 0.993 MeV. The matrix element of the calculated residual interaction between $1g_{9/2} \otimes 0$ and $1g_{9/2} \otimes 2_1^+$ is η=-1.284 MeV. The

reduced OPVC matrix one can write is then of the form

$$\begin{pmatrix} -4.971 & -1.284 \\ -1.284 & 0.993 \end{pmatrix}$$

The eigenvectors of this matrix are $\begin{pmatrix} -0.979 \\ -0.202 \end{pmatrix}$ with eigenvalue -5.236 MeV and $\begin{pmatrix} 0.202 \\ 0.979 \end{pmatrix}$ with eigenvalue 1.258 MeV. As one can easily see, the first eigenvector coincides, to some extent, with the single-nucleon state and shows an energy shift of -0.265 keV with respect to the uncoupled configuration. This simple model accounts, though, for the 27.9% of the total shift of the $1g_{9/2}$ state, which is equal to -0.949 MeV.

In Tab. 5.7 we report, for each low single-nucleon state, the uncoupled (ϵ_i) and dressed ($\overline{E}_i$) energies. Besides, we provide the closer pure state (with energy E_k), together with the ratio $|\eta^i_k/(E_k-\epsilon_i)|$ and the caused partial shift $\delta\epsilon_i$. The ratio $|\eta^i_k/(E_k-\epsilon_i)|$ is an index for the intensity of the mixing: if it is big, i.e., the residual interaction is of the order of the energy gap, the two states will be efficiently mixed, while, if it is little, i.e., if the energy gap is big with respect to residual interaction, the two states will be poorly mixed. We report the results only for SkI3 interaction (with the exception of $1g_{7/2}$), since they are similar for SLy5 force.

pure state	ϵ_i	$\overline{E}_i$ ($\Delta\epsilon_i$)	coupl. state (E_k, $\lvert\eta^i_k/(E_k-\epsilon_i)\rvert$, $\delta\epsilon_i$, $\delta\epsilon_i/\Delta\epsilon_i$%)
$1g_{9/2}\otimes 0$	-4.971	-5.920 (-0.949)	$1g_{9/2}\otimes 2^+_1$ (0.993, 0.323, -0.265, 27.9)
$2d_{5/2}\otimes 0$	-0.009	-1.016 (-1.007)	$1g_{9/2}\otimes 2^+_1$ (0.993, 0.930, -0.557, 55.3)
$3s_{1/2}\otimes 0$	0.311	-0.256 (-0.567)	$2d_{5/2}\otimes 2^+_1$ (5.955, 0.131, -0.095, 16.7)
$2d_{3/2}\otimes 0$	1.408	0.712 (-0.696)	$2d_{5/2}\otimes 2^+_1$ (5.955, 0.147, -0.102, 14.6)
$3p_{3/2}\otimes 0$	2.522	2.489 (-0.033)	$1g_{9/2}\otimes 3^-_2$ (4.053, 0.049, -0.004, 12.1)
$3p_{1/2}\otimes 0$	2.613	2.577 (-0.036)	$2d_{5/2}\otimes 3^-_1$ (4.772, 0.079, -0.014, 38.9)
$1g_{7/2}\otimes 0$	3.462	3.394 (-0.068)	$2d_{3/2}\otimes 2^+_1$ (7.372, 0.146, -0.082, 120.5)
$1g_{7/2}\otimes 0$ (SLy5)	3.710	2.879 (-0.831)	$2d_{3/2}\otimes 2^+_1$ (5.987, 0.234, -0.118, 14.2)
$4s_{1/2}\otimes 0$	4.247	3.773 (-0.474)	$2d_{5/2}\otimes 2^+_1$ (5.955, 0.178, -0.053, 11.2)

Table 5.7
Properties of some dressed single-nucleon states in ^{69}Ni. ϵ_i is the HF single-nucleon energy, whereas $\overline{E}_i$ is the energy of that particle state after OPVC diagonalization ($\Delta\epsilon_i$ is the energy shift). In the last column we list the nucleon-plus-vibration state which contributes most to the coupling, together with its energy E_k, the ratio $|\eta^i_k/(E_k-\epsilon_i)|$, the caused partial energy shift $\delta\epsilon_i$ and its percentage on $\Delta\epsilon_i$. All energies are measured in MeV.

As we can see from the table, just one coupling state is sufficient to understand the order of magnitude of the total shift. For example, in the case of $1g_{9/2}\otimes 0$, as we have already seen, the coupling with $1g_{9/2}\otimes 2^+_1$ provides almost 1/3 of the global shift, and almost 1/2 of the shift of $2d_{5/2}\otimes 0$ is provided by the coupling with the same $1g_{9/2}\otimes 2^+_1$. In the case of $3p_{3/2}\otimes 0$, instead, the most important coupling provides a shift of only 4 keV, explaining qualitatively the absence of energy shift.

As a general consideration, the coupling between two states lowers the energy of the state with uncoupled lower energy and raises the energy of the state with higher energy. This consideration allows to understand why, in the case of $1g_{7/2}\otimes 0$, the coupling with a $2d_{3/2}\otimes 2^+_1$ state provides more than the total shift. The reason is that there will be minor couplings with states lower in energy than $1g_{7/2}\otimes 0$, which will provide a compensating up-shift.

In Fig. 5.7(a) we plot the coefficients $\mathcal{C}^\alpha_k$ as a function of the uncoupled energy E_k, being α the index of the dressed $1g_{9/2}\otimes 0$ state (the interaction is again SkI3). As we can see from the figure, the uncoupled state k which contributes most to the state α is, of course, $1g_{9/2}\otimes 0$. The other contributions decrease in importance with energy, as one expects, starting from the closest state, $1g_{9/2}\otimes 2^+_1$, and going to $2d_{5/2}\otimes 2^+_1$, $3p_{3/2}\otimes 3^-_2$, $1g_{9/2}\otimes 2^+_4$ and so on. In Fig. 5.7(b) we plot, instead, the coefficients $\mathcal{C}^i_\beta$ as a function of the energy of the dressed states. In this case, β is the index for the uncoupled $1g_{9/2}\otimes 0$ state. As we can see from this figure, the coefficient is,

as one expects, close to 1 for the dressed $1g_{9/2} \otimes 0$ state, while is fastly descreases with increasing energy starting from $1g_{9/2} \otimes 2_1^+$, $2d_{5/2} \otimes 2_1^+$ and $1h_{11/2} \otimes 3_1^-$.

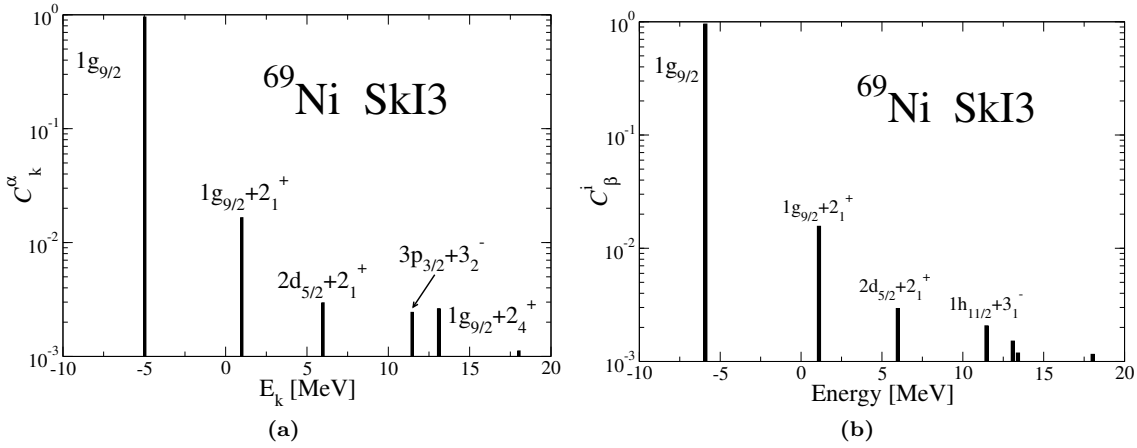

Figure 5.7
In panel (a) we plot the coefficients $\mathcal{C}_k^\alpha$ as a function of the uncoupled energy E_k, being α the index of the dressed $1g_{9/2} \otimes 0$ state. In panel (b), instead, we plot the coefficients $\mathcal{C}_\beta^i$ as a function of the energy of the dressed states. In this case, β is the index for the uncoupled $1g_{9/2} \otimes 0$ state. The Skyrme interaction is SkI3.

Single-nucleon level splitting

The situation is different far from the Fermi surface, where many $\mathcal{C}_k^i$ different from 1 can be identified. This means that the original single-nucleon states do mix appreciably with other pure states, splitting into many components. This is true for the $2f_{7/2} \otimes 0$ orbital for SkI3 force and for $4s_{1/2} \otimes 0$, $3d_{5/2} \otimes 0$ and $2f_{7/2} \otimes 0$ orbitals for SLy5 force. The reason for the fragmentation is quite clear. Because of the increasing energy, there will be many pure states very close in energy to these single-nucleon states. These states can participate in the mixing and so the fragmentation, absent at low energy, will become more and more important. The presence of a large number of mixing states prevents a simple argument which shows the quantitative origin of the fragmentation. In Tab. 5.8 we report those states in which the $2f_{7/2} \otimes 0$ state (for SkI3 force) is split, together with a weighted average of the dressed $2f_{7/2} \otimes 0$ energy.

part. state k	ϵ_k	$\overline{E}_i$, $\mathcal{C}_k^i$ (other imp. state)	$\overline{E}_k$ weighted ($\Delta\epsilon_k$)
$2f_{7/2} \otimes 0$	4.278	$\begin{cases} 4.022 & 0.261 & (1g_{9/2} \otimes 3_2^-) \\ 4.109 & 0.556 & (1g_{9/2} \otimes 3_2^-) \\ 4.776 & 0.135 & (2d_{5/2} \otimes 3_1^-) \end{cases}$	4.180 (-0.098)

Table 5.8
Properties of the highly mixed $2f_{7/2} \otimes 0$ particle states in ^{69}Ni. ϵ_k is the HF single-nucleon energy, whereas $\overline{E}_i$ is the energy of each fragment in which the original single-nucleon state splits. It is listed together with its amplitude $\mathcal{C}_k^i$ (we list only those states more important than 5%) and with the other important uncoupled state involved in the mixing to the state i. $\overline{E}_k$ is the energy of the dressed $2f_{7/2} \otimes 0$ single-nucleon state after OPVC diagonalization (obtained as a weighted average of the previous). All energies are measured in MeV and the interaction is SkI3.

Strength function for dipole response

The complete diagonalization of the OPVC matrices allows the calculation of the matrix elements (4.20) of the transition between the ground state and any excited state, and so the evaluation

of the strength function for dipole transitions. In Fig. 5.8 we report the results for the complete dipole response in the OPVC model for ^{69}Ni for SkI3 (panel (a)) and SLy5 (panel (b)) interactions. In the same figure, a comparison is made with the response of ^{68}Ni and ^{69}Ni in the zero-coupling limit.

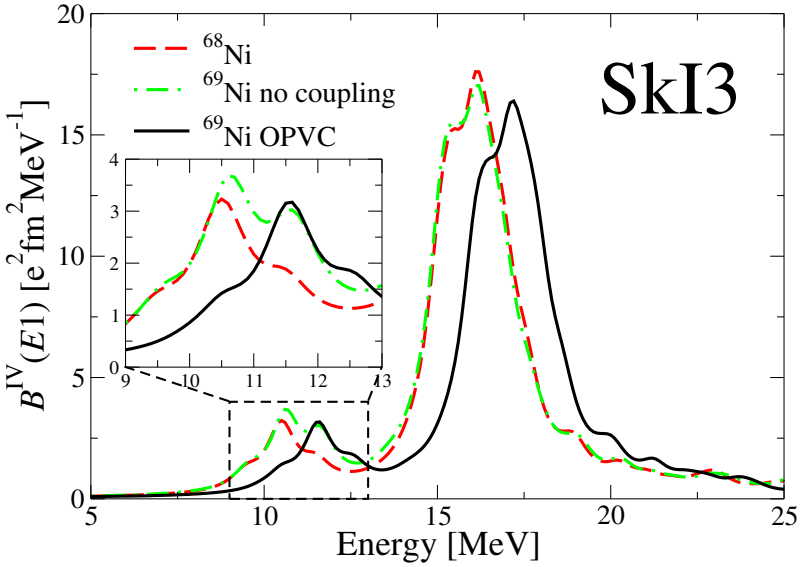

(a)

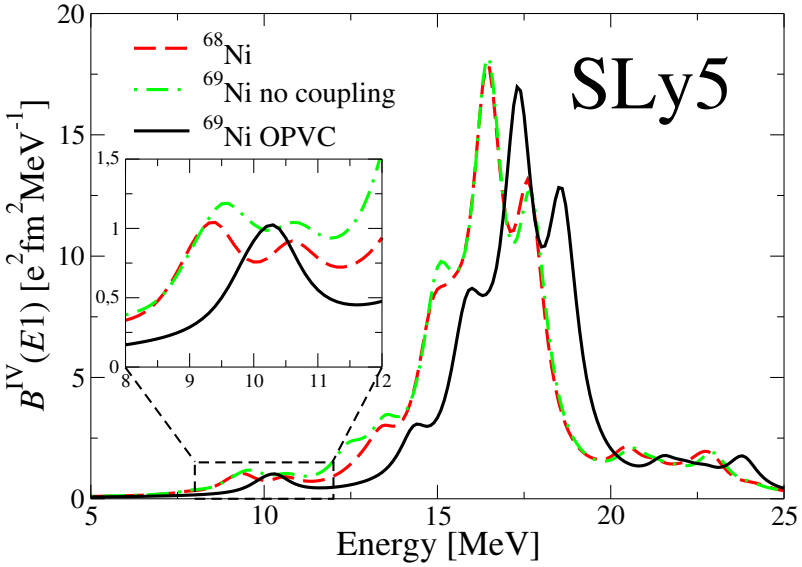

(b)

Figure 5.8
Results for the complete dipole response in the OPVC model for ^{69}Ni for SkI3 (panel (a)) and SLy5 (panel (b)) interactions. In the same figure, a comparison is made with the response of ^{68}Ni and ^{69}Ni in the zero-coupling limit.

As we can see from the figure, the strength function of ^{69}Ni in the fully coupled model appears to be up-shifted of about 950 keV with respect to the two other curves both in the case of SkI3 and SLy5 interactions. This feature turns out to be the greatest modifications, since the shape remains substantially unhaltered.

The main reason for this (almost rigid) shift is the variation in the single-nucleon level energies one obtaines introducing the coupling with other single-nucleon and nucleon-plus-vibration states.

Since the energy of the ground state, in the uncoupled system, is just the energy of the single-nucleon state $1g_{9/2} \otimes 0$, and down-shifts of almost 950 keV introducing the coupling, the overall spectrum up-shifts of about 950 keV.

As we said in Chapter 4, one of the main tasks in the analysis of the response of an odd nucleus is the correct interpretation of the multiplet splitting. This aspect is authomatically taken into account in our model, since the expression (4.20) accounts for transition to a state of definite angular momentum and parity. This allows to separate the dipole strength function in contributions coming from transitions to different J^π subspaces, i.e., to obtain the multiplet itself. In Fig. 5.9 we plot the total OPVC strength function for ^{69}Ni and the contributions coming from transitions to $\frac{7}{2}^-$, $\frac{9}{2}^-$ and $\frac{11}{2}^-$ subspaces.

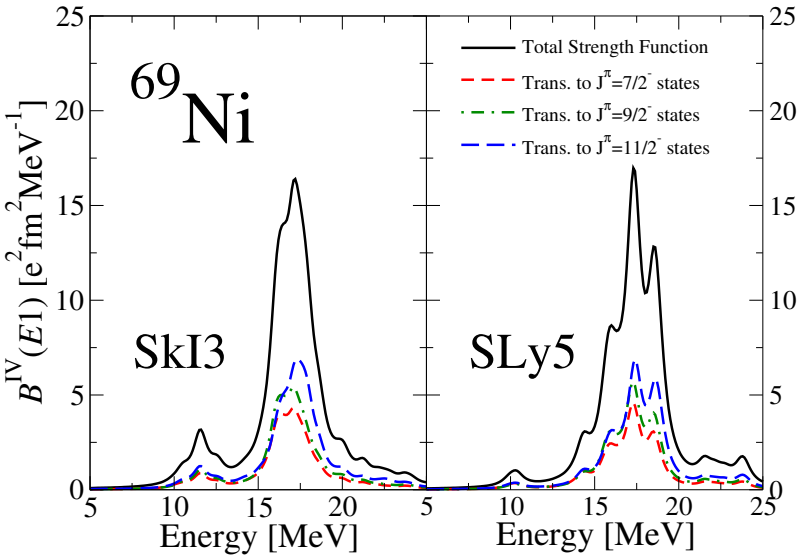

Figure 5.9
Total OPVC strength function for ^{69}Ni and the contributions coming from transitions to $\frac{7}{2}^-$, $\frac{9}{2}^-$ and $\frac{11}{2}^-$ subspaces. The plot is depicted for SkI3 and SLy5.

Sum rules for the dipole response

As we said before, there are no rules concerning a conservation of the energy weighted sum rule in our model nor implying a strict proportionality between the mass number A and the total exhausted EWSR. A check we can do, nonetheless, is to calculate the EWSR of ^{69}Ni as coming from the OPVC model, $m_1^{\rm OPVC}$, and compare it to the EWSR exhausted by the RPA response of ^{68}Ni, $m_1^{\rm RPA}$. In Tab. 5.9 we report the data for $m_1^{\rm OPVC}$ and $m_1^{\rm RPA}$, together with the value of $\hat{A} = A^{\rm core} \cdot m_1^{\rm OPVC}/m_1^{\rm RPA}$, which will correspond, almost exactly, to 69 if our model were EWSR conserving. As we can see, the value one obtaines is greater, spanning from 71.1 in the case of SLy5 to 73.7 in the case of SkI3. It has to be noticed that, for consistency, since the OPVC has been evaluated considering only the RPA phonons which exhausted at least 1% of the total isoscalar or isovector sum rule, also $m_1^{\rm RPA}$ has been evaluated, in this case, considering only those phonons. This consideration accounts for the difference between $m_1^{\rm RPA}$ in Tabs. 5.9 and 5.3.

Moreover, one can compare the total EWSR exhausted by ^{69}Ni in the zero-coupling limit, $m_1^{\rm zc}$, and in the full OPVC calculation, $m_1^{\rm OPVC}$. The results are reported in Tab. 5.10. For consistency, the EWSR in the zero-coupling limit has been evaluated only including the RPA phonons which exhausted at least 1% of the total isoscalar or isovector sum rule. This consideration accounts for the difference between $m_1^{\rm zc}$ in Tabs. 5.10 and 5.5. As one can see from the table, the value of $m_1^{\rm OPVC}$ is sistematically larger than that of $m_1^{\rm zc}$, as one expects as an effect of the up-shift of the spectrum.

interaction	m_1^{OPVC} (m_1^{RPA})	$\hat{A}$
SkI3	1122.9 (1035.8)	73.7
SLy5	1106.7 (1058.3)	71.1

Table 5.9
Comparison between the EWSR calculated for ^{69}Ni in the OPVC model, m_1^{OPVC}, and for the pure even-even core, m_1^{RPA}, by means of standard RPA calculation. The value of $\hat{A} = A^{\mathrm{core}} \cdot m_1^{\mathrm{OPVC}}/m_1^{\mathrm{RPA}}$ is also indicated. All sume rules are measured in [e^2fm^{2}MeV].

interaction	m_1^{OPVC}	m_1^{zc}	$m_1^{\mathrm{OPVC}}/m_1^{\mathrm{zc}}\%$
SkI3	1122.9	1062.4	105.7
SLy5	1106.7	1078.3	102.6

Table 5.10
Comparison between the total EWSR exhausted by ^{69}Ni in the zero-coupling limit, m_1^{zc}, and in the full OPVC calculation, m_1^{OPVC}. All sume rules are measured in [e^2fm^{2}MeV].

As a test of the calculation, one can check that the ESWR scales correctly for the components of the multiplet. This request means that the total EWSR for transitions to a J^π subspace must be proportional to $2J+1$. This is equivalent to ask that, defining $\mathcal{J} = \sum_J (2J+1)$, the EWSR of each component of the multiplet be compatible with the fraction $m_1^{\mathrm{OPVC}} \times (2J+1)/\mathcal{J}$. In Tab. 5.11 we report the results: m_1^{MULT} is the EWSR exhausted by each component of the multiplet and $m_1^{\mathrm{MULT,EXP}}$ is equal to the expected value $m_1^{\mathrm{OPVC}} \times (2J+1)/\mathcal{J}$.

interaction	J^π, m_1^{MULT}, $m_1^{\mathrm{MULT,EXP}}$, $m_1^{\mathrm{MULT}}/m_1^{\mathrm{MULT,EXP}}\%$
SkI3	$7/2^-$, 291.6, 299.4, 97.4 $9/2^-$, 361.3, 374.3, 96.5 $11/2^-$, 470.0, 449.2, 104.6
SLy5	$7/2^-$, 288.0, 295.1, 97.6 $9/2^-$, 357.7, 368.9, 97.0 $11/2^-$, 461.1, 442.7, 104.1

Table 5.11
For SkI3 and SLy5 interactions, we list the EWSR m_1^{MULT} related to dipole transitions from the ground state $9/2^+$ of ^{69}Ni to all possible final J^π configurations allowed by angular momentum and parity selection rules. These data are compared to the expected values $m_1^{\mathrm{MULT,EXP}}$. All sume rules are measured in [e^2fm^{2}MeV].

As one can see from the table, the sum rule calculated for each multiplet is, in each case, fully compatible with the expected value.

5.5.3 Dipole response in ^{67}Ni

Diagonalization of OPVC matrix

After the diagonalization of the OPVC matrices, one is faced with a number of new states of the odd nucleus in the coupled representation.

In Fig. 5.10, we plot, for SkI3 and SLy5 interactions, a comparison between pure and dressed levels for ^{67}Ni below the Fermi surface. In the left column we plot single-nucleon levels coming from Skyrme-Hartree-Fock calculation, whereas, on the right column, we plot those dressed states i whose $\mathcal{C}_k^i$ (see Section 4.1) is bigger than 0.05, being k any single-nucleon state. In this latter case, the length of the lines is proportional to $\mathcal{C}_k^i$. The colors have been chosen so that states with

the same orbital angular momentum have the same color. For the sake of clarity, when two dressed states are closer in energy than 500 keV they are plotted as one (sum) line.

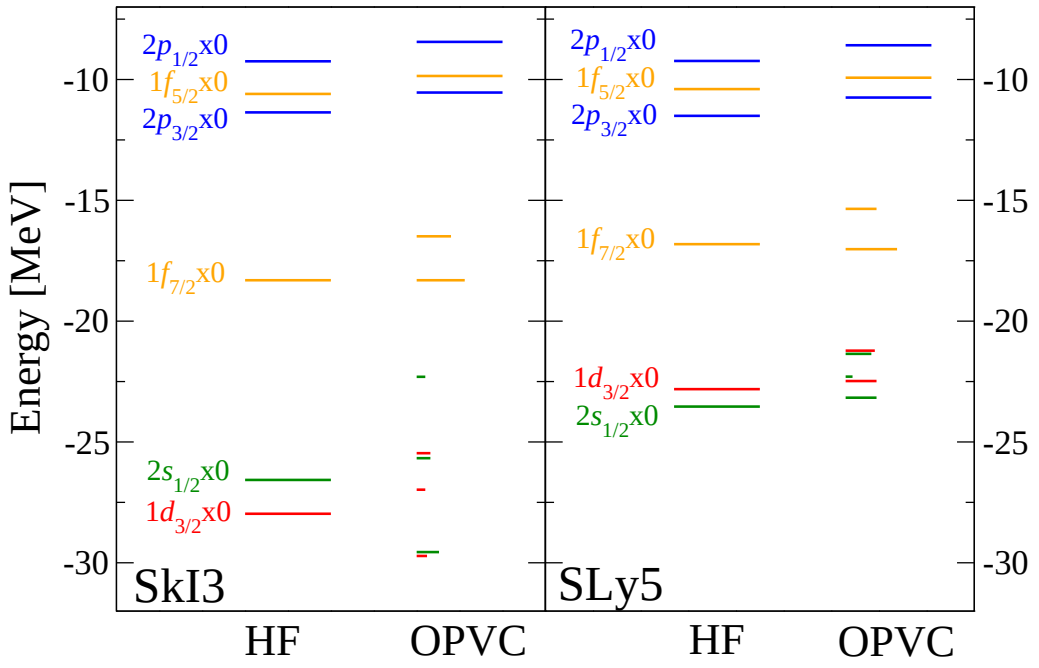

Figure 5.10
Comparison between pure and dressed single-nucleon levels for ^{67}Ni. For further comments, see the label of Fig. 5.6.

Single-nucleon level shift

As we can see from Fig. 5.10, the coefficient $\mathcal{C}_k^i$ is very close to 1 for states near the Fermi surface, indicating a limited amount of mixture between a pure single-nucleon state and other pure states. It is easy, though, to identify the original pure state and the corresponding poorly dressed state, which will be called *dressed single-nucleon state*. Besides, these states, $2p_{3/2} \otimes 0$, $1f_{5/2} \otimes 0$ and $2p_{1/2} \otimes 0$, appear to be up-shifted of about 1 MeV.

This occurrence can be easily explained with a simple model involving a drastic reduction of the huge OPVC matrix, as done in the case of ^{69}Ni. In fact, one expects, since the considered single-nucleon states are high in energy, not to be many possible pure states available for the coupling and close to them in energy. Since one would expect a strong mixing only between states somewhat close in energy, the dimension of the matrix can be reduced retaining but one single state for the mixing with the initial single-nucleon state. This picture is of course approximate, but it can give the order of magnitude of the energy shift caused by the coupling with different states.

In Tab. 5.12 we report, for each high single-nucleon state, the uncoupled (ϵ_i) and dressed ($\overline{E}_i$) energies. Besides, we provide the closer pure state (with energy E_k), together with the ratio $|\eta_k^i/(E_k - \epsilon_i)|$ and the caused partial shift $\delta\epsilon_i$. The ratio $|\eta_k^i/(E_k - \epsilon_i)|$ is an index for the intensity of the mixing: if it is big, i.e., the residual interaction is of the order of the energy gap, the two states will be efficiently mixed, while, if the energy gap is big with respect to residual interaction, the two states will be poorly mixed. We report the results only for SkI3 interaction, since they are similar for SLy5 force.

As we can see from the table, just one coupling state is sufficient to understand the order of magnitude of the total shift. For example, in the case of $2p_{1/2} \otimes 0$, the coupling with $1f_{5/2} \otimes 2_1^+$ provides almost 1/7 of the global shift, and almost 1/5 of the shift of $1f_{5/2} \otimes 0$ is provided by the coupling with the same $1f_{5/2} \otimes 2_1^+$.

hole state	ϵ_i	$\overline{E}_i$ ($\Delta\epsilon_i$)	coupl. state (E_k, $\lvert\eta^i_k/(E_k-\epsilon_i)\rvert$, $\delta\epsilon_i$, $\delta\epsilon_i/\Delta\epsilon_i\%$)
$2p_{1/2}\otimes 0$	-9.247	-8.433 ($+0.814$)	$1f_{5/2}\otimes 2^+_1$ (-16.485, 0.124, $+0.109$, 13.4)
$1f_{5/2}\otimes 0$	-10.597	-9.854 ($+0.743$)	$1f_{5/2}\otimes 2^+_1$ (-16.485, 0.157, $+0.141$, 19.0)
$2p_{3/2}\otimes 0$	-11.360	-10.539 ($+0.821$)	$2p_{3/2}\otimes 2^+_1$ (-17.247, 0.109, $+0.070$, 8.5)

Table 5.12
Properties of some dressed single-nucleon states in ^{67}Ni. For further comments, see the label of Tab. 5.7.

Single-nucleon level splitting

The situation is different far from the Fermi surface, where many $\mathcal{C}^i_k$ different from 1 can be identified. This means that the original single-nucleon states do mix appreciably with other pure states, splitting into many components. This is true for the $1d_{3/2}\otimes 0$, $2s_{1/2}\otimes 0$ and $1f_{7/2}\otimes 0$ orbitals for both SkI3 and SLy5. The reason for the fragmentation is quite clear. Because of the increasing energy, there will be many pure states very close in energy to these single-nucleon states. These states can participate in the mixing and so the fragmentation, absent at low energy, will become more and more important. The presence of a large number of mixing states prevents a simple argument which shows the quantitative origin of the fragmentation. In Tab. 5.13 we report the properties of some highly mixed single-nucleon states in ^{67}Ni.

part. state k	ϵ_k	$\overline{E}_i$, $\mathcal{C}^i_k$ (other imp. state)	$\overline{E}_k$ weighted ($\Delta\epsilon_k$)
$1f_{7/2}\otimes 0$	-18.293	-18.307 0.556 ($2p_{3/2}\otimes 2^+_1$) -16.648 0.175 ($1f_{5/2}\otimes 2^+_1$) -16.328 0.217 ($1f_{5/2}\otimes 2^+_1$)	-17.547 ($+0.746$)
$2s_{1/2}\otimes 0$	-26.566	-29.830 0.157 ($2p_{3/2}\otimes 1^-_{18}$) -29.282 0.095 ($2p_{3/2}\otimes 1^-_{15}$) -25.933 0.063 ($2p_{1/2}\otimes 1^-_{12}$) -25.413 0.096 ($2p_{1/2}\otimes 1^-_{11}$) -22.305 0.102 ($1f_{7/2}\otimes 3^-_1$)	-26.930 (-0.364)
$1d_{3/2}\otimes 0$	-27.973	-29.719 0.115 ($2p_{1/2}\otimes 1^+_{18}$) -26.974 0.086 ($2p_{3/2}\otimes 1^+_8$) -25.592 0.070 ($1f_{5/2}\otimes 1^-_5$) -25.335 0.091 ($1f_{5/2}\otimes 1^-_4$)	-27.116 ($+0.857$)

Table 5.13
Properties of some highly mixed single-nucleon states in ^{67}Ni. For further comments, see the label of Tab. 5.8.

In Fig. 5.11(a) we plot the coefficients $\mathcal{C}^i_\alpha$ as a function of the energy of the dressed states i, being α the index for the uncoupled $1d_{3/2}\otimes 0$ state (the interaction is again SkI3). In Fig. 5.11(b) we plot, instead, the coefficients $\mathcal{C}^i_\beta$, being β the index for the uncoupled $1f_{7/2}\otimes 0$ state. As one can see from the figure, many dressed states i have a significant projection upon $1d_{3/2}\otimes 0$ and $1f_{7/2}\otimes 0$, originating in a huge split of the original single-nucleon state.

Strength function for dipole response

The complete diagonalization of the OPVC matrices allows the calculation of the matrix elements (4.20) of the transition between the ground state and any excited state, and so the evaluation of the strength function for dipole transitions. In Fig. 5.12 we report the results for the complete dipole response in the OPVC model for ^{67}Ni for SkI3 (panel (a)) and SLy5 (panel (b)) interactions. In the same figure, a comparison is made with the response of ^{68}Ni and ^{67}Ni in the zero-coupling limit.

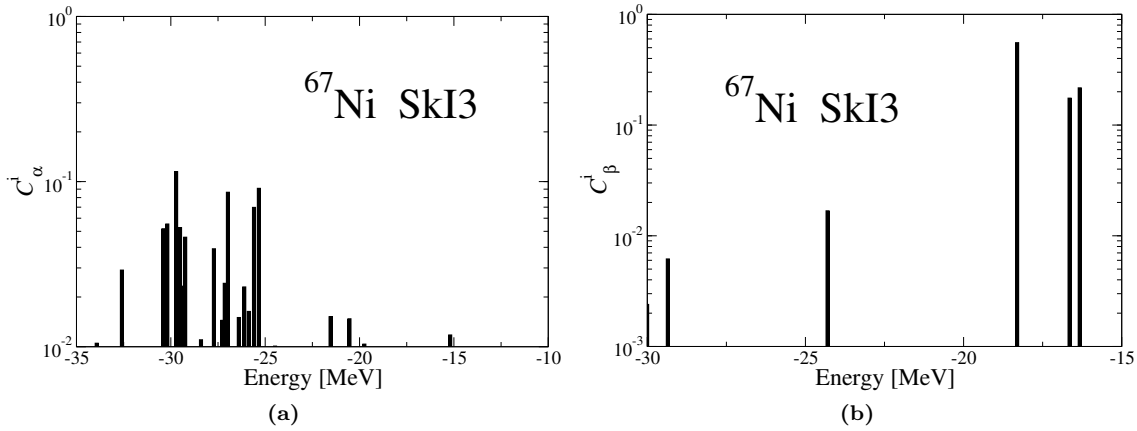

Figure 5.11
In panel (a) we plot the coefficients $\mathcal{C}^i_\alpha$ as a function of the energy of the dressed states, being α the index for the uncoupled $1d_{3/2} \otimes 0$ state. In panel (b), instead, we plot the coefficients $\mathcal{C}^i_\beta$, being β the index for the uncoupled $1f_{7/2} \otimes 0$ state. The Skyrme interaction is SkI3.

As we can see from the figure, the strength function of ^{67}Ni in the fully coupled model appears to be down-shifted of about 850 keV with respect to the two other curves both in the case of SkI3 and SLy5 interactions. This feature turns out to be the greatest modifications, since the shape remains again substantially unhaltered.

The main reason for this (almost rigid) shift is the variation in the single-nucleon level energies one obtaines introducing the coupling with single-nucleon and nucleon-plus-vibration states. Since the energy of the ground state, in the uncoupled system, is just the energy of the single-nucleon state $2p_{1/2} \otimes 0$, and up-shifts of almost 850 keV introducing the coupling, the overall spectrum down-shifts of about 850 keV.

In Fig. 5.13 we plot the total OPVC strength function and the contributions coming from transitions to $\frac{1}{2}^+$ and $\frac{3}{2}^+$ subspaces, which consitute the multiplet in the case of ^{67}Ni.

Sum rules for the dipole response

As we said before, there are no rules concerning a conservation of the energy weighted sum rule in our model nor implying a strict proportionality between the mass number A and the total exhausted EWSR. A check we can do, nonetheless, is to calculate the EWSR of ^{67}Ni as coming from the OPVC model, m_1^{OPVC}, and compare it to the EWSR exhausted by the RPA response of ^{68}Ni, m_1^{RPA}. In Tab. 5.14 we report the data for m_1^{OPVC} and m_1^{RPA}, together with the value of $\hat{A} = A^{\mathrm{core}} \cdot m_1^{\mathrm{OPVC}}/m_1^{\mathrm{RPA}}$, which will correspond, almost exactly, to 67 if our model were EWSR conserving. As we can see, the value one obtaines is lower, spanning from 60.7 in the case of SLy5 to 62.6 in the case of SkI3. It has to be noticed that, for consistency, since the OPVC has been evaluated considering only the RPA phonons which exhausted at least 1% of the total isoscalar or isovector sum rule, also m_1^{RPA} has been evaluating, in this case, considering only phonons. This consideration accounts for the difference between m_1^{RPA} in Tabs. 5.14 and 5.3.

interaction	m_1^{OPVC} (m_1^{RPA})	$\hat{A}$
SkI3	953.7 (1035.8)	62.6
SLy5	945.1 (1058.3)	60.7

Table 5.14
Comparison between the EWSR calculated for ^{67}Ni in the OPVC model and for the core in standard RPA. For further comments, see the label of Tab.(5.14).

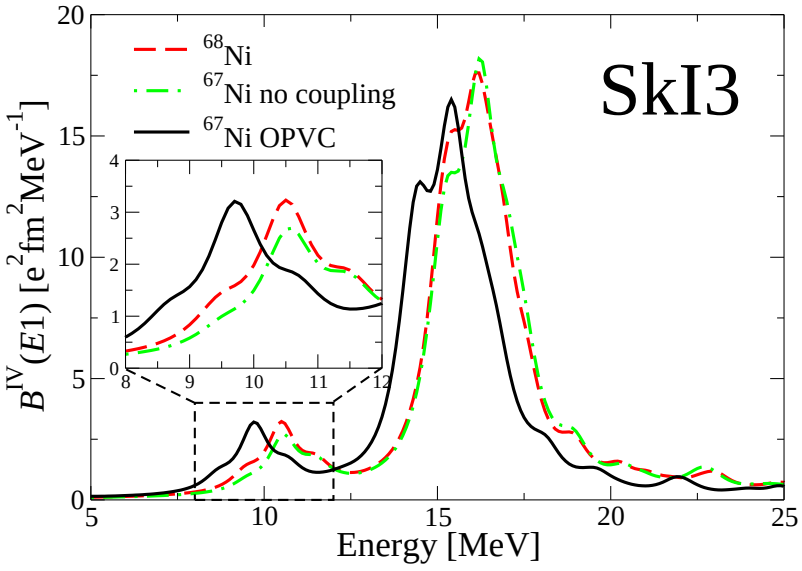

(a)

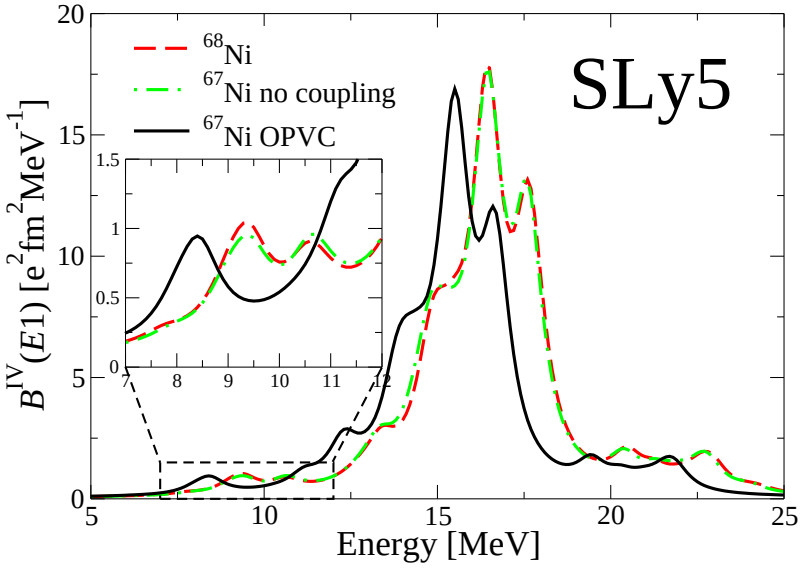

(b)

Figure 5.12
Results for the complete dipole response in the OPVC model for ^{67}Ni for SkI3 (panel (a)) and SLy5 (panel (b)) interactions. In the same figure, a comparison is made with the response of ^{68}Ni and ^{67}Ni in the zero-coupling limit.

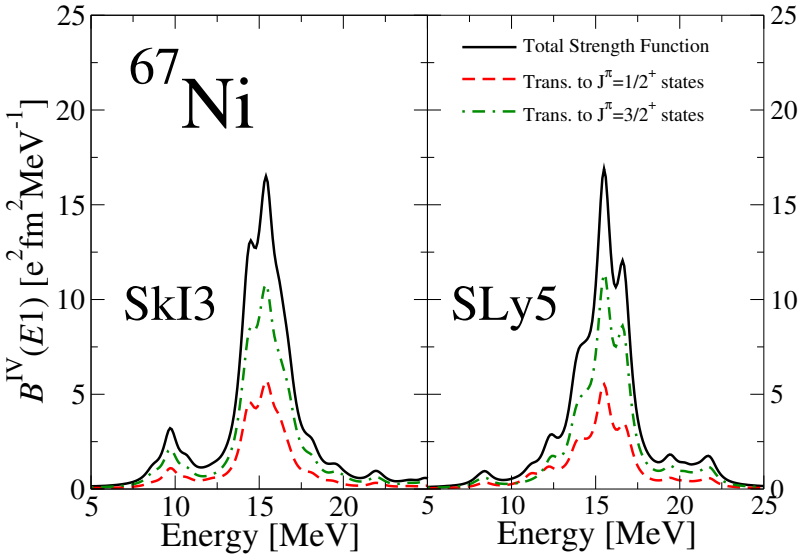

Figure 5.13
Total OPVC strength function for ^{67}Ni and the contributions coming from transitions to $\frac{1}{2}^+$ and $\frac{3}{2}^+$ subspaces. The plot is depicted for SkI3 and SLy5.

Moreover, one can compare the total EWSR exhausted by ^{67}Ni in the zero-coupling limit, $m_1^{\rm zc}$, and in the full OPVC calculation, $m_1^{\rm OPVC}$. The results are reported in Tab. 5.15. For consistency, the EWSR in the zero-coupling limit has been evaluated only including the RPA phonons which exhausted at least 1% of the total isoscalar or isovector sum rule. This consideration accounts for the difference between $m_1^{\rm zc}$ in Tabs. 5.15 and 5.5. As one can see from the table, the value of $m_1^{\rm OPVC}$ is sistematically smaller than that of $m_1^{\rm zc}$, as one expects as an effect of the down-shift of the spectrum.

interaction	$m_1^{\rm OPVC}$	$m_1^{\rm zc}$	$m_1^{\rm OPVC}/m_1^{\rm zc}\%$
SkI3	953.7	1030.7	92.5
SLy5	945.1	1038.3	91.0

Table 5.15
Comparison between the total EWSR exhausted by ^{67}Ni in the zero-coupling limit, $m_1^{\rm zc}$, and in the full OPVC calculation, $m_1^{\rm OPVC}$. All sume rules are measured in $[e^2{\rm fm}^2{\rm MeV}]$.

As a test of the calculation, one can check that the ESWR scales correctly for the components of the multiplet. This request means that the total EWSR for transitions to a J^π subspace is proportional to $2J+1$ or, equivalently, is compatible with the fraction $m_1^{\rm OPVC} \times (2J+1)/\mathcal{J}$. In Tab. 5.16 we report the results. As one can see from the table, the sum rule calculated for each multiplet is, in each case, fully compatible with the expected value.

interaction	J^π,	$m_1^{\rm MULT}$,	$m_1^{\rm MULT,EXP}$,	$m_1^{\rm MULT}/m_1^{\rm MULT,EXP}\%$
SkI3	$1/2^+$,	322.8,	317.9,	101.5
	$3/2^+$,	630.9,	635.8,	99.2
SLy5	$1/2^+$,	316.8,	315.0,	100.6
	$3/2^+$,	628.3,	630.1,	99.7

Table 5.16
Check of the correct scaling of EWSR for the multiplet. For further comments, see the label of Tab.(5.11).

Conclusions

In this work, we have introduced an original microscopic self-consistent model for the multipole response in odd nuclei, the OPVC model, which is valid for nuclei near closed-shell, doubly-magic configurations. This hypothesis has allowed us to neglect the effect of nuclear deformations and pairing correlations.

The simplest possible picture of such an odd nucleus is that of an even-even core plus an odd-nucleon, which can be either a particle or a hole. If the core and the odd-nucleon were completely independent, the excitation spectrum would be just the sum of the vibrational spectrum of the core plus the single-particle excitation spectrum of the odd-nucleon. The states of the uncoupled system, that is, the limit in which the odd-nucleon and the core are completely independent, can be either single-nucleon states, i.e., configurations in which the odd-nucleon is in a given quantum state and core vibrations are absent, or nucleon-plus-vibration states, i.e., configurations in which the odd-nucleon is in a given quantum state and the core is vibrating.

In a realistic picture, nonetheless, the core and the odd-nucleon are not independent. The following problem has to be dealt with: how the excitation energies and the wave functions of the even-even core (i.e. of the phonons) and the odd-particle (or hole) are mutually affected. According to the OPVC model, the interaction between the even-even core and the odd-nucleon acts on the states of the uncoupled system introducing a coupling effect. The effect of this coupling is to linearly mix the simple single-nucleon and nucleon-plus-vibration states, giving rise to a spectrum of more complicated states for the odd system. The coefficients of the mixing and the energies of the excited states of the odd nucleus can be obtained via the diagonalization of a matrix including the energies of single-nucleon and nucleon-plus-vibration states with the same angular momentum and parity, J^π, as well as the matrix elements of the reciprocal residual interaction. This matrix represents, from a qualitative point of view, an extension of the classical particle-vibration coupling matrix introduced in the 1970s. The element of novelty is that the energies of particles and phonons, as well as the phonon verteces, are calculated in the microscopic self-consistent framework of Hartree-Fock (HF), random phase approximation (RPA) and particle-vibration coupling (PVC) theories based on the effective Skyrme interaction.

The expansion for the eigenstates of the odd nucleus has been employed to extract a complete expression for the transition matrix element associated with the action of an external multipole field, and then to provide a formula for the strength function associated with multipole nuclear transitions in the odd system. This formula takes automatically into account the problem of the multiplet splitting associated with multipole excitations in odd nuclei. The transition matrix elements have been written as the sum of four different and independent contributions, for which a suitable interpretation in terms of Feynman graphs has been provided.

It has to be noticed that our model is valid in the hypothesis of time-reversal and spherical symmetry. This condition is, in principle, not fulfilled by an odd nucleus, since the odd-particle (or hole) breaks the symmetries of the even-even core. For this reason we have adopted (in building the HF-RPA basis for the calculation) the equal filling approximation (EFA), according to which the unpaired nucleon is distributed among all possible angular momentum projections with equal probability, thus preserving the symmetries of the system.

The OPVC model has been implemented to analyze the dipole response in ^{67}Ni and ^{69}Ni. The nuclear problem has been solved, at the mean field level, with a Hartree-Fock calculation employing two effective Skyrme interactions: SLy5, which is a standard force fitted on pure neutron matter properties, and SkI3, which mimics relativistic RMF calculations and, thus, among other things, predicts a stiffer equation of state (i.e., a larger slope at nuclear saturation). A set of random phase approximation equations for the even-even core, modified to take care of the equal filling approximation, have then been solved to obtain the complete core vibrational spectrum. As an effect of the screening due to the Pauli blocking, the RPA-EFA dipole response of the core has been found to be up-shifted of about 100 and 150 keV, respectively, in ^{67}Ni and ^{69}Ni, with respect to the common RPA response.

First, the calculation of the strength function for dipole excitations in ^{67}Ni and ^{69}Ni has been evaluated in the zero-coupling limit. In this case, the total strength function is just the sum of the core response and of the single-particle contribution associated to odd-nucleon excitations. We have found that, as expected, the single-particle contribution is almost negligible with respect to that of the core, expecially in the case of ^{67}Ni. In the case of ^{69}Ni, a somewhat bigger enhancement has been found in the low-lying region of the excitation spectrum. The main source of modification with respect to ^{68}Ni, both in the two nuclei and for the two interactions, turns out to be the energy-shift related to the EFA.

The complete calculation within the OPVC model provides different results: in the case of ^{67}Ni, the dipole spectrum is down-shifted of about 850 keV with respect to that of ^{68}Ni, while, in the case of ^{69}Ni, it appears to be up-shifted of about 950 keV. The main reason has been found in the level shifting caused by the coupling and involving single-nucleon states close to the Fermi surface. The coupling with different states, in fact, induces a down-shift and an up-shift in single-nucleon states in ^{67}Ni and ^{69}Ni, respectively. This is a common feature of particle-vibration coupling calculations, whose effect, as a rule, is to down-shift particle states and to up-shifts hole states. Moreover, the ground state of the odd nucleus correspond, in the zero-coupling limit, to single-nucleon states close to the Fermi surface, which are much affected by the level shifting. The net effect of the coupling for the dipole response is, thus, a modification of the ground state energy of ^{67}Ni and ^{69}Ni, and, thus, a shift in the excitation spectrum. This result is almost independent of the choice of the Skyrme interaction. We have also demonstrated that it is possible to predict the order of magnitude of the single-nucleon level shifting just considering the coupling with low-lying nucleon-plus-vibration states in which the phonon is a highly collective 2^+ or 3^- vibration.

The result of our calculation in the case of ^{67}Ni is in good agreement with experimental results. The pygmy dipole structure shifting in the excitation spectrum of ^{67}Ni is, thus, theoretically explained as an effect of the coupling between the odd-nucleon and the core vibrations. As our argument explaining the level shifting is quite general, and not strictly dependent on the odd nucleus under investigation, we expect a similar shift of the spectrum to be a common feature of odd nuclei in different mass regions. Thus, we expect that all odd nuclei obtained by adding a hole to a doubly-magic core will show a down-shift of the excitation spectrum with respect to that of the core. This conclusion is confirmed by the experimental data in ^{131}Sn and neighboring doubly-magic ^{132}Sn.

As possible improvements to the present work, it could be of interest to implement the calculation also for nuclei in other mass regions, for example to odd-neighbors of ^{132}Sn and ^{208}Pb, so as to check if the energy shift of the spectrum with respect to the even-even core is lower or higher than that characterizing ^{67}Ni and ^{69}Ni. As further perspectives for the model itself, it would be useful to determine analytical sum rules which would help to understand the physics underlying the odd nuclei problem.

Appendix A

Angular Momentum

In this appendix we briefly expose some important concepts and relations concerning angular momentum. For a wider review, refer to [BS62] or [VMK88]; phase conventions are consistent with [BM69] and [BM75].

A.1 Coupling of angular momenta

A.1.1 Coupling of two angular momenta

Clebsch-Gordan coefficients

If two components in the system have angular momenta j_1 and j_2, the coupling of these two components may produce states with resultant angular momentum

$$J = |j_1 - j_2|, |j_1 - j_2| + 1, \cdots, j_1 + j_2. \tag{A.1}$$

The coupled states JM can be written in the form

$$|j_1 j_2\rangle_{(j_1 j_2)JM} = \sum_{m_1 m_2} \langle j_1 m_1 j_2 m_2 | JM\rangle |j_1 m_1, j_2 m_2\rangle \tag{A.2}$$

where the expansion coefficients, $\langle j_1 m_1 j_2 m_2 | JM\rangle$, are referred to as *Clebsch-Gordan* (CG) *coefficients*.

The CG coefficients obey the orthogonality relations

$$\sum_{m_1 m_2} \langle j_1 m_1 j_2 m_2 | JM\rangle \langle j_1 m_1 j_2 m_2 | J'M'\rangle = \delta_{J,J'}\delta_{M,M'} \tag{A.3}$$

$$\sum_{JM} \langle j_1 m_1 j_2 m_2 | JM\rangle \langle j_1 m_1' j_2 m_2' | JM\rangle = \delta_{m_1,m_1'}\delta_{m_2,m_2'} \tag{A.4}$$

and possess several important symmetry properties:

$$\begin{aligned}
\langle j_1 m_1 j_2 m_2 | j_3 m_3\rangle &= (-1)^{j_1+j_2-j_3} \langle j_1 - m_1 j_2 - m_2 | j_3 - m_3\rangle && \text{(A.5)}\\
&= (-1)^{j_1+j_2-j_3} \langle j_2 m_2 j_1 m_1 | j_3 m_3\rangle && \text{(A.6)}\\
&= (-1)^{j_1-m_1} \sqrt{\frac{2j_3+1}{2j_2+1}} \langle j_1 m_1 j_3 - m_3 | j_2 - m_2\rangle && \text{(A.7)}\\
&= (-1)^{j_2+m_2} \sqrt{\frac{2j_3+1}{2j_1+1}} \langle j_3 - m_3 j_2 m_2 | j_1 - m_1\rangle; && \text{(A.8)}
\end{aligned}$$

special cases of CG coefficients are

$$\langle j_1 m_1 j_2 m_2 | 00 \rangle = (-1)^{j_1 - m_1} \frac{1}{\sqrt{2j_1+1}} \delta_{j_1,j_2} \delta_{m_1,-m_2} \tag{A.9}$$

$$\langle j_1 m_1 00 | j_2 m_2 \rangle = \delta_{j_1,j_2} \delta_{m_1,m_2} \tag{A.10}$$

We have assumed the CG coefficients to be real quantities, as it is implied by the phase convention

$$\mathcal{R}\mathcal{T}|jm\rangle = |jm\rangle \tag{A.11}$$

where $\mathcal{R}$ and $\mathcal{T}$ are, respectively, the rotation operator $\mathcal{R}_y(\pi)$ and the time reversal operator (see below).

Wigner 3-j symbols

Wigner 3-j symbols are defined in relation with CG coefficients as

$$\langle a\alpha b\beta | c - \gamma \rangle = (-1)^{a-b-\gamma} \sqrt{2c+1} \begin{pmatrix} a & b & c \\ \alpha & \beta & \gamma \end{pmatrix}. \tag{A.12}$$

They obey the following orthogonality relations

$$\sum_{\alpha\beta} (2c+1) \begin{pmatrix} a & b & c \\ \alpha & \beta & \gamma \end{pmatrix} \begin{pmatrix} a & b & c' \\ \alpha & \beta & \gamma' \end{pmatrix} = \delta_{cc'} \delta_{\gamma\gamma'} \tag{A.13}$$

$$\sum_{c\gamma} (2c+1) \begin{pmatrix} a & b & c \\ \alpha & \beta & \gamma \end{pmatrix} \begin{pmatrix} a & b & c \\ \alpha' & \beta' & \gamma \end{pmatrix} = \delta_{\alpha\alpha'} \delta_{\beta\beta'} \tag{A.14}$$

and are invariant under interchange of rows and columns (reflection about diagonals), and are multiplied by $(-1)^{a+b+c}$ upon interchange of two adjacent rows or columns. In particular this means that

$$\begin{pmatrix} a & b & c \\ -\alpha & -\beta & -\gamma \end{pmatrix} = (-1)^{a+b+c} \begin{pmatrix} a & b & c \\ \alpha & \beta & \gamma \end{pmatrix} \tag{A.15}$$

and that the 3-j is invariant under cyclic permutation of its columns and multiplied by $(-1)^{a+b+c}$ by non-cyclic ones

$$\begin{pmatrix} a & b & c \\ \alpha & \beta & \gamma \end{pmatrix} = \begin{pmatrix} b & c & a \\ \beta & \gamma & \alpha \end{pmatrix} = (-1)^{a+b+c} \begin{pmatrix} b & a & c \\ \beta & \alpha & \gamma \end{pmatrix}. \tag{A.16}$$

A.1.2 Coupling of three angular momenta

Racah coefficients

Three angular momenta $\mathbf{j}_1$,$\mathbf{j}_2$ and $\mathbf{j}_3$ can be coupled in several ways to a resultant $\mathbf{J}$. Thus, we can first perform the coupling $\mathbf{j}_1 + \mathbf{j}_2 = \mathbf{J}_{12}$ and subsequently $\mathbf{J}_{12} + \mathbf{j}_3 = \mathbf{J}$; another possibility is $\mathbf{j}_2 + \mathbf{j}_3 = \mathbf{J}_{23}$ followed by $\mathbf{j}_1 + \mathbf{J}_{23} = \mathbf{J}$. The transformation between these two coupling schemes

$$\begin{aligned} |j_1 j_2 j_3\rangle_{(j_1 j_2) J_{12}, j_3; JM} &= \sum_{m_1 m_2 m_3 M_{12}} \langle j_1 m_1 j_2 m_2 | J_{12} M_{12} \rangle \langle J_{12} M_{12} j_3 m_3 | JM \rangle \\ &\quad \times |j_1 m_1, j_2 m_2, j_3 m_3\rangle \\ &= \sum_{J_{23}} \langle j_1, (j_2 j_3) J_{23}; J | (j_1 j_2) J_{12}, j_3; J \rangle |j_1 j_2 j_3\rangle_{j_1, (j_2 j_3) J_{23}; JM} \end{aligned} \tag{A.17}$$

involves a set of expansion coefficients referred to as *recoupling coefficients* or *Racah coefficients*, $\langle j_1, (j_2 j_3) J_{23}; J | (j_1 j_2) J_{12}, j_3; J \rangle$.

6-j symbols

The Racah coefficients possess a number of symmetry properties, which are conveniently expressed in terms of the *6-j symbols* defined by

$$\langle j_1,(j_2j_3)J_{23};J|(j_1j_2)J_{12},j_3;J\rangle = (-1)^{j_1+j_2+j_3+J}\sqrt{2J_{12}+1}\sqrt{2J_{23}+1}\begin{Bmatrix} j_1 & j_2 & J_{12} \\ j_3 & J & J_{23}\end{Bmatrix}. \tag{A.18}$$

The 6-j symbol is invariant under the interchange of any two columns, and also for interchange of the upper and lower arguments in each of any two columns. Besides, given the 6-j symbol $\begin{Bmatrix} a & b & c \\ d & e & f\end{Bmatrix}$, four triangular coupling condition have to be satisfied: $[abc]$, $[aef]$, $[dbf]$, $[dec]$.

If one of the six angular momenta vanishes, the 6-j symbol reduces to

$$\begin{Bmatrix} j_1 & j_2 & j_3 \\ j_2 & j_1 & 0\end{Bmatrix} = (-1)^{j_1+j_2+j_3}\frac{1}{\sqrt{(2j_1+1)(2j_2+1)}}. \tag{A.19}$$

The following sum rules hold for 6-j symbols:

$$\sum_k (-1)^{2k}(2k+1)\begin{Bmatrix} a & b & k \\ a & b & f\end{Bmatrix} = 1 \tag{A.20}$$

$$\sum_k (-1)^{a+b+k}(2k+1)\begin{Bmatrix} a & b & k \\ b & a & f\end{Bmatrix} = \delta_{f0}\sqrt{2a+1}\sqrt{2b+1} \tag{A.21}$$

$$\sum_k (2k+1)(2f+1)\begin{Bmatrix} a & b & k \\ c & d & f\end{Bmatrix}\begin{Bmatrix} a & b & k \\ c & d & g\end{Bmatrix} = \delta_{fg} \tag{A.22}$$

$$\sum_k (-1)^{f+g+k}(2k+1)\begin{Bmatrix} a & b & k \\ c & d & f\end{Bmatrix}\begin{Bmatrix} a & b & k \\ d & c & g\end{Bmatrix} = \begin{Bmatrix} a & d & f \\ b & c & g\end{Bmatrix}. \tag{A.23}$$

6-j symbols and Wigner 3-j symbols are related by some contraction rules:

$$\sum_{\alpha\beta\gamma\alpha'\beta'} (-1)^{A+B+C+\alpha+\beta+\gamma}\begin{pmatrix} A & B & c \\ \alpha & -\beta & \gamma'\end{pmatrix}\begin{pmatrix} B & C & a \\ \beta & -\gamma & \alpha'\end{pmatrix}\begin{pmatrix} C & A & b \\ \gamma & -\alpha & \beta'\end{pmatrix}\begin{pmatrix} a & b & c_1 \\ \alpha' & \beta' & \gamma_1'\end{pmatrix} = \frac{1}{2c+1}\delta_{cc_1}\delta_{\gamma'\gamma_1'}\begin{Bmatrix} a & b & c \\ A & B & C\end{Bmatrix} \tag{A.24}$$

$$\sum_{\alpha\beta\gamma} (-1)^{A+B+C+\alpha+\beta+\gamma}\begin{pmatrix} A & B & c \\ \alpha & -\beta & \gamma'\end{pmatrix}\begin{pmatrix} B & C & a \\ \beta & -\gamma & \alpha'\end{pmatrix}\begin{pmatrix} C & A & b \\ \gamma & -\alpha & \beta'\end{pmatrix} = \begin{pmatrix} a & b & c \\ \alpha' & \beta' & \gamma'\end{pmatrix}\begin{Bmatrix} a & b & c \\ A & B & C\end{Bmatrix} \tag{A.25}$$

A.1.3 Coupling of four angular momenta

Recoupling coefficients

Four angular momenta can be coupled in many different ways, such as

$$\begin{array}{lll} \mathbf{j}_1+\mathbf{j}_2=\mathbf{J}_{12} & \mathbf{j}_3+\mathbf{j}_4=\mathbf{J}_{34} & \mathbf{J}_{12}+\mathbf{J}_{34}=\mathbf{J} \\ \mathbf{j}_1+\mathbf{j}_3=\mathbf{J}_{13} & \mathbf{j}_2+\mathbf{j}_4=\mathbf{J}_{24} & \mathbf{J}_{13}+\mathbf{J}_{24}=\mathbf{J}\end{array}$$

The transformation between these two coupling schemes involves recoupling coefficients depending on nine angular momenta,

$$|j_1j_2j_3j_4\rangle_{(j_1j_2)J_{12},(j_3j_4)J_{34};JM} = \sum_{J_{23}J_{34}}\langle(j_1j_3)J_{13},(j_2j_4)J_{24};J|(j_1j_2)J_{12},(j_3j_4)J_{34};J\rangle|j_1j_2j_3j_4\rangle_{(j_1j_3)J_{13},(j_2j_4)J_{24};JM} \tag{A.26}$$

9-j symbols

It is often convenient to express the coefficients associated with the recoupling of four angular momenta in terms of the *9-j symbols*, defined by

$$\begin{aligned}&\langle (j_1 j_2) J_{12}, (j_3 j_4) J_{34}; J | (j_1 j_3) J_{13}, (j_2 j_4) J_{24}; J \rangle \\ &\quad = \sqrt{(2J_{12}+1)(2J_{34}+1)(2J_{13}+1)(2J_{24}+1)} \begin{Bmatrix} j_1 & j_2 & J_{12} \\ j_3 & j_4 & J_{34} \\ J_{13} & J_{24} & J \end{Bmatrix}. \end{aligned} \tag{A.27}$$

The 9-j symbol has a simple permutation symmetry. Thus, any even permutation of rows or columns, or a transposition (replacement of rows by columns) leaves the 9-j symbol invariant, while an odd permutation of rows or columns induces a phase factor $(-1)^{\Sigma}$, where Σ is the sum of all the nine angular momenta.

If one of the j values vanishes, the 9-j symbol reduces to a 6-j symbol,

$$\begin{Bmatrix} j_1 & j_2 & j_3 \\ j_4 & j_5 & j_3 \\ j_6 & j_6 & 0 \end{Bmatrix} = (-1)^{j_2+j_3+j_4+j_6} \frac{1}{\sqrt{(2j_3+1)(2j_6+1)}} \begin{Bmatrix} j_1 & j_2 & j_3 \\ j_5 & j_4 & j_6 \end{Bmatrix} \tag{A.28}$$

A.2 Spherical tensors and reduced matrix elements

A.2.1 Definition of spherical tensors

Any rotation $\mathcal{R}$ through an angle α about an axis $\mathbf{n}$ can be represented as a function of the generator of rotation, the angular momentum operator $\mathbf{J}$:

$$\mathcal{R}_{\mathbf{n}}(\alpha) = e^{-i(\mathbf{J}\cdot\mathbf{n})\alpha}. \tag{A.29}$$

No rotation can change the magnitude of j: starting from a state $|jm\rangle$ and applying various finite rotations we are always confined to the family of states with different m and same j. Thus, any state $|jm\rangle$ transforms under rotation $\mathcal{R}$ into a superposition of the states belonging to the same multiplet of $|jm\rangle$. This fact can be written explicitly as

$$\mathcal{R}|jm\rangle = \sum_{m'} \mathcal{D}^{j}_{m'm}(\mathcal{R}) |jm'\rangle \tag{A.30}$$

where

$$\mathcal{D}^{j}_{m'm}(\mathcal{R}) = \langle jm'|\mathcal{R}|jm\rangle \tag{A.31}$$

are the matrix element of the finite rotation $\mathcal{R}$ in a given representation. The unitarity of rotations implies the unitarity of $\mathcal{D}^j$ matrices (*Wigner matrices*), $(\mathcal{D}^j)^\dagger = (\mathcal{D}^j)^{-1}$. In algebraic terms, the $\mathcal{D}^j$ matrices give a unitary representation of the rotation group of dimension $2j+1$; the representation $\mathcal{D}^j$ is also irreducible: the multiplet $|jm\rangle$ does not contain any smaller subset of states that transform only within this subset under all rotations.

The operators can be classified by their behavior under rotations: the set of $2\lambda+1$ operators $T_{\lambda\mu}$, where λ is an integer of half-integer and $\mu = -\lambda, -\lambda+1, \ldots, \lambda$, is said to form a *spherical tensor* of rank λ if the operators of the set are transformed under rotations according to the same rules (A.30) as the state vectors $|jm\rangle$,

$$\mathcal{R} T_{\lambda\mu} \mathcal{R}^{-1} = \sum_{\mu'} \mathcal{D}^{\lambda}_{\mu'\mu}(\mathcal{R}) T_{\lambda\mu'}. \tag{A.32}$$

Equivalently, one can also characterize operators by the amount of angular momentum they transfer to the state on which they act. In this picture, a spherical tensor of rank λ is a set of operators $T_{\lambda\mu}$ transferring an angular momentum λ with the different component μ.

A tensor of rank $\lambda = 0$ is a rotational invariant (a scalar); a vector $\mathbf{v}$, instead, is a spherical tensor of rank $\lambda = 1$. Further examples of tensors are the spherical harmonics $Y_{\lambda\mu}(\vartheta, \phi)$, which are tensors of rank λ. In particular, any operator can be expanded in a series of spherical harmonics: for example, the electric multipole moments are the tensors resulting from the expansion of the electric charge density.

A.2.2 Wigner-Eckhart theorem

The *Wigner-Eckhart Theorem* states that the dependence of the matrix element of an operator $T_{\lambda\mu}$ between two states $|j_2 m_2\rangle$ and $|j_1 m_1\rangle$, namely $\langle j_2 m_2|T_{\lambda\mu}|j_1 m_1\rangle$, on the magnetic quantum numbers μ, m_1 and m_2 is given entirely by a CG coefficient. In particular

$$\langle j_2 m_2|T_{\lambda\mu}|j_1 m_1\rangle = \frac{1}{\sqrt{2j_2+1}}\langle j_1 m_1 \lambda\mu|j_2 m_2\rangle\langle j_2||T_\lambda||j_1\rangle \tag{A.33}$$

and this expression defines the *reduced matrix element* $\langle j_2||T_\lambda||j_1\rangle$. Besides

$$\langle j_2||T_\lambda||j_1\rangle = \sqrt{2j_2+1}\sum_{m_1\mu}\langle j_1 m_1 \lambda\mu|j_2 m_2\rangle\langle j_2 m_2|T_{\lambda\mu}|j_1 m_1\rangle \tag{A.34}$$

$$= \frac{1}{\sqrt{2j_2+1}}\sum_{m_1 m_2 \mu}\langle j_1 m_1 \lambda\mu|j_2 m_2\rangle\langle j_2 m_2|T_{\lambda\mu}|j_1 m_1\rangle. \tag{A.35}$$

A.2.3 Reduced probability for nuclear transitions

A nuclear transition $j_1 \to j_2$ involving the transfer of angular momentum λ can be described in terms of a transition operator $T_{\lambda\mu}$, such that the transition amplitudes are proportional to the matrix element (A.33). The total transition probability, summed over μ and over the polarization m_2 of the final state, is independent of m_1 and given by the *reduced transition probability*

$$B(T_\lambda; j_1 \to j_2) = \sum_{\mu m_2}|\langle j_2 m_2|T_{\lambda\mu}|j_1 m_1\rangle|^2. \tag{A.36}$$

Averaging over initial states, we get

$$B(T_\lambda; j_1 \to j_2) = \frac{1}{2j_1+1}\sum_{\mu m_1 m_2}|\langle j_2 m_2|T_{\lambda\mu}|j_1 m_1\rangle|^2; \tag{A.37}$$

applying now the Wigner-Eckhart theorem and the orthogonality relations for CG coefficients, we obtain

$$B(T_\lambda; j_1 \to j_2) = \frac{1}{2j_1+1}|\langle j_2||T_\lambda||j_1\rangle|^2. \tag{A.38}$$

For the inverse transition, $j_2 \to j_1$, we have

$$B(T_\lambda; j_2 \to j_1) = \frac{2j_1+1}{2j_2+1}B(T_\lambda; j_1 \to j_2) \tag{A.39}$$

since the absolute value of the reduced matrix element is invariant under the interchange of j_1 and j_2 (see Eq.(A.48)); the relation (A.39) expresses detailed balance for reaction rates averaged over polarization.

The *strength function* associated with the transitions from the initial state j_1 is defined as

$$S(E) = \sum_{j_2}\frac{|\langle j_2||T_\lambda||j_1\rangle|^2}{2j_1+1}\delta(E-(E_2-E_1)) = \sum_{j_2}B(T_\lambda; j_1 \to j_2)\delta(E-(E_2-E_1)) \tag{A.40}$$

A.2.4 Transformation under time reversal and Hermitian conjugation

The reduced matrix element is, in general, a complex number. Its phase is related to the transformation of $T_{\lambda\mu}$ under time reversal. Since the time reversal transformation, $\mathcal{T}$, inverts angular momenta, it transforms $T_{\lambda\mu}$ into a tensor of components $\lambda,-\mu$. It is thus convenient to consider the combined transformation $\mathcal{RT}$, where $\mathcal{R}$ is now the rotation $\mathcal{R}_y(\pi)$. Usually, the tensors encountered transform into themselves under $\mathcal{RT}$, except for a phase factor

$$\mathcal{RT}T_{\lambda\mu}(\mathcal{RT})^{-1} = c_{\mathcal{T}}T_{\lambda\mu}. \tag{A.41}$$

Eq.(A.41) is equivalent to

$$\mathcal{T}T_{\lambda\mu}\mathcal{T} = c_{\mathcal{T}}(-1)^{\lambda+\mu}T_{\lambda-\mu}. \tag{A.42}$$

The phase factor $c_{\mathcal{T}}$ is not an intrinsic property of T_λ, since it depends on the phase of the operator. Thus, by multiplying T_λ with a suitable phase factor, we can always achieve $c_{\mathcal{T}} = +1$. For example, in the case of electromagnetic multipoles, $c_{\mathcal{T}} = +1$ is obtained by multiplying electric moments by i^λ and magnetic moments by $i^{\lambda-1}$.

If we assume that the nuclear states are phased according to Eq.(A.11), we obtain that

$$\langle j_2||T_\lambda||j_1\rangle^* = c_{\mathcal{T}}\langle j_2||T_\lambda||j_1\rangle. \tag{A.43}$$

Thus, the phase choice leading to $c_{\mathcal{T}} = +1$ implies that all matrix elements are real.

The symmetry of the reduced matrix element with respect to the interchange of initial and final states is related to the behavior of $T_{\lambda\mu}$ under Hermitian conjugation. The Hermitian conjugate $T^\dagger_{\lambda\mu}$ of a spherical tensor removes the angular momentum $\lambda\mu$ from the state on which it acts, and the operator

$$T^{\mathcal{H}}_{\lambda\mu} \equiv (-1)^{\lambda+\mu}(T_{\lambda-\mu})^\dagger \tag{A.44}$$

is thus again a spherical tensor. From Eq.(A.33), we obtain

$$\langle j_1||T^{\mathcal{H}}_\lambda||j_2\rangle = (-1)^{j_1+\lambda-j_2}\langle j_2||T_\lambda||j_1\rangle^*. \tag{A.45}$$

If $T_{\lambda\mu}$ is self-adjoint, that is, if

$$T_{\lambda\mu} = c_{\mathcal{H}}T^{\mathcal{H}}_{\lambda\mu}, \tag{A.46}$$

the relation (A.45) can be written

$$\langle j_1||T_\lambda||j_2\rangle = c_{\mathcal{H}}(-1)^{j_1+\lambda-j_2}\langle j_2||T_\lambda||j_1\rangle^*. \tag{A.47}$$

Combining eqs. (A.47) and (A.43), we obtain

$$\langle j_1||T_\lambda||j_2\rangle = -c(-1)^{j_1+\lambda-j_2}\langle j_2||T_\lambda||j_1\rangle \tag{A.48}$$

where

$$c = -c_{\mathcal{T}}c_{\mathcal{H}}. \tag{A.49}$$

While $c_{\mathcal{T}}$ and $c_{\mathcal{H}}$ depend on the phase of $T_{\lambda\mu}$ and may take complex values, the product c is independent on the overall phase of $T_{\lambda\mu}$ and equals $+1$ or -1. Examples of operators with $c = -1$ are $F(\mathbf{r})$ and $(\mathbf{l}\cdot\mathbf{s})F(\mathbf{r})$, whereas operators with $c = +1$ are $\mathbf{s}F(\mathbf{r})$ or $\mathbf{l}$.

Thus, if $F_\lambda = i^\lambda Y_\lambda$,

$$\langle j_1||i^\lambda Y_\lambda||j_2\rangle = (-1)^{j_1+\lambda-j_2}\langle j_2||i^\lambda Y_\lambda||j_1\rangle \tag{A.50}$$

A.2.5 Tensor properties of particle and hole creation operators

Let us consider a nuclear system in which the single-particle states jm are labelled by their energy, ϵ_j. In this system we define the *normal state* (or *ground state*) as the configuration in which the particles occupy all the lowest possible energy levels, i.e. the state with lowest total energy. We can talk about *occupation number* for a single-particle orbit, that is, if the single-particle states are occupied or not.

The states obtained by adding a particle in an unfilled orbit (zero occupancy) are represented by $a^\dagger_{jm}|0\rangle$, where $a^\dagger_{jm}$ is the particle creation operator, while $|0\rangle$ is the ground state of the system; these states are referred to as *particle states*. The transformation of $a^\dagger_{jm}$ under time reversal is given by

$$\mathcal{T} a^\dagger_{jm} \mathcal{T}^{-1} = a^\dagger_{\widetilde{jm}} = (-1)^{j+m} a^\dagger_{j-m}; \tag{A.51}$$

the matrix elements of $a^\dagger_{jm}$ are real in a representation with the phase convention (A.11).

The Hermitian conjugate of $a^\dagger_{jm}$ is the annihilation operator a_{jm}, from which we can construct the tensor

$$b^\dagger_{jm} \equiv a_{\widetilde{jm}} = (-1)^{j+m} a_{j-m}. \tag{A.52}$$

The operator $b^\dagger_{jm}$ acts on the ground state removing a particle in the state $j-m$, that is, creating a hole in the state jm. The states $b^\dagger_{jm}|0\rangle$ are referred to as *hole states*.

From Eq.(A.45) we thus obtain

$$\langle j_2||a_{\widetilde{j}}||j_1\rangle = \langle j_2||b^\dagger_j||j_1\rangle = (-1)^{j_2+j-j_1}\langle j_1||a^\dagger_j||j_2\rangle. \tag{A.53}$$

From products of $a^\dagger$ and a operators, one can form the spherical tensors

$$F_{\lambda\mu} = a^\dagger_{j_2} a_{\widetilde{j_1}\,(j_1 j_2)\lambda\mu} = a^\dagger_{j_2} b^\dagger_{j_1\,(j_1 j_2)\lambda\mu}. \tag{A.54}$$

These are unit tensor operators from which arbitrary one-particle operators can be constructed, as is the case of phonon creation and destruction operators $\Gamma^\dagger$ and Γ (see Chapter 3.2).

A.3 One-particle wave functions and matrix elements

A.3.1 One particle wave functions

The wave function for a particle with spin $s = \frac{1}{2}$ moving in a spherically symmetric and parity-conserving potential can be written in the form

$$\begin{aligned}\phi_i(\mathbf{r},\sigma,\tau) &= \frac{u_\alpha(r)}{r}[i^l Y_l(\hat{r})\chi_{\frac{1}{2}}(\sigma)]_{(l\frac{1}{2})jm}\chi_q(\tau) \\ &= \frac{u_\alpha(r)}{r}\sum_{m_l m_s}\langle l m_l \frac{1}{2} m_s|jm\rangle i^l Y_{lm_l}(\hat{r})\chi_{\frac{1}{2}m_s}(\sigma)\chi_q(\tau).\end{aligned} \tag{A.55}$$

In the previous equation, the indexes i and α stands for the sets of quantum numbers $i \equiv q,n,l,j,m$ and $\alpha \equiv q,n,l,j$: q is the isospin quantum number, n is the principal quantum number, l the orbital angular momentum, j the total angular momentum and m is the projection of the total angular momentum upon the z-axis. Finally, $\chi_{\frac{1}{2}m_s}$ and χ_q are the two-component spinor and isospin, respectively. The factor i^l has been inserted in Eq.(A.55) in order to ensure the standard transformation under time reversal,

$$\mathcal{T}|nljm\rangle = (-1)^{j+m}|nlj-m\rangle. \tag{A.56}$$

The radial function may be taken to be real (for a time-reversal invariant potential), and we choose the phase in such a manner that u is positive for large r (for r greater than the outermost nodal point).

A.3.2 Evaluation of matrix elements for one-particle operators

A tensor operator depending only on the position $\mathbf{r}$ of a particle has the general form

$$T_{\lambda\mu} = i^\lambda f(r) Y_{\lambda\mu}(\vartheta,\phi). \tag{A.57}$$

For a self-adjoint tensor (which transforms into itself under Hermitian conjugation), the radial function $f(r)$ may be taken to be real. We have added the factor i^λ so as to obtain the phase factor $c_{\mathcal{T}} = c_{\mathcal{H}} = 1$ for time reversal and Hermitian conjugation and in order the matrix elements of $T_{\lambda\mu}$ to be real (see Section A.2.4).

The reduced matrix element of $T_{\lambda\mu}$ is

$$\begin{aligned}\langle n_2 l_2 j_2 || i^\lambda f(r) Y_{\lambda\mu} || n_1 l_1 j_1 \rangle = i^{l_1+\lambda-l_2}(-1)^{j_1+\lambda-j_2}\sqrt{\frac{(2\lambda+1)(2j_1+1)}{4\pi}} \\ \times \langle j_1 \frac{1}{2} \lambda 0 | j_2 \frac{1}{2} \rangle \langle j_2 | f | j_1 \rangle \begin{cases} 1 & \text{if } l_1+\lambda-l_2 \quad \text{even} \\ 0 & \text{if } l_1+\lambda-l_2 \quad \text{odd} \end{cases}\end{aligned} \tag{A.58}$$

with the radial matrix element

$$\langle j_2 | f | j_1 \rangle = \int_0^\infty u_{n_2 l_2 j_2}(r) f(r) u_{n_1 l_1 j_1} dr. \tag{A.59}$$

Appendix B

Explicit calculation of the OPVC reduced transition matrix element

In this Appendix we will derive the expression for the OPVC reduced transition matrix element (4.18) for the odd nucleus in the microscopic Hartree-Fock (see Section 3.1) and Random Phase Approximation (see Section 3.2) context.

The matrix element from which we have to start, $\langle \nu_2 l_2 j_2 m_2 | F_{\lambda\mu} | \nu_1 l_1 j_1 m_1 \rangle$ is, by definition (see Chapter 4),

$$
\begin{aligned}
\langle \nu_2 l_2 j_2 m_2 | F_{\lambda\mu} | \nu_1 l_1 j_1 m_1 \rangle &= \langle 0 | c_{\nu_2 l_2 j_2 m_2} F_{\lambda\mu} c^\dagger_{\nu_1 l_1 j_1 m_1} | 0 \rangle \\
&= \langle 0 | \left\{ \sum_{n_2} \mathcal{A}^{\nu_2 l_2 j_2}_{n_2} \left[d^\dagger_{n_2 l_2 j_2} \otimes \mathbb{I} \right]^\dagger_{j_2 m_2} + \sum_{n'_2 l'_2 j'_2 \xi_2 L_2} \mathcal{B}^{\nu_2 l_2 j_2}_{n'_2 l'_2 j'_2 \xi_2 L_2} \left[d^\dagger_{n'_2 l'_2 j'_2} \otimes \Gamma^\dagger_{\xi_2}(L_2) \right]^\dagger_{j_2 m_2} \right\} F_{\lambda\mu} \\
&\quad \times \left\{ \sum_{n_1} \mathcal{A}^{\nu_1 l_1 j_1}_{n_1} \left[d^\dagger_{n_1 l_1 j_1} \otimes \mathbb{I} \right]_{j_1 m_1} + \sum_{n'_1 l'_1 j'_1 \xi_1 L_1} \mathcal{B}^{\nu_1 l_1 j_1}_{n'_1 l'_1 j'_1 \xi_1 L_1} \left[d^\dagger_{n'_1 l'_1 j'_1} \otimes \Gamma^\dagger_{\xi_1}(L_1) \right]_{j_1 m_1} \right\} | 0 \rangle \\
&= \sum_{n_2} \sum_{n_1} \mathcal{A}^{\nu_2 l_2 j_2}_{n_2} \mathcal{A}^{\nu_1 l_1 j_1}_{n_1} \langle 0 | \left[d^\dagger_{n_2 l_2 j_2} \otimes \mathbb{I} \right]^\dagger_{j_2 m_2} F_{\lambda\mu} \left[d^\dagger_{n_1 l_1 j_1} \otimes \mathbb{I} \right]_{j_1 m_1} | 0 \rangle \\
&\quad + \sum_{n_2} \sum_{n'_1 l'_1 j'_1 \xi_1 L_1} \mathcal{A}^{\nu_2 l_2 j_2}_{n_2} \mathcal{B}^{\nu_1 l_1 j_1}_{n'_1 l'_1 j'_1 \xi_1 L_1} \langle 0 | \left[d^\dagger_{n_2 l_2 j_2} \otimes \mathbb{I} \right]^\dagger_{j_2 m_2} F_{\lambda\mu} \left[d^\dagger_{n'_1 l'_1 j'_1} \otimes \Gamma^\dagger_{\xi_1}(L_1) \right]_{j_1 m_1} | 0 \rangle \\
&\quad + \sum_{n'_2 l'_2 j'_2 \xi_2 L_2} \sum_{n_1} \mathcal{B}^{\nu_2 l_2 j_2}_{n'_2 l'_2 j'_2 \xi_2 L_2} \mathcal{A}^{\nu_1 l_1 j_1}_{n_1} \langle 0 | \left[d^\dagger_{n'_2 l'_2 j'_2} \otimes \Gamma^\dagger_{\xi_2}(L_2) \right]^\dagger_{j_2 m_2} F_{\lambda\mu} \left[d^\dagger_{n_1 l_1 j_1} \otimes \mathbb{I} \right]_{j_1 m_1} | 0 \rangle \\
&\quad + \sum_{n'_2 l'_2 j'_2 \xi_2 L_2} \sum_{n'_1 l'_1 j'_1 \xi_1 L_1} \mathcal{B}^{\nu_2 l_2 j_2}_{n'_2 l'_2 j'_2 \xi_2 L_2} \mathcal{B}^{\nu_1 l_1 j_1}_{n'_1 l'_1 j'_1 \xi_1 L_1} \\
&\qquad \times \langle 0 | \left[d^\dagger_{n'_2 l'_2 j'_2} \otimes \Gamma^\dagger_{\xi_2}(L_2) \right]^\dagger_{j_2 m_2} F_{\lambda\mu} \left[d^\dagger_{n'_1 l'_1 j'_1} \otimes \Gamma^\dagger_{\xi_1}(L_1) \right]_{j_1 m_1} | 0 \rangle \qquad \text{(B.1)} \\
&\equiv \mathcal{M}_{\mathcal{AA}} + \mathcal{M}_{\mathcal{AB}} + \mathcal{M}_{\mathcal{BA}} + \mathcal{M}_{\mathcal{BB}}. \qquad \text{(B.2)}
\end{aligned}
$$

Since the Wigner-Eckhart Theorem (see Appendix A.2.2) is additive,

$$
\langle \nu_2 l_2 j_2 || F_\lambda || \nu_1 l_1 j_1 \rangle = \mathcal{M}^{red}_{\mathcal{AA}} + \mathcal{M}^{red}_{\mathcal{AB}} + \mathcal{M}^{red}_{\mathcal{BA}} + \mathcal{M}^{red}_{\mathcal{BB}} \qquad \text{(B.3)}
$$

and so we can calculate separately four reduced matrix elements and, then, sum them up to obtain the desired $\langle \nu_2 l_2 j_2 || F_\lambda || \nu_1 l_1 j_1 \rangle$.

The operator $F_{\lambda\mu}$ is a one-body operator and so

$$F_{\lambda\mu} = \sum_{im_i km_k} \langle im_i|F_{\lambda\mu}|km_k\rangle a^\dagger_{im_i} a_{km_k}. \tag{B.4}$$

In the case of the odd nucleus, this operator will act separately on the odd-nucleon and on the even-even core; thus it could be written as

$$F_{\lambda\mu} = \left[F^{odd}_\lambda \otimes \mathbb{I}^{core}\right]_{\lambda\mu} + \left[\mathbb{I}^{odd} \otimes F^{core}_\lambda\right]_{\lambda\mu} \tag{B.5}$$

B.1 Transition matrix elements for particle-plus-core odd nuclei

Let us consider first the case in which the odd nucleus is formed by an even-even core plus a particle.

The $\mathcal{M}_{\mathcal{AA}}$ term of the transition matrix element

The first term in Eq. (B.2) is simply, using Eq. (B.5) for the operator $F_{\lambda\mu}$,

$$\begin{aligned}
\mathcal{M}_{\mathcal{AA}} &= \sum_{n_2}\sum_{n_1} \mathcal{A}^{\nu_2 l_2 j_2}_{n_2} \mathcal{A}^{\nu_1 l_1 j_1}_{n_1} \langle 0_{odd}|a_{2m_2} F_{\lambda\mu} a^\dagger_{1m_1}|0_{odd}\rangle \\
&= \sum_{n_2}\sum_{n_1} \mathcal{A}^{\nu_2 l_2 j_2}_{n_2} \mathcal{A}^{\nu_1 l_1 j_1}_{n_1} \sum_{im_i km_k} \langle im_i|F_{\lambda\mu}|km_k\rangle \langle 0_{odd}|a_{2m_2} a^\dagger_{im_i} a_{km_k} a^\dagger_{1m_1}|0_{odd}\rangle \\
&\simeq \sum_{n_2}\sum_{n_1} \mathcal{A}^{\nu_2 l_2 j_2}_{n_2} \mathcal{A}^{\nu_1 l_1 j_1}_{n_1} \sum_{im_i km_k} \langle im_i|F_{\lambda\mu}|km_k\rangle \langle HF_{odd}|a_{2m_2} a^\dagger_{im_i} a_{km_k} a^\dagger_{1m_1}|HF_{odd}\rangle \\
&= \sum_{n_2}\sum_{n_1} \mathcal{A}^{\nu_2 l_2 j_2}_{n_2} \mathcal{A}^{\nu_1 l_1 j_1}_{n_1} \langle 2m_2|F_{\lambda\mu}|1m_1\rangle
\end{aligned} \tag{B.6}$$

Then, for the reduced matrix element we obtain

$$\mathcal{M}^{red}_{\mathcal{AA}} = \frac{1}{\sqrt{2j_2+1}} \sum_{m_1 m_2 \mu} \langle j_1 m_1 \lambda\mu|j_2 m_2\rangle \mathcal{M}_{\mathcal{AA}} \simeq \sum_{n_1 n_2} \mathcal{A}^{\nu_1 l_1 j_1}_{n_1} \mathcal{A}^{\nu_2 l_2 j_2}_{n_2} \langle 2||F_\lambda||1\rangle. \tag{B.7}$$

The $\mathcal{M}_{\mathcal{AB}}$ term of the transition matrix element

The second term in Eq. (B.2) is

$$\begin{aligned}
\mathcal{M}_{\mathcal{AB}} = \sum_{n_2} \sum_{n'_1 l'_1 j'_1 \xi_1 L_1} & \mathcal{A}^{\nu_2 l_2 j_2}_{n_2} \mathcal{B}^{\nu_1 l_1 j_1}_{n'_1 l'_1 j'_1 \xi_1 L_1} \sum_{m'_1 M_1} \langle j'_1 m'_1 L_1 M_1|j_1 m_1\rangle \\
& \times \langle 0|a_{2m_2} F_{\lambda\mu} a^\dagger_{1'm'_1} \Gamma^\dagger_{\xi_1}(L_1 M_1)|0\rangle.
\end{aligned} \tag{B.8}$$

Now, because of Eq. (B.5),

$$\begin{aligned}
\langle 0|a_{2m_2} F_{\lambda\mu} a^\dagger_{1'm'_1} \Gamma^\dagger_{\xi_1}(L_1 M_1)|0\rangle = & \langle 0_{odd}|a_{2m_2} F_{\lambda\mu} a^\dagger_{1'm'_1}|0_{odd}\rangle \langle 0_{core}|\Gamma^\dagger_{\xi_1}(L_1 M_1)|0_{core}\rangle \\
& + \langle 0_{odd}|a_{2m_2} a^\dagger_{1'm'_1}|0_{odd}\rangle \langle 0_{core}|F_{\lambda\mu}\Gamma^\dagger_{\xi_1}(L_1 M_1)|0_{core}\rangle.
\end{aligned} \tag{B.9}$$

Since the term $\langle 0_{core}|\Gamma^\dagger_{\xi_1}(L_1 M_1)|0_{core}\rangle$ is identically zero, just like a term $\Gamma_{\xi_1}(L_1 M_1)|0_{core}\rangle$, one can write

$$\begin{aligned}
\langle 0|a_{2m_2} F_{\lambda\mu} a^\dagger_{1'm'_1} \Gamma^\dagger_{\xi_1}(L_1 M_1)|0\rangle &= \langle 0_{odd}|a_{2m_2} a^\dagger_{1'm'_1}|0_{odd}\rangle \langle 0_{core}|\left[F_{\lambda\mu}, \Gamma^\dagger_{\xi_1}(L_1 M_1)\right]|0_{core}\rangle \\
&\simeq \langle HF_{odd}|a_{2m_2} a^\dagger_{1'm'_1}|HF_{odd}\rangle \langle RPA_{core}|\left[F_{\lambda\mu}, \Gamma^\dagger_{\xi_1}(L_1 M_1)\right]|RPA_{core}\rangle \\
&\simeq \delta_{21'} \langle RPA_{core}|\left[F_{\lambda\mu}, \Gamma^\dagger_{\xi_1}(L_1 M_1)\right]|RPA_{core}\rangle
\end{aligned} \tag{B.10}$$

Now, in RPA approximation,

$$\left[F_{\lambda\mu},\Gamma^{\dagger}_{\xi_1}(L_1M_1)\right]=\sum_{ph}X^{\xi_1L_1}_{ph}\left[F_{\lambda\mu},A^{\dagger}_{ph}(L_1M_1)\right]-Y^{\xi_1L_1}_{ph}\left[F_{\lambda\mu},A_{ph}(\widetilde{L_1M_1})\right] \tag{B.11}$$

where

$$\begin{aligned}\left[F_{\lambda\mu},A^{\dagger}_{ph}(L_1M_1)\right] &= \sum_{m_pm_h}(-1)^{j_h-m_h}\langle j_pm_pj_h-m_h|L_1M_1\rangle\left[F_{\lambda\mu},a^{\dagger}_{pm_p}a_{hm_h}\right]\\ &= \sum_{m_pm_h}(-1)^{j_h-m_h}\langle j_pm_pj_h-m_h|L_1M_1\rangle\sum_{im_ikm_k}\langle im_i|F_{\lambda\mu}|km_k\rangle\\ &\quad\times\left[a^{\dagger}_{im_i}a_{km_k},a^{\dagger}_{pm_p}a_{hm_h}\right].\end{aligned} \tag{B.12}$$

If we make the approximation that the RPA ground state of the core, $|RPA_{core}\rangle$, does not differ very much from the Hartree-Fock ground state of the core itself, $|HF_{core}\rangle$, one can write, by means of the *quasi-boson approximation*,

$$\begin{aligned}&\langle RPA_{core}|\left[a^{\dagger}_{im_i}a_{km_k},a^{\dagger}_{pm_p}a_{hm_h}\right]|RPA_{core}\rangle\\ &\quad\simeq\langle HF_{core}|\left[a^{\dagger}_{im_i}a_{km_k},a^{\dagger}_{pm_p}a_{hm_h}\right]|HF_{core}\rangle=\delta_{ih}\delta_{kp},\end{aligned} \tag{B.13}$$

and thus

$$\begin{aligned}&\langle RPA_{core}|\left[F_{\lambda\mu},A^{\dagger}_{ph}(L_1M_1)\right]|RPA_{core}\rangle\\ &\quad\simeq\sum_{m_pm_h}(-1)^{j_h-m_h}\langle j_pm_pj_h-m_h|L_1M_1\rangle\langle hm_h|F_{\lambda\mu}|pm_p\rangle.\end{aligned} \tag{B.14}$$

Similarly,

$$\begin{aligned}&\langle RPA_{core}|\left[F_{\lambda\mu},A_{ph}(\widetilde{L_1M_1})\right]|RPA_{core}\rangle\\ &\quad\simeq-\sum_{m_pm_h}(-1)^{j_h-m_h+L_1+M_1}\langle j_pm_pj_h-m_h|L_1-M_1\rangle\langle pm_p|F_{\lambda\mu}|hm_h\rangle.\end{aligned} \tag{B.15}$$

Writing down the reduced matrix element $\mathcal{M}^{red}_{\mathcal{AB}}$ with the previous approximations, we obtain

$$\begin{aligned}\mathcal{M}^{red}_{\mathcal{AB}} &= \frac{1}{\sqrt{2j_2+1}}\sum_{m_1m_2\mu}\langle j_1m_1\lambda\mu|j_2m_2\rangle\mathcal{M}_{\mathcal{AB}}\\ &\simeq\frac{1}{\sqrt{2j_2+1}}\sum_{m_1m_2\mu}\langle j_1m_1\lambda\mu|j_2m_2\rangle\sum_{n_2}\sum_{\xi_1L_1}\mathcal{A}^{\nu_2l_2j_2}_{n_2}\mathcal{B}^{\nu_1l_1j_1}_{n_2l_2j_2\xi_1L_1}\sum_{M_1}\langle j_2m_2L_1M_1|j_1m_1\rangle\\ &\quad\times\sum_{ph}\Bigg\{X^{\xi_1L_1}_{ph}\sum_{m_pm_h}(-1)^{j_h-m_h}\langle j_pm_pj_h-m_h|L_1M_1\rangle\langle hm_h|F_{\lambda\mu}|pm_p\rangle\\ &\quad+Y^{\xi_1L_1}_{ph}\sum_{m_pm_h}(-1)^{j_h-m_h+L_1+M_1}\langle j_pm_pj_h-m_h|L_1-M_1\rangle\langle pm_p|F_{\lambda\mu}|hm_h\rangle\Bigg\}.\end{aligned} \tag{B.16}$$

Now we substitute the particle-hole matrix elements with their reduced expression to obtain

$$\begin{aligned}\mathcal{M}^{red}_{\mathcal{AB}} \simeq \frac{1}{\sqrt{2j_2+1}} \sum_{m_1 m_2 \mu} \langle j_1 m_1 \lambda\mu | j_2 m_2\rangle \sum_{n_2} \sum_{\xi_1 L_1} \mathcal{A}^{\nu_2 l_2 j_2}_{n_2} \mathcal{B}^{\nu_1 l_1 j_1}_{n_2 l_2 j_2 \xi_1 L_1} \sum_{M_1} \langle j_2 m_2 L_1 M_1 | j_1 m_1\rangle \\ \times \sum_{ph} \Bigg\{ X^{\xi_1 L_1}_{ph} \sum_{m_p m_h} (-1)^{j_h - m_h} \langle j_p m_p j_h - m_h | L_1 M_1\rangle \\ \times \frac{1}{\sqrt{2j_h+1}} \langle j_p m_p \lambda\mu | j_h m_h\rangle \langle h || F_\lambda || p\rangle \\ + Y^{\xi_1 L_1}_{ph} \sum_{m_p m_h} (-1)^{j_h - m_h + L_1 + M_1} \langle j_p m_p j_h - m_h | L_1 - M_1\rangle \\ \times \frac{1}{\sqrt{2j_p+1}} \langle j_h m_h \lambda\mu | j_p m_p\rangle \langle p || F_\lambda || h\rangle \Bigg\}. \end{aligned} \tag{B.17}$$

The Clebsch-Gordan simmetries (Eqs. (A.5) to (A.8)) allow us to write

$$\langle j_1 m_1 \lambda\mu | j_2 m_2\rangle = \frac{\sqrt{2j_2+1}}{\sqrt{2\lambda+1}} (-1)^{j_1 - m_1} \langle j_1 m_1 j_2 - m_2 | \lambda - \mu\rangle \tag{B.18}$$

$$\begin{aligned}\langle j_2 m_2 L_1 M_1 | j_1 m_1\rangle &= \frac{\sqrt{2j_1+1}}{\sqrt{2L_1+1}} (-1)^{j_2 - m_2} \langle j_2 m_2 j_1 - m_1 | L_1 - M_1\rangle \\ &= \frac{\sqrt{2j_1+1}}{\sqrt{2L_1+1}} (-1)^{j_2 - m_2} (-1)^{j_2 + j_1 - L_1} \langle j_1 - m_1 j_2 m_2 | L_1 - M_1\rangle \\ &= \frac{\sqrt{2j_1+1}}{\sqrt{2L_1+1}} (-1)^{j_2 - m_2} (-1)^{j_2 + j_1 - L_1} (-1)^{j_2 + j_1 - L_1} \langle j_1 m_1 j_2 - m_2 | L_1 M_1\rangle \\ &= \frac{\sqrt{2j_1+1}}{\sqrt{2L_1+1}} (-1)^{j_2 - m_2} \langle j_1 m_1 j_2 - m_2 | L_1 M_1\rangle \end{aligned} \tag{B.19}$$

$$\langle j_p m_p \lambda\mu | j_h m_h\rangle = \frac{\sqrt{2j_h+1}}{\sqrt{2\lambda+1}} (-1)^{j_p - m_p} \langle j_p m_p j_h - m_h | \lambda - \mu\rangle \tag{B.20}$$

$$\begin{aligned}\langle j_h m_h \lambda\mu | j_p m_p\rangle &= \frac{\sqrt{2j_p+1}}{\sqrt{2\lambda+1}} (-1)^{j_h - m_h} \langle j_h m_h j_p - m_p | \lambda - \mu\rangle \\ &= \frac{\sqrt{2j_p+1}}{\sqrt{2\lambda+1}} (-1)^{j_h - m_h} (-1)^{j_h + j_p - \lambda} \langle j_p - m_p j_h m_h | \lambda - \mu\rangle \\ &= \frac{\sqrt{2j_p+1}}{\sqrt{2\lambda+1}} (-1)^{j_h - m_h} (-1)^{j_h + j_p - \lambda} (-1)^{j_h + j_p - \lambda} \langle j_p m_p j_h - m_h | \lambda\mu\rangle \\ &= \frac{\sqrt{2j_p+1}}{\sqrt{2\lambda+1}} (-1)^{j_h - m_h} \langle j_p m_p j_h - m_h | \lambda\mu\rangle \end{aligned} \tag{B.21}$$

and so

$$\begin{aligned}\mathcal{M}^{red}_{\mathcal{AB}} \simeq \frac{\sqrt{2j_1+1}}{2\lambda+1} \sum_{n_2} \sum_{\xi_1 L_1} \frac{1}{\sqrt{2L_1+1}} \mathcal{A}^{\nu_2 l_2 j_2}_{n_2} \mathcal{B}^{\nu_1 l_1 j_1}_{n_2 l_2 j_2 \xi_1 L_1} \sum_{m_1 m_2 \mu} \sum_{M_1} (-1)^{j_1 - m_1 + j_2 - m_2} \\ \times \langle j_1 m_1 j_2 - m_2 | \lambda - \mu\rangle \langle j_1 m_1 j_2 - m_2 | L_1 M_1\rangle \\ \times \sum_{ph} \Bigg\{ X^{\xi_1 L_1}_{ph} \sum_{m_p m_h} (-1)^{j_h - m_h + j_p - m_p} \langle j_p m_p j_h - m_h | L_1 M_1\rangle \\ \times \langle j_p m_p j_h - m_h | \lambda - \mu\rangle \langle h || F_\lambda || p\rangle \\ + Y^{\xi_1 L_1}_{ph} \sum_{m_p m_h} (-1)^{L_1 + M_1} \langle j_p m_p j_h - m_h | L_1 - M_1\rangle \langle j_p m_p j_h - m_h | \lambda\mu\rangle \langle p || F_\lambda || h\rangle \Bigg\}. \end{aligned} \tag{B.22}$$

The Clebsch-Gordan coefficients of the previous expression imply that $m_2 - m_1 = M_1$ and $m_p - m_h = M_1$; besides, the following orthogonality relations hold (Eq. (A.3))

$$\sum_{m_1 m_2} \langle j_1 m_1 j_2 - m_2 | \lambda - \mu \rangle \langle j_1 m_1 j_2 - m_2 | L_1 M_1 \rangle = \delta_{\lambda, L_1} \delta_{-\mu, M_1} \tag{B.23}$$

$$\sum_{m_p m_h} \langle j_p m_p j_h - m_h | L_1 M_1 \rangle \langle j_p m_p j_h - m_h | \lambda - \mu \rangle = \delta_{\lambda, L_1} \delta_{-\mu, M_1} \tag{B.24}$$

$$\sum_{m_p m_h} \langle j_p m_p j_h - m_h | L_1 - M_1 \rangle \langle j_p m_p j_h - m_h | \lambda \mu \rangle = \delta_{\lambda, L_1} \delta_{\mu, -M_1} \tag{B.25}$$

and so we get

$$\begin{aligned} \mathcal{M}^{red}_{\mathcal{AB}} \simeq & \frac{\sqrt{2j_1+1}}{(2\lambda+1)^{3/2}} \sum_{n_2} \sum_{\xi_1} \mathcal{A}^{\nu_2 l_2 j_2}_{n_2} \mathcal{B}^{\nu_1 l_1 j_1}_{n_2 l_2 j_2 \xi_1 \lambda} \sum_{\mu} (-1)^{j_1 + j_2} \\ & \times \sum_{ph} \left\{ X^{\xi_1 \lambda}_{ph} (-1)^{j_h + j_p} \langle h || F_\lambda || p \rangle + Y^{\xi_1 \lambda}_{ph} (-1)^{\lambda+1} \langle p || F_\lambda || h \rangle \right\} \end{aligned} \tag{B.26}$$

We now observe that, for reduced matrix elements and operators proportional to i^λ, Eq. (A.50) implies that

$$\langle h || F_\lambda || p \rangle = (-1)^{j_h - j_p + \lambda} \langle p || F_\lambda || h \rangle. \tag{B.27}$$

Besides the sum over μ is now mute and so we can obtain finally the following result

$$\mathcal{M}^{red}_{\mathcal{AB}} \simeq \frac{\sqrt{2j_1+1}}{\sqrt{2\lambda+1}} \sum_{n_2} \sum_{\xi_1} \mathcal{A}^{\nu_2 l_2 j_2}_{n_2} \mathcal{B}^{\nu_1 l_1 j_1}_{n_2 l_2 j_2 \xi_1 \lambda} (-1)^{j_1 + \lambda - j_2} \sum_{ph} \left\{ X^{\xi_1 \lambda}_{ph} + Y^{\xi_1 \lambda}_{ph} \right\} \langle p || F_\lambda || h \rangle. \tag{B.28}$$

The $\mathcal{M}_{\mathcal{BA}}$ term of the transition matrix element

The third term in Eq. (B.2) is

$$\begin{aligned} \mathcal{M}_{\mathcal{BA}} = & \sum_{n_2' l_2' j_2' \xi_2 L_2} \sum_{n_1} \mathcal{B}^{\nu_2 l_2 j_2}_{n_2' l_2' j_2' \xi_2 L_2} \mathcal{A}^{\nu_1 l_1 j_1}_{n_1} \sum_{m_2' M_2} \langle j_2' m_2' L_2 M_2 | j_2 m_2 \rangle \\ & \times \langle 0 | \Gamma_{\xi_2}(L_2 M_2) a_{2' m_2'} F_{\lambda \mu} a^\dagger_{1 m_1} | 0 \rangle \end{aligned} \tag{B.29}$$

We proceed exactly as for the previous term:

$$\langle 0 | \Gamma_{\xi_2}(L_2 M_2) a_{\alpha_2' m_2'} F_{\lambda \mu} a^\dagger_{\alpha_1 m_1} | 0 \rangle \simeq \delta_{12'} \langle RPA_{core} | \left[\Gamma_{\xi_2}(L_2 M_2), F_{\lambda \mu} \right] | RPA_{core} \rangle \tag{B.30}$$

$$\left[\Gamma_{\xi_2}(L_2 M_2), F_{\lambda \mu} \right] = \sum_{ph} X^{\xi_2 L_2}_{ph} \left[A_{ph}(L_2 M_2), F_{\lambda \mu} \right] - Y^{\xi_2 L_2}_{ph} \left[A^\dagger_{ph}(\widetilde{L_2 M_2}), F_{\lambda \mu} \right] \tag{B.31}$$

$$\left[A_{ph}(L_2 M_2), F_{\lambda \mu} \right] \simeq \sum_{m_p m_h} (-1)^{j_h - m_h} \langle j_p m_p j_h - m_h | L_2 M_2 \rangle \langle p m_p | F_{\lambda \mu} | h m_h \rangle \tag{B.32}$$

$$\left[A^\dagger_{ph}(\widetilde{L_2 M_2}), F_{\lambda \mu} \right] \simeq - \sum_{m_p m_h} (-1)^{j_h - m_h + L_2 + M_2} \langle j_p m_p j_h - m_h | L_2 - M_2 \rangle \langle h m_h | F_{\lambda \mu} | p m_p \rangle \tag{B.33}$$

$$\mathcal{M}^{red}_{\mathcal{BA}} \simeq \frac{1}{\sqrt{2j_2+1}} \sum_{m_1 m_2 \mu} \langle j_1 m_1 \lambda\mu | j_2 m_2\rangle \sum_{\xi_2 L_2} \sum_{n_1} \mathcal{B}^{\nu_2 l_2 j_2}_{n_1 l_1 j_1 \xi_2 L_2} \mathcal{A}^{\nu_1 l_1 j_1}_{n_1} \sum_{M_2} \langle j_1 m_1 L_2 M_2 | j_2 m_2\rangle$$
$$\times \sum_{ph} \Bigg\{ X^{\xi_2 L_2}_{ph} \sum_{m_p m_h} (-1)^{j_h - m_h} \langle j_p m_p j_h - m_h | L_2 M_2\rangle$$
$$\times \frac{1}{\sqrt{2j_p+1}} \langle j_h m_h \lambda\mu | j_p m_p\rangle \langle p||F_\lambda||h\rangle$$
$$+ Y^{\xi_2 L_2}_{ph} \sum_{m_p m_h} (-1)^{j_h - m_h + L_2 + M_2} \langle j_p m_p j_h - m_h | L_2 - M_2\rangle$$
$$\times \frac{1}{\sqrt{2j_h+1}} \langle j_p m_p \lambda\mu | j_h m_h\rangle \langle h||F_\lambda||p\rangle \Bigg\} \tag{B.34}$$

$$\langle j_1 m_1 \lambda\mu | j_2 m_2\rangle = \frac{\sqrt{2j_2+1}}{\sqrt{2\lambda+1}} (-1)^{j_1 - m_1} \langle j_1 m_1 j_2 - m_2 | \lambda - \mu\rangle \tag{B.35}$$

$$\langle j_1 m_1 L_2 M_2 | j_2 m_2\rangle = \frac{\sqrt{2j_2+1}}{\sqrt{2L_2+1}} (-1)^{j_1 - m_1} \langle j_1 m_1 j_2 - m_2 | L_2 - M_2\rangle \tag{B.36}$$

$$\langle j_h m_h \lambda\mu | j_p m_p\rangle = \frac{\sqrt{2j_p+1}}{\sqrt{2\lambda+1}} (-1)^{j_h - m_h} \langle j_p m_p j_h - m_h | \lambda\mu\rangle \tag{B.37}$$

$$\langle j_p m_p \lambda\mu | j_h m_h\rangle = \frac{\sqrt{2j_h+1}}{\sqrt{2\lambda+1}} (-1)^{j_p - m_p} \langle j_p m_p j_h - m_h | \lambda\mu\rangle \tag{B.38}$$

$$\mathcal{M}^{red}_{\mathcal{BA}} \simeq \frac{\sqrt{2j_2+1}}{(2\lambda+1)^{3/2}} \sum_{\xi_2} \sum_{n_1} \mathcal{B}^{\nu_2 l_2 j_2}_{n_1 l_1 j_1 \xi_2 \lambda} \mathcal{A}^{\nu_1 l_1 j_1}_{n_1} \sum_{\mu}$$
$$\times \sum_{ph} \Bigg\{ X^{\xi_2 \lambda}_{ph} \langle p||F_\lambda||h\rangle + Y^{\xi_2 \lambda}_{ph} (-1)^{j_p + j_h + \lambda + 1} \langle h||F_\lambda||p\rangle \Bigg\} \tag{B.39}$$

We finally obtain the following result

$$\mathcal{M}^{red}_{\mathcal{BA}} \simeq \frac{\sqrt{2j_2+1}}{\sqrt{2\lambda+1}} \sum_{\xi_2} \sum_{n_1} \mathcal{B}^{\nu_2 l_2 j_2}_{n_1 l_1 j_1 \xi_2 \lambda} \mathcal{A}^{\nu_1 l_1 j_1}_{n_1} \sum_{ph} \Bigg\{ X^{\xi_2 \lambda}_{ph} + Y^{\xi_2 \lambda}_{ph} \Bigg\} \langle p||F_\lambda||h\rangle \tag{B.40}$$

The $\mathcal{M}_{\mathcal{BB}}$ term of the transition matrix element

The fourth term in Eq. (B.2) is

$$\mathcal{M}_{\mathcal{BB}} = \sum_{n'_2 l'_2 j'_2 \xi_2 L_2} \sum_{n'_1 l'_1 j'_1 \xi_1 L_1} \mathcal{B}^{\nu_2 l_2 j_2}_{n'_2 l'_2 j'_2 \xi_2 L_2} \mathcal{B}^{\nu_1 l_1 j_1}_{n'_1 l'_1 j'_1 \xi_1 L_1} \sum_{m'_2 M_2} \sum_{m'_1 M_1} \langle j'_2 m'_2 L_2 M_2 | j_2 m_2\rangle$$
$$\times \langle j'_1 m'_1 L_1 M_1 | j_1 m_1\rangle \langle 0 | \Gamma_{\xi_2}(L_2 M_2) a_{2' m'_2} F_{\lambda\mu} a^\dagger_{1' m'_1} \Gamma^\dagger_{\xi_1}(L_1 M_1) | 0\rangle \tag{B.41}$$

Because of Eq. (B.5),

$$\begin{aligned}
&\langle 0|\Gamma_{\xi_2}(L_2M_2)a_{2'm_2'}F_{\lambda\mu}a^\dagger_{1'm_1'}\Gamma^\dagger_{\xi_1}(L_1M_1)|0\rangle \\
&\quad= \langle 0_{odd}|a_{2'm_2'}a^\dagger_{1'm_1'}|0_{odd}\rangle\langle 0_{core}|\Gamma_{\xi_2}(L_2M_2)F_{\lambda\mu}\Gamma^\dagger_{\xi_1}(L_1M_1)|0_{core}\rangle \\
&\qquad+ \langle 0_{odd}|a_{2'm_2'}F_{\lambda\mu}a^\dagger_{1'm_1'}|0_{odd}\rangle\langle 0_{core}|\Gamma_{\xi_2}(L_2M_2)\Gamma^\dagger_{\xi_1}(L_1M_1)|0_{core}\rangle \\
&\quad= \langle 0_{odd}|a_{2'm_2'}a^\dagger_{1'm_1'}|0_{odd}\rangle\langle 0_{core}|\left[\Gamma_{\xi_2}(L_2M_2),\left[F_{\lambda\mu},\Gamma^\dagger_{\xi_1}(L_1M_1)\right]\right]|0_{core}\rangle \\
&\qquad+ \langle 0_{odd}|a_{2'm_2'}F_{\lambda\mu}a^\dagger_{1'm_1'}|0_{odd}\rangle\langle 0_{core}|\Gamma_{\xi_2}(L_2M_2)\Gamma^\dagger_{\xi_1}(L_1M_1)|0_{core}\rangle \\
&\quad\simeq \langle HF_{odd}|a_{2'm_2'}a^\dagger_{1'm_1'}|HF_{odd}\rangle\langle RPA_{core}|\left[\Gamma_{\xi_2}(L_2M_2),\left[F_{\lambda\mu},\Gamma^\dagger_{\xi_1}(L_1M_1)\right]\right]|RPA_{core}\rangle \\
&\qquad+ \langle HF_{odd}|a_{2'm_2'}F_{\lambda\mu}a^\dagger_{1'm_1'}|HF_{odd}\rangle\langle RPA_{core}|\Gamma_{\xi_2}(L_2M_2)\Gamma^\dagger_{\xi_1}(L_1M_1)|RPA_{core}\rangle \\
&\quad= \delta_{1'2'}\langle HF_{core}|\left[\Gamma_{\xi_2}(L_2M_2),\left[F_{\lambda\mu},\Gamma^\dagger_{\xi_1}(L_1M_1)\right]\right]|HF_{core}\rangle \\
&\qquad+ \langle HF_{odd}|a_{2'm_2'}F_{\lambda\mu}a^\dagger_{1'm_1'}|HF_{odd}\rangle\delta_{\xi_1\xi_2}.
\end{aligned} \tag{B.42}$$

By definition,

$$\begin{aligned}
&\langle HF_{core}|\left[\Gamma_{\xi_2}(L_2M_2),\left[F_{\lambda\mu},\Gamma^\dagger_{\xi_1}(L_1M_1)\right]\right]|HF_{core}\rangle \\
&\quad= \sum_{p_1h_1p_2h_2}\Big\{X^{\xi_2L_2}_{p_2h_2}X^{\xi_1L_1}_{p_1h_1}\langle HF_{core}|\left[A_{p_2h_2}(L_2M_2),\left[F_{\lambda\mu},A^\dagger_{p_1h_1}(L_1M_1)\right]\right]|HF_{core}\rangle \\
&\qquad- X^{\xi_2L_2}_{p_2h_2}Y^{\xi_1L_1}_{p_1h_1}\langle HF_{core}|\left[A_{p_2h_2}(L_2M_2),\left[F_{\lambda\mu},A_{p_1h_1}(\widetilde{L_1M_1})\right]\right]|HF_{core}\rangle \\
&\qquad- Y^{\xi_2L_2}_{p_2h_2}X^{\xi_1L_1}_{p_1h_1}\langle HF_{core}|\left[A^\dagger_{p_2h_2}(\widetilde{L_2M_2}),\left[F_{\lambda\mu},A^\dagger_{p_1h_1}(L_1M_1)\right]\right]|HF_{core}\rangle \\
&\qquad+ Y^{\xi_2L_2}_{p_2h_2}Y^{\xi_1L_1}_{p_1h_1}\langle HF_{core}|\left[A^\dagger_{p_2h_2}(\widetilde{L_2M_2}),\left[F_{\lambda\mu},A_{p_1h_1}(\widetilde{L_1M_1})\right]\right]|HF_{core}\rangle\Big\}.
\end{aligned} \tag{B.43}$$

For the first commutator we have,

$$\begin{aligned}
&\langle HF_{core}|\left[A_{p_2h_2}(L_2M_2),\left[F_{\lambda\mu},A^\dagger_{p_1h_1}(L_1M_1)\right]\right]|HF_{core}\rangle \\
&\quad= \sum_{m_{p_1}m_{h_1}m_{p_2}m_{h_2}}(-1)^{j_{h_1}-m_{h_1}+j_{h_2}-m_{h_2}} \\
&\qquad\times\langle j_{p_1}m_{p_1}j_{h_1}-m_{h_1}|L_1M_1\rangle\langle j_{p_2}m_{p_2}j_{h_2}-m_{h_2}|L_2M_2\rangle \\
&\qquad\times\sum_{im_ikm_k}\langle im_i|F_{\lambda\mu}|km_k\rangle\langle HF_{core}|\left[a^\dagger_{h_2m_{h_2}}a_{p_2m_{p_2}},\left[a^\dagger_{im_i}a_{km_k},a^\dagger_{p_1m_{p_1}}a_{h_1m_{h_1}}\right]\right]|HF_{core}\rangle
\end{aligned} \tag{B.44}$$

but, for Wick's Theorem,

$$\langle HF_{core}|\left[a^\dagger_{h_2m_{h_2}}a_{p_2m_{p_2}},\left[a^\dagger_{im_i}a_{km_k},a^\dagger_{p_1m_{p_1}}a_{h_1m_{h_1}}\right]\right]|HF_{core}\rangle = \delta_{p_1p_2}\delta_{h_2k}\delta_{h_1i}+\delta_{h_1h_2}\delta_{p_1k}\delta_{p_2i} \tag{B.45}$$

and so

$$\begin{aligned}
&\langle HF_{core}|\Big[A_{p_2h_2}(L_2M_2),\Big[F_{\lambda\mu},A^{\dagger}_{p_1h_1}(L_1M_1)\Big]\Big]|HF_{core}\rangle \\
&\quad=\sum_{m_{p_1}m_{h_1}m_{p_2}m_{h_2}}(-1)^{j_{h_1}-m_{h_1}+j_{h_2}-m_{h_2}} \\
&\quad\times\langle j_{p_1}m_{p_1}j_{h_1}-m_{h_1}|L_1M_1\rangle\langle j_{p_2}m_{p_2}j_{h_2}-m_{h_2}|L_2M_2\rangle \\
&\quad\times\Big\{\langle h_1m_{h_1}|F_{\lambda\mu}|h_2m_{h_2}\rangle\delta_{p_1p_2}+\langle p_2m_{p_2}|F_{\lambda\mu}|p_1m_{p_1}\rangle\delta_{h_1h_2}\Big\}. \qquad \text{(B.46)}
\end{aligned}$$

Similarly we obtain also that

$$\langle HF_{core}|\Big[A_{p_2h_2}(L_2M_2),\Big[F_{\lambda\mu},A_{p_1h_1}(\widetilde{L_1M_1})\Big]\Big]|HF_{core}\rangle=0 \qquad \text{(B.47)}$$

$$\langle HF_{core}|\Big[A^{\dagger}_{p_2h_2}(\widetilde{L_2M_2}),\Big[F_{\lambda\mu},A^{\dagger}_{p_1h_1}(L_1M_1)\Big]\Big]|HF_{core}\rangle=0 \qquad \text{(B.48)}$$

$$\begin{aligned}
&\langle HF_{core}|\Big[A^{\dagger}_{p_2h_2}(\widetilde{L_2M_2}),\Big[F_{\lambda\mu},A_{p_1h_1}(\widetilde{L_1M_1})\Big]\Big]|HF_{core}\rangle \\
&\quad=\sum_{m_{p_1}m_{h_1}m_{p_2}m_{h_2}}(-1)^{j_{h_1}-m_{h_1}+j_{h_2}-m_{h_2}+L_1+M_1+L_2+M_2} \\
&\quad\times\langle j_{p_1}m_{p_1}j_{h_1}-m_{h_1}|L_1-M_1\rangle\langle j_{p_2}m_{p_2}j_{h_2}-m_{h_2}|L_2-M_2\rangle \\
&\quad\times\Big\{\langle h_2m_{h_2}|F_{\lambda\mu}|h_1m_{h_1}\rangle\delta_{p_1p_2}+\langle p_1m_{p_1}|F_{\lambda\mu}|p_2m_{p_2}\rangle\delta_{h_1h_2}\Big\}. \qquad \text{(B.49)}
\end{aligned}$$

Equations from (B.41) to (B.49) imply that

$$\mathcal{M}_{\mathcal{BB}}\simeq\mathcal{M}^{s.p.}_{\mathcal{BB}}+\mathcal{M}^{XX}_{\mathcal{BB}}+\mathcal{M}^{YY}_{\mathcal{BB}} \qquad \text{(B.50)}$$

and so, because of the additivity of the Wigner-Eckhart Theorem,

$$\mathcal{M}^{red}_{\mathcal{BB}}\simeq\mathcal{M}^{sp,red}_{\mathcal{BB}}+\mathcal{M}^{XX,red}_{\mathcal{BB}}+\mathcal{M}^{YY,red}_{\mathcal{BB}}. \qquad \text{(B.51)}$$

We start with $\mathcal{M}^{sp,red}_{\mathcal{BB}}$, which comes from the second term in Eq. (B.42):

$$\begin{aligned}
\mathcal{M}^{sp,red}_{\mathcal{BB}}\simeq&\frac{1}{\sqrt{2j_2+1}}\sum_{n_2'l_2'j_2'}\sum_{n_1'l_1'j_1'\xi_1L_1}\mathcal{B}^{\nu_2l_2j_2}_{n_2'l_2'j_2'\xi_1L_1}\mathcal{B}^{\nu_1l_1j_1}_{n_1'l_1'j_1'\xi_1L_1}\sum_{m_2'}\sum_{m_1'M_1}\sum_{m_1m_2\mu} \\
&\times\langle j_1m_1\lambda\mu|j_2m_2\rangle\langle j_2'm_2'L_2M_2|j_2m_2\rangle\langle j_1'm_1'L_1M_1|j_1m_1\rangle\langle j_1'm_1'\lambda\mu|j_2'm_2'\rangle \\
&\times\frac{1}{\sqrt{2j_2'+1}}\langle 2'||F_\lambda||1'\rangle. \qquad \text{(B.52)}
\end{aligned}$$

Using the definition of 3-j symbols and their properties (Eqs. (A.12),(A.15),(A.16),(A.24)), we

have

$$\begin{aligned}
\mathcal{M}^{sp,red}_{\mathcal{BB}} \simeq & \frac{1}{\sqrt{2j_2+1}} \sum_{n'_2 l'_2 j'_2} \sum_{n'_1 l'_1 j'_1 \xi_1 L_1} \mathcal{B}^{\nu_2 l_2 j_2}_{n'_2 l'_2 j'_2 \xi_1 L_1} \mathcal{B}^{\nu_1 l_1 j_1}_{n'_1 l'_1 j'_1 \xi_1 L_1} \sum_{m'_2} \sum_{m'_1 M_1} \sum_{m_1 m_2 \mu} \\
& \times (-1)^{j_1+m_1+j'_2-m'_2+1} (2j_2+1) \sqrt{2j_1+1} \sqrt{2j'_2+1} \\
& \times \begin{pmatrix} j_1 & \lambda & j_2 \\ m_1 & \mu & -m_2 \end{pmatrix} \begin{pmatrix} j'_2 & L_1 & j_2 \\ m'_2 & M_1 & -m_2 \end{pmatrix} \begin{pmatrix} j'_1 & L_1 & j_1 \\ m'_1 & M_1 & -m_1 \end{pmatrix} \begin{pmatrix} j'_1 & \lambda & j'_2 \\ m'_1 & \mu & -m'_2 \end{pmatrix} \\
& \times \frac{1}{\sqrt{2j'_2+1}} \langle 2' || F_\lambda || 1' \rangle \\
\simeq & \sqrt{2j_1+1} \sqrt{2j_2+1} \sum_{n'_2 l'_2 j'_2} \sum_{n'_1 l'_1 j'_1 \xi_1 L_1} \mathcal{B}^{\nu_2 l_2 j_2}_{n'_2 l'_2 j'_2 \xi_1 L_1} \mathcal{B}^{\nu_1 l_1 j_1}_{n'_1 l'_1 j'_1 \xi_1 L_1} \sum_{m'_2} \sum_{m'_1 M_1} \sum_{m_1 m_2 \mu} \\
& \times (-1)^{j_1+j_2+L_1+m_1+m_2+M_1} (-1)^{-j_1-L_1-m_2-M_1+j'_2-m'_2+\lambda} \\
& \times \begin{pmatrix} j_1 & j_2 & \lambda \\ m_1 & -m_2 & \mu \end{pmatrix} \begin{pmatrix} j_2 & L_1 & j'_2 \\ m_2 & -M_1 & -m'_2 \end{pmatrix} \begin{pmatrix} L_1 & j_1 & j'_1 \\ M_1 & -m_1 & m'_1 \end{pmatrix} \begin{pmatrix} j'_2 & j'_1 & \lambda \\ -m'_2 & m'_1 & \mu \end{pmatrix} \\
& \times \langle 2' || F_\lambda || 1' \rangle \\
\simeq & \sqrt{2j_1+1} \sqrt{2j_2+1} \sum_{n'_2 l'_2 j'_2} \sum_{n'_1 l'_1 j'_1 \xi_1 L_1} \mathcal{B}^{\nu_2 l_2 j_2}_{n'_2 l'_2 j'_2 \xi_1 L_1} \mathcal{B}^{\nu_1 l_1 j_1}_{n'_1 l'_1 j'_1 \xi_1 L_1} \sum_{m'_2} \sum_{m'_1 M_1} \sum_{m_1 m_2 \mu} \\
& \times (-1)^{j_1+j_2+L_1+m_1+m_2+M_1} (-1)^{j_1+L_1+j'_2+\lambda} \\
& \times \begin{pmatrix} j_1 & j_2 & \lambda \\ m_1 & -m_2 & \mu \end{pmatrix} \begin{pmatrix} j_2 & L_1 & j'_2 \\ m_2 & -M_1 & -m'_2 \end{pmatrix} \begin{pmatrix} L_1 & j_1 & j'_1 \\ M_1 & -m_1 & m'_1 \end{pmatrix} \begin{pmatrix} j'_2 & j'_1 & \lambda \\ -m'_2 & m'_1 & \mu \end{pmatrix} \\
& \times \langle 2' || F_\lambda || 1' \rangle \\
\simeq & \sqrt{2j_1+1} \sqrt{2j_2+1} \sum_{n'_2 l'_2 j'_2} \sum_{n'_1 l'_1 j'_1 \xi_1 L_1} \mathcal{B}^{\nu_2 l_2 j_2}_{n'_2 l'_2 j'_2 \xi_1 L_1} \mathcal{B}^{\nu_1 l_1 j_1}_{n'_1 l'_1 j'_1 \xi_1 L_1} \sum_{\mu} (-1)^{j_1+L_1+j'_2+\lambda} \\
& \times \begin{Bmatrix} j'_2 & j'_1 & \lambda \\ j_1 & j_2 & L_1 \end{Bmatrix} \frac{1}{2\lambda+1} \langle 2' || F_\lambda || 1' \rangle
\end{aligned} \tag{B.53}$$

Since the sum over μ is mute, we obtain the final result for the term $\mathcal{M}^{sp,red}_{\mathcal{BB}}$:

$$\begin{aligned}
\mathcal{M}^{sp,red}_{\mathcal{BB}} \simeq & \sqrt{2j_1+1} \sqrt{2j_2+1} \sum_{n'_2 l'_2 j'_2} \sum_{n'_1 l'_1 j'_1} \sum_{\xi_1 L_1} \mathcal{B}^{\nu_2 l_2 j_2}_{n'_2 l'_2 j'_2 \xi_1 L_1} \mathcal{B}^{\nu_1 l_1 j_1}_{n'_1 l'_1 j'_1 \xi_1 L_1} (-1)^{j_1+L_1+j'_2+\lambda} \\
& \times \begin{Bmatrix} j'_2 & j'_1 & \lambda \\ j_1 & j_2 & L_1 \end{Bmatrix} \langle 2' || F_\lambda || 1' \rangle
\end{aligned} \tag{B.54}$$

Now we calculate the term $\mathcal{M}^{XX,red}_{\mathcal{BB}}$, which comes from the commutator of Eq. (B.46):

$$\begin{aligned}
\mathcal{M}^{XX,red}_{\mathcal{BB}} \simeq & \frac{1}{\sqrt{2j_2+1}} \sum_{\xi_2 L_2} \sum_{n'_1 l'_1 j'_1 \xi_1 L_1} \mathcal{B}^{\nu_2 l_2 j_2}_{n'_1 l'_1 j'_1 \xi_2 L_2} \mathcal{B}^{\nu_1 l_1 j_1}_{n'_1 l'_1 j'_1 \xi_1 L_1} \sum_{m'_1} \sum_{M_1 M_2} \sum_{m_1 m_2 \mu} \\
& \times \langle j_1 m_1 \lambda \mu | j_2 m_2 \rangle \langle j'_1 m'_1 L_2 M_2 | j_2 m_2 \rangle \langle j'_1 m'_1 L_1 M_1 | j_1 m_1 \rangle \\
& \times \sum_{p_1 h_1 p_2 h_2} X^{\xi_2 L_2}_{p_2 h_2} X^{\xi_1 L_1}_{p_1 h_1} \sum_{m_{p_1} m_{h_1} m_{p_2} m_{h_2}} (-1)^{j_{h_1}-m_{h_1}+j_{h_2}-m_{h_2}} \\
& \times \langle j_{p_1} m_{p_1} j_{h_1} - m_{h_1} | L_1 M_1 \rangle \langle j_{p_2} m_{p_2} j_{h_2} - m_{h_2} | L_2 M_2 \rangle \\
& \times \left\{ \frac{1}{\sqrt{2j_{h_1}+1}} \langle j_{h_2} m_{h_2} \lambda \mu | j_{h_1} m_{h_1} \rangle \langle h_1 || F_\lambda || h_2 \rangle \delta_{p_1 p_2} \right. \\
& \left. + \frac{1}{\sqrt{2j_{p_2}+1}} \langle j_{p_1} m_{p_1} \lambda \mu | j_{p_2} m_{p_2} \rangle \langle p_2 || F_\lambda || p_1 \rangle \delta_{h_1 h_2} \right\}
\end{aligned} \tag{B.55}$$

By means of the definition of 3-j symbols and their properties (Eqs. (A.12),(A.15),(A.16),(A.25)),

we have

$$
\begin{aligned}
\mathcal{M}^{XX,red}_{\mathcal{BB}} \simeq & \sqrt{2j_1+1}\sqrt{2j_2+1} \\
& \times \sum_{\xi_2 L_2} \sum_{n_1' l_1' j_1' \xi_1 L_1} \sqrt{2L_1+1}\sqrt{2L_2+1} \mathcal{B}^{\nu_2 l_2 j_2}_{n_1' l_1' j_1' \xi_2 L_2} \mathcal{B}^{\nu_1 l_1 j_1}_{n_1' l_1' j_1' \xi_1 L_1} \sum_{m_1'} \sum_{M_1 M_2} \sum_{m_1 m_2 \mu} \\
& \times (-1)^{j_1+m_1-L_1-L_2} \begin{pmatrix} j_1 & \lambda & j_2 \\ m_1 & \mu & -m_2 \end{pmatrix} \begin{pmatrix} j_1' & L_2 & j_2 \\ m_1' & M_2 & -m_2 \end{pmatrix} \begin{pmatrix} j_1' & L_1 & j_1 \\ m_1' & M_1 & -m_1 \end{pmatrix} \\
& \times \sum_{p_1 h_1 p_2 h_2} X^{\xi_2 L_2}_{p_2 h_2} X^{\xi_1 L_1}_{p_1 h_1} \sum_{m_{p_1} m_{h_1} m_{p_2} m_{h_2}} \\
& \times \begin{pmatrix} j_{p_1} & j_{h_1} & L_1 \\ m_{p_1} & -m_{h_1} & -M_1 \end{pmatrix} \begin{pmatrix} j_{p_2} & j_{h_2} & L_2 \\ m_{p_2} & -m_{h_2} & -M_2 \end{pmatrix} \\
& \times \Bigg\{ (-1)^{-m_{h_2}+j_{p_1}+M_1+j_{p_2}+M_2+j_{h_2}} \begin{pmatrix} j_{h_2} & \lambda & j_{h_1} \\ m_{h_2} & \mu & -m_{h_1} \end{pmatrix} \langle h_1 || F_\lambda || h_2 \rangle \delta_{p_1 p_2} \\
& + (-1)^{m_{h_1}-m_{h_2}+M_1+j_{p_2}+M_2+m_{p_2}} \begin{pmatrix} j_{p_1} & \lambda & j_{p_2} \\ m_{p_1} & \mu & -m_{p_2} \end{pmatrix} \langle p_2 || F_\lambda || p_1 \rangle \delta_{h_1 h_2} \Bigg\} \\
\simeq & \sqrt{2j_1+1}\sqrt{2j_2+1} \\
& \times \sum_{\xi_2 L_2} \sum_{n_1' l_1' j_1' \xi_1 L_1} \sqrt{2L_1+1}\sqrt{2L_2+1} \mathcal{B}^{\nu_2 l_2 j_2}_{n_1' l_1' j_1' \xi_2 L_2} \mathcal{B}^{\nu_1 l_1 j_1}_{n_1' l_1' j_1' \xi_1 L_1} \sum_{m_1'} \sum_{M_1 M_2} \sum_{m_1 m_2 \mu} \\
& \times (-1)^{j_1+j_2+j_1'+m_1+m_2+m_1'} (-1)^{j_2+j_1'+M_2+\lambda} \\
& \times \begin{pmatrix} j_1 & j_2 & \lambda \\ m_1 & -m_2 & \mu \end{pmatrix} \begin{pmatrix} j_2 & j_1' & L_2 \\ m_2 & -m_1' & -M_2 \end{pmatrix} \begin{pmatrix} j_1' & j_1 & L_1 \\ m_1' & -m_1 & M_1 \end{pmatrix} \\
& \times \sum_{p_1 h_1 p_2 h_2} X^{\xi_2 L_2}_{p_2 h_2} X^{\xi_1 L_1}_{p_1 h_1} \\
& \times \Bigg\{ \sum_{m_{p_1} m_{h_1} m_{h_2}} (-1)^{j_{p_1}+j_{h_1}+j_{h_2}-m_{p_1}-m_{h_1}-m_{h_2}} (-1)^{j_{p_1}+j_{h_2}+M_2+L_1+L_2} \delta_{p_1 p_2} \\
& \times \begin{pmatrix} j_{p_1} & j_{h_1} & L_1 \\ -m_{p_1} & m_{h_1} & M_1 \end{pmatrix} \begin{pmatrix} j_{h_1} & j_{h_2} & \lambda \\ -m_{h_1} & m_{h_2} & \mu \end{pmatrix} \begin{pmatrix} j_{h_2} & j_{p_1} & L_2 \\ -m_{h_2} & m_{p_1} & -M_2 \end{pmatrix} \langle h_1 || F_\lambda || h_2 \rangle \\
& + \sum_{m_{p_1} m_{p_2} m_{h_1}} (-1)^{j_{p_1}+j_{h_1}+j_{p_2}-m_{p_1}-m_{h_1}-m_{p_2}} (-1)^{j_{h_1}+j_{p_2}+M_2+L_1+L_2} \delta_{h_1 h_2} \\
& \times \begin{pmatrix} j_{p_1} & j_{h_1} & L_1 \\ -m_{p_1} & m_{h_1} & M_1 \end{pmatrix} \begin{pmatrix} j_{h_1} & j_{p_2} & L_2 \\ -m_{h_1} & m_{p_2} & -M_2 \end{pmatrix} \begin{pmatrix} j_{p_2} & j_{p_1} & \lambda \\ -m_{p_2} & m_{p_1} & \mu \end{pmatrix} \langle p_2 || F_\lambda || p_1 \rangle \Bigg\} \\
\simeq & \sqrt{2j_1+1}\sqrt{2j_2+1} \\
& \times \sum_{\xi_2 L_2} \sum_{n_1' l_1' j_1' \xi_1 L_1} \sqrt{2L_1+1}\sqrt{2L_2+1} \mathcal{B}^{\nu_2 l_2 j_2}_{n_1' l_1' j_1' \xi_2 L_2} \mathcal{B}^{\nu_1 l_1 j_1}_{n_1' l_1' j_1' \xi_1 L_1} \sum_{M_1 M_2} \sum_{\mu} \\
& \times (-1)^{j_2+j_1'+M_2+\lambda} \\
& \times \begin{pmatrix} L_2 & L_1 & \lambda \\ -M_2 & M_1 & \mu \end{pmatrix} \begin{Bmatrix} L_2 & L_1 & \lambda \\ j_1 & j_2 & j_1' \end{Bmatrix} \sum_{p_1 h_1 p_2 h_2} X^{\xi_2 L_2}_{p_2 h_2} X^{\xi_1 L_1}_{p_1 h_1} \\
& \times \Bigg\{ (-1)^{j_{p_1}+j_{h_2}+M_2+L_1+L_2} \begin{pmatrix} \lambda & L_2 & L_1 \\ \mu & -M_2 & M_1 \end{pmatrix} \begin{Bmatrix} \lambda & L_2 & L_1 \\ j_{p_1} & j_{h_1} & j_{h_2} \end{Bmatrix} \langle h_1 || F_\lambda || h_2 \rangle \delta_{p_1 p_2} \\
& + (-1)^{j_{h_1}+j_{p_2}+M_2+L_1+L_2} \begin{pmatrix} L_2 & \lambda & L_1 \\ -M_2 & \mu & M_1 \end{pmatrix} \begin{Bmatrix} L_2 & \lambda & L_1 \\ j_{p_1} & j_{h_1} & j_{p_2} \end{Bmatrix} \langle p_2 || F_\lambda || p_1 \rangle \delta_{h_1 h_2} \Bigg\}
\end{aligned}
\tag{B.56}
$$

Using the orthogonality relation Eq. (A.13) and the symmetry relation Eq. (B.27) we then

obtain the final result

$$\begin{aligned}\mathcal{M}^{XX,red}_{\mathcal{BB}} \simeq & \sqrt{2j_1+1}\sqrt{2j_2+1}\sum_{n'_1l'_1j'_1}\sum_{\xi_1L_1}\sum_{\xi_2L_2}\mathcal{B}^{\nu_1l_1j_1}_{n'_1l'_1j'_1\xi_1L_1}\mathcal{B}^{\nu_2l_2j_2}_{n'_1l'_1j'_1\xi_2L_2} \\ & \times\sqrt{2L_1+1}\sqrt{2L_2+1}(-)^{j_2+\lambda+j'_1} \\ & \times\begin{Bmatrix} L_1 & \lambda & L_2 \\ j_2 & j'_1 & j_1\end{Bmatrix}\sum_{p_1p_2h_1h_2}X^{\xi_1L_1}_{p_1h_1}X^{\xi_2L_2}_{p_2h_2} \\ & \times\Bigg((-)^{j_{p_1}+j_{h_1}}\delta_{h_1h_2}\begin{Bmatrix} L_1 & \lambda & L_2 \\ j_{p_2} & j_{h_1} & j_{p_1}\end{Bmatrix}\langle p_1||F_\lambda||p_2\rangle \\ & +(-)^{j_{p_1}+j_{h_2}+L_1+L_2}\delta_{p_1p_2}\begin{Bmatrix} L_1 & \lambda & L_2 \\ j_{h_2} & j_{p_1} & j_{h_1}\end{Bmatrix}\langle h_1||F_\lambda||h_2\rangle\Bigg)\end{aligned} \tag{B.57}$$

The term $\mathcal{M}^{YY,red}_{\mathcal{BB}}$ comes from the commutator in Eq. (B.49) and is

$$\begin{aligned}\mathcal{M}^{YY,red}_{\mathcal{BB}} \simeq & \frac{1}{\sqrt{2j_2+1}}\sum_{\xi_2L_2}\sum_{n'_1l'_1j'_1\xi_1L_1}\mathcal{B}^{\nu_2l_2j_2}_{n'_1l'_1j'_1\xi_2L_2}\mathcal{B}^{\nu_1l_1j_1}_{n'_1l'_1j'_1\xi_1L_1}\sum_{m'_1}\sum_{M_1M_2}\sum_{m_1m_2\mu} \\ & \times\langle j_1m_1\lambda\mu|j_2m_2\rangle\langle j'_1m'_1L_2M_2|j_2m_2\rangle\langle j'_1m'_1L_1M_1|j_1m_1\rangle \\ & \times\sum_{p_1h_1p_2h_2}Y^{\xi_2L_2}_{p_2h_2}Y^{\xi_1L_1}_{p_1h_1}\sum_{m_{p_1}m_{h_1}m_{p_2}m_{h_2}}(-1)^{j_{h_1}-m_{h_1}+L_1+M_1+j_{h_2}-m_{h_2}+L_2+M_2} \\ & \times\langle j_{p_1}m_{p_1}j_{h_1}-m_{h_1}|L_1-M_1\rangle\langle j_{p_2}m_{p_2}j_{h_2}-m_{h_2}|L_2-M_2\rangle \\ & \times\Bigg\{\frac{1}{\sqrt{2j_{h_2}+1}}\langle j_{h_1}m_{h_1}\lambda\mu|j_{h_2}m_{h_2}\rangle\langle h_2||F_\lambda||h_1\rangle\delta_{p_1p_2} \\ & +\frac{1}{\sqrt{2j_{p_1}+1}}\langle j_{p_2}m_{p_2}\lambda\mu|j_{p_1}m_{p_1}\rangle\langle p_1||F_\lambda||p_2\rangle\delta_{h_1h_2}\Bigg\}.\end{aligned} \tag{B.58}$$

The calculation is similar to that for the term $\mathcal{M}^{XX,red}_{\mathcal{BB}}$; we just report the result

$$\begin{aligned}\mathcal{M}^{YY,red}_{\mathcal{BB}} \simeq & \sqrt{2j_1+1}\sqrt{2j_2+1}\sum_{n'_1l'_1j'_1}\sum_{\xi_1L_1}\sum_{\xi_2l_2L_2}\mathcal{B}^{\nu_1l_1j_1}_{n'_1l'_1j'_1\xi_1L_1}\mathcal{B}^{\nu_2j_2}_{n'_1l'_1j'_1\xi_2L_2} \\ & \times\sqrt{2L_1+1}\sqrt{2L_2+1}(-)^{j_2+\lambda+j'_1} \\ & \times\begin{Bmatrix} L_1 & \lambda & L_2 \\ j_2 & j'_1 & j_1\end{Bmatrix}\sum_{p_1p_2h_1h_2}Y^{\xi_1L_1}_{p_1h_1}Y^{\xi_2L_2}_{p_2h_2} \\ & \times\Bigg((-)^{j_{p_1}+j_{h_1}}\delta_{h_1h_2}\begin{Bmatrix} L_1 & \lambda & L_2 \\ j_{p_2} & j_{h_1} & j_{p_1}\end{Bmatrix}\langle p_1||F_\lambda||p_2\rangle \\ & +(-)^{j_{p_1}+j_{h_2}+L_1+L_2}\delta_{p_1p_2}\begin{Bmatrix} L_1 & \lambda & L_2 \\ j_{h_2} & j_{p_1} & j_{h_1}\end{Bmatrix}\langle h_1||F_\lambda||h_2\rangle\Bigg).\end{aligned} \tag{B.59}$$

B.2 Transition matrix elements for hole-plus-core odd nuclei

Let us consider now the case in which the odd nucleus is formed by an even-even core plus a hole.

The $\mathcal{M}_{\mathcal{A}\mathcal{A}}$ term of the transition matrix element

The first term in Eq. (B.2) is, using Eq. (B.5) for the operator $F_{\lambda\mu}$,

$$\begin{aligned}
\mathcal{M}_{\mathcal{A}\mathcal{A}} &= \sum_{n_2}\sum_{n_1} \mathcal{A}_{n_2}^{\nu_2 l_2 j_2}\mathcal{A}_{n_1}^{\nu_1 l_1 j_1}\langle 0_{odd}|b_{2m_2}F_{\lambda\mu}b^{\dagger}_{1m_1}|0_{odd}\rangle \\
&= \sum_{n_2}\sum_{n_1} \mathcal{A}_{n_2}^{\nu_2 l_2 j_2}\mathcal{A}_{n_1}^{\nu_1 l_1 j_1}(-1)^{j_1+m_1+j_2+m_2}\langle 0_{odd}|a^{\dagger}_{2-m_2}F_{\lambda\mu}a_{1-m_1}|0_{odd}\rangle \\
&= \sum_{n_2}\sum_{n_1} \mathcal{A}_{n_2}^{\nu_2 l_2 j_2}\mathcal{A}_{n_1}^{\nu_1 l_1 j_1}(-1)^{j_1+m_1+j_2+m_2}\sum_{im_ikm_k}\langle im_i|F_{\lambda\mu}|km_k\rangle \\
&\quad\times\langle 0_{odd}|a^{\dagger}_{2-m_2}a^{\dagger}_{im_i}a_{km_k}a_{1-m_1}|0_{odd}\rangle \\
&\simeq \sum_{n_2}\sum_{n_1} \mathcal{A}_{n_2}^{\nu_2 l_2 j_2}\mathcal{A}_{n_1}^{\nu_1 l_1 j_1}(-1)^{j_1+m_1+j_2+m_2}\sum_{im_ikm_k}\langle im_i|F_{\lambda\mu}|km_k\rangle \\
&\quad\times\langle HF_{odd}|a^{\dagger}_{2-m_2}a^{\dagger}_{im_i}a_{km_k}a_{1-m_1}|HF_{odd}\rangle \\
&= \sum_{n_2}\sum_{n_1} \mathcal{A}_{n_2}^{\nu_2 l_2 j_2}\mathcal{A}_{n_1}^{\nu_1 l_1 j_1}(-1)^{j_1+m_1+j_2+m_2}\langle 1-m_1|F_{\lambda\mu}|2-m_2\rangle
\end{aligned}$$

where we have made use of the definition (A.52) for the hole creation operators. Consequently, for the reduced matrix element we obtain

$$\begin{aligned}
\mathcal{M}^{red}_{\mathcal{A}\mathcal{A}} &= \frac{1}{\sqrt{2j_2+1}}\sum_{m_1m_2\mu}\langle j_1m_1\lambda\mu|j_2m_2\rangle\mathcal{M}_{\mathcal{A}\mathcal{A}} \\
&= \frac{1}{\sqrt{2j_2+1}}\sum_{m_1m_2\mu}\langle j_2-m_2\lambda\mu|j_1-m_1\rangle(-1)^{j_1+m_1+j_2+m_2+\lambda+\mu} \\
&\quad\times\frac{\sqrt{2j_2+1}}{\sqrt{2j_1+1}}\sum_{n_2}\sum_{n_1}\mathcal{A}_{n_2}^{\nu_2 l_2 j_2}\mathcal{A}_{n_1}^{\nu_1 l_1 j_1}\langle 1-m_1|F_{\lambda\mu}|2-m_2\rangle.
\end{aligned}$$

Now, the Clebsch-Gordan coefficient in the previous equation implies that $m_1+\mu=m_2$; besides, for the Wigner-Eckhart theorem,

$$\langle 1||F_\lambda||2\rangle = \frac{1}{\sqrt{2j_1+1}}\sum_{m_1m_2\mu}\langle j_2-m_2\lambda\mu|j_1-m_1\rangle\langle 1-m_1|F_{\lambda\mu}|2-m_2\rangle,$$

and so, from Eq. (A.50),

$$\begin{aligned}
\mathcal{M}^{red}_{\mathcal{A}\mathcal{A}} &= \sum_{n_2}\sum_{n_1}\mathcal{A}_{n_2}^{\nu_2 l_2 j_2}\mathcal{A}_{n_1}^{\nu_1 l_1 j_1}(-1)^{j_1+j_2+\lambda+1}\langle 1||F_\lambda||2\rangle \\
&= \sum_{n_2}\sum_{n_1}\mathcal{A}_{n_2}^{\nu_2 l_2 j_2}\mathcal{A}_{n_1}^{\nu_1 l_1 j_1}(-1)^{j_1+j_2+\lambda+1}(-1)^{j_1-j_2+\lambda}\langle 2||F_\lambda||1\rangle \\
&= \sum_{n_2}\sum_{n_1}\mathcal{A}_{n_2}^{\nu_2 l_2 j_2}\mathcal{A}_{n_1}^{\nu_1 l_1 j_1}\langle 2||F_\lambda||1\rangle.
\end{aligned} \tag{B.60}$$

Eqs. (B.7) and (B.60) imply that the contribution to the total transition matrix element coming from the $\mathcal{M}_{\mathcal{A}\mathcal{A}}$ term is exactly the same both in the cases of particle-plus-core and hole-plus-core odd nuclei.

The $\mathcal{M}_{\mathcal{A}\mathcal{B}}$ and $\mathcal{M}_{\mathcal{B}\mathcal{A}}$ terms of the transition matrix element

The second term in Eq. (B.2) is

$$\begin{aligned}
\mathcal{M}_{\mathcal{A}\mathcal{B}} &= \sum_{n_2}\sum_{n_1'l_1'j_1'\xi_1L_1}\mathcal{A}_{n_2}^{\nu_2 l_2 j_2}\mathcal{B}^{\nu_1 l_1 j_1}_{n_1'l_1'j_1'\xi_1L_1}\sum_{m_1'M_1}\langle j_1'm_1'L_1M_1|j_1m_1\rangle \\
&\quad\times\langle 0|b_{2m_2}F_{\lambda\mu}b^{\dagger}_{1'm_1'}\Gamma^{\dagger}_{\xi_1}(L_1M_1)|0\rangle.
\end{aligned} \tag{B.61}$$

Now, because of Eq. (B.5),

$$\langle 0|b_{2m_2}F_{\lambda\mu}b^\dagger_{1'm'_1}\Gamma^\dagger_{\xi_1}(L_1M_1)|0\rangle = \langle 0_{odd}|b_{2m_2}F_{\lambda\mu}b^\dagger_{1'm'_1}|0_{odd}\rangle\langle 0_{core}|\Gamma^\dagger_{\xi_1}(L_1M_1)|0_{core}\rangle + \langle 0_{odd}|b_{2m_2}b^\dagger_{1'm'_1}|0_{odd}\rangle\langle 0_{core}|F_{\lambda\mu}\Gamma^\dagger_{\xi_1}(L_1M_1)|0_{core}\rangle. \tag{B.62}$$

Since the term $\langle 0_{core}|\Gamma^\dagger_{\xi_1}(L_1M_1)|0_{core}\rangle$ is identically zero, just like a term $\Gamma_{\xi_1}(L_1M_1)|0_{core}\rangle$, one can write

$$\begin{aligned}\langle 0|b_{2m_2}F_{\lambda\mu}b^\dagger_{1'm'_1}\Gamma^\dagger_{\xi_1}(L_1M_1)|0\rangle &= \langle 0_{odd}|b_{2m_2}b^\dagger_{1'm'_1}|0_{odd}\rangle\langle 0_{core}|\Big[F_{\lambda\mu},\Gamma^\dagger_{\xi_1}(L_1M_1)\Big]|0_{core}\rangle \\ &\simeq \langle HF_{odd}|b_{2m_2}b^\dagger_{1'm'_1}|HF_{odd}\rangle\langle RPA_{core}|\Big[F_{\lambda\mu},\Gamma^\dagger_{\xi_1}(L_1M_1)\Big]|RPA_{core}\rangle \\ &\simeq \delta_{21'}\langle RPA_{core}|\Big[F_{\lambda\mu},\Gamma^\dagger_{\xi_1}(L_1M_1)\Big]|RPA_{core}\rangle.\end{aligned} \tag{B.63}$$

The third term in Eq. (B.2) is, instead,

$$\begin{aligned}\mathcal{M}_{\mathcal{BA}} = &\sum_{n'_2l'_2j'_2\xi_2L_2}\sum_{n_1}\mathcal{B}^{\nu_2l_2j_2}_{n'_2l'_2j'_2\xi_2L_2}\mathcal{A}^{\nu_1l_1j_1}_{n_1}\sum_{m'_2M_2}\langle j'_2m'_2L_2M_2|j_2m_2\rangle \\ &\times\langle 0|\Gamma_{\xi_2}(L_2M_2)b_{2'm'_2}F_{\lambda\mu}b^\dagger_{1m_1}|0\rangle\end{aligned} \tag{B.64}$$

where

$$\langle 0|\Gamma_{\xi_2}(L_2M_2)b_{2'm'_2}F_{\lambda\mu}b^\dagger_{1m_1}|0\rangle \simeq \delta_{12'}\langle RPA_{core}|\Big[\Gamma_{\xi_2}(L_2M_2),F_{\lambda\mu}\Big]|RPA_{core}\rangle. \tag{B.65}$$

Since Eq. (B.63) coincides with Eq. (B.10), and Eq. (B.65) with Eq. (B.30), one can easily conclude that the contribution to the total transition matrix element coming from the $\mathcal{M}_{\mathcal{AB}}$ and $\mathcal{M}_{\mathcal{BA}}$ terms must be exactly the same both in the cases of particle-plus-core and hole-plus-core odd nuclei.

The $\mathcal{M}_{\mathcal{BB}}$ term of the transition matrix element

The fourth term in Eq. (B.2) is

$$\begin{aligned}\mathcal{M}_{\mathcal{BB}} = &\sum_{n'_2l'_2j'_2\xi_2L_2}\sum_{n'_1l'_1j'_1\xi_1L_1}\mathcal{B}^{\nu_2l_2j_2}_{n'_2l'_2j'_2\xi_2L_2}\mathcal{B}^{\nu_1l_1j_1}_{n'_1l'_1j'_1\xi_1L_1}\sum_{m'_2M_2}\sum_{m'_1M_1}\langle j'_2m'_2L_2M_2|j_2m_2\rangle \\ &\times\langle j'_1m'_1L_1M_1|j_1m_1\rangle\langle 0|\Gamma_{\xi_2}(L_2M_2)a_{2'm'_2}F_{\lambda\mu}a^\dagger_{1'm'_1}\Gamma^\dagger_{\xi_1}(L_1M_1)|0\rangle\end{aligned} \tag{B.66}$$

Because of Eq. (B.5),

$$\begin{aligned}&\langle 0|\Gamma_{\xi_2}(L_2M_2)b_{2'm'_2}F_{\lambda\mu}b^\dagger_{1'm'_1}\Gamma^\dagger_{\xi_1}(L_1M_1)|0\rangle \\ &\quad= \delta_{1'2'}\langle HF_{core}|\Big[\Gamma_{\xi_2}(L_2M_2),\Big[F_{\lambda\mu},\Gamma^\dagger_{\xi_1}(L_1M_1)\Big]\Big]|HF_{core}\rangle \\ &\quad\quad+\langle HF_{odd}|b_{2'm'_2}F_{\lambda\mu}b^\dagger_{1'm'_1}|HF_{odd}\rangle\delta_{\xi_1\xi_2}.\end{aligned} \tag{B.67}$$

Now,

$$
\begin{aligned}
&\langle HF_{odd}|b_{2'm'_2}F_{\lambda\mu}b^{\dagger}_{1'm'_1}|HF_{odd}\rangle \\
&\quad= (-1)^{j'_1+m'_1+j'_2+m'_2}\langle HF_{odd}|a^{\dagger}_{2'm'_2}F_{\lambda\mu}a_{1'm'_1}|HF_{odd}\rangle \\
&\quad= (-1)^{j'_1+m'_1+j'_2+m'_2}\langle 1'-m'_1|F_{\lambda\mu}|2'-m'_2\rangle \\
&\quad= (-1)^{j'_1+m'_1+j'_2+m'_2}\frac{1}{\sqrt{2j'_1+1}}\langle j'_2-m'_2\lambda\mu|j'_1-m'_1\rangle\langle 1'||F_\lambda||2'\rangle \\
&\quad= (-1)^{j'_1+m'_1+j'_2+m'_2}\frac{1}{\sqrt{2j'_1+1}}\frac{\sqrt{2j'_1+1}}{\sqrt{2j'_2+1}}\langle j'_1m'_1\lambda\mu|j'_2m'_2\rangle(-1)^{j'_1+\lambda-j'_2}\langle 2'||F_\lambda||1'\rangle \\
&\quad= \frac{1}{\sqrt{2j'_2+1}}\langle j'_1m'_1\lambda\mu|j'_2m'_2\rangle\langle 2'||F_\lambda||1'\rangle \\
&\quad= \langle HF_{odd}|a_{2'm'_2}F_{\lambda\mu}a^{\dagger}_{1'm'_1}|HF_{odd}\rangle. \qquad \text{(B.68)}
\end{aligned}
$$

Since Eqs. (B.67) and (B.42) coincide, one concludes that the contribution to the total transition matrix element coming from the $\mathcal{M}_{\mathcal{BB}}$, too, term must be exactly the same both in the cases of particle-plus-core and hole-plus-core odd nuclei.

B.3 Final result for the transition matrix element

The final result for $\langle\nu_2l_2j_2||F_\lambda||\nu_1l_1j_1\rangle$ comes from the sum of $\mathcal{M}^{red}_{\mathcal{AA}}$, $\mathcal{M}^{red}_{\mathcal{AB}}$, $\mathcal{M}^{red}_{\mathcal{BA}}$, $\mathcal{M}^{sp,red}_{\mathcal{BB}}$, $\mathcal{M}^{XX,red}_{\mathcal{BB}}$ and $\mathcal{M}^{YY,red}_{\mathcal{BB}}$. As we demonstrated, the result does not depend on whether the nucleus is a particle-plus-core or an hole-plus-core one. In its full glory it is

$$
\begin{aligned}
&\langle\nu_2l_2j_2||F_\lambda||\nu_1l_1j_1\rangle \\
&\quad\simeq \sum_{n_1n_2}\mathcal{A}^{\nu_1l_1j_1}_{n_1}\mathcal{A}^{\nu_2l_2j_2}_{n_2}\langle n_2l_2j_2||F_\lambda||n_1l_1j_1\rangle \\
&\qquad+\frac{\sqrt{2j_1+1}}{\sqrt{2\lambda+1}}\sum_{n_2\xi}\mathcal{A}^{\nu_2l_2j_2}_{n_2}\mathcal{B}^{\nu_1l_1j_1}_{n_2l_2j_2\xi\lambda}(-1)^{j_1+\lambda-j_2}\sum_{ph}\left\{X^{\xi\lambda}_{ph}+Y^{\xi\lambda}_{ph}\right\}\langle p||F_\lambda||h\rangle \\
&\qquad+\frac{\sqrt{2j_2+1}}{\sqrt{2\lambda+1}}\sum_{n_1\xi}\mathcal{B}^{\nu_2l_2j_2}_{n_1l_1j_1\xi\lambda}\mathcal{A}^{\nu_1l_1j_1}_{n_1}\sum_{ph}\left\{X^{\xi\lambda}_{ph}+Y^{\xi\lambda}_{ph}\right\}\langle p||F_\lambda||h\rangle \\
&\qquad+\sqrt{2j_1+1}\sqrt{2j_2+1}\sum_{n'_1l'_1j'_1}\sum_{n'_2l'_2j'_2}\sum_{\xi L}\mathcal{B}^{\nu_1l_1j_1}_{n'_1l'_1j'_1\xi L}\mathcal{B}^{\nu_2l_2j_2}_{n'_2l'_2j'_2\xi L} \\
&\qquad\quad\times(-)^{j_1+\lambda+j'_2+L}\begin{Bmatrix}j'_2 & j'_1 & \lambda\\ j_1 & j_2 & L\end{Bmatrix}\langle n'_2l'_2j'_2||F_\lambda||n'_1l'_1j'_1\rangle \\
&\qquad+\sqrt{2j_1+1}\sqrt{2j_2+1}\sum_{n'l'j'}\sum_{\xi_1L_1}\sum_{\xi_2L_2}\mathcal{B}^{\nu_1l_1j_1}_{n'l'j'\xi_1L_1}\mathcal{B}^{\nu_2l_2j_2}_{n'l'j'\xi_2L_2} \\
&\qquad\quad\times\sqrt{2L_1+1}\sqrt{2L_2+1}(-)^{j_2+\lambda+j'} \\
&\qquad\quad\times\begin{Bmatrix}L_1 & \lambda & L_2\\ j_2 & j' & j_1\end{Bmatrix}\sum_{p_1p_2h_1h_2}(X^{\xi_1L_1}_{p_1h_1}X^{\xi_2L_2}_{p_2h_2}+Y^{\xi_1L_1}_{p_1h_1}Y^{\xi_2L_2}_{p_2h_2}) \\
&\qquad\quad\times\Bigg((-)^{j_{p_1}+j_{h_1}}\delta_{h_1h_2}\begin{Bmatrix}L_1 & \lambda & L_2\\ j_{p_2} & j_{h_1} & j_{p_1}\end{Bmatrix}\langle p_1||F_\lambda||p_2\rangle \\
&\qquad\quad+(-)^{j_{p_1}+j_{h_2}+L_1+L_2}\delta_{p_1p_2}\begin{Bmatrix}L_1 & \lambda & L_2\\ j_{h_2} & j_{p_1} & j_{h_1}\end{Bmatrix}\langle h_1||F_\lambda||h_2\rangle\Bigg). \qquad \text{(B.69)}
\end{aligned}
$$

Bibliography

[A+05] P. Adrich et al. Evidence for pygmy and giant dipole resonances in ^{130}Sn and ^{132}Sn. *Phys. Rev. Lett.*, 95, 2005.

[BBB98] P.F. Bortignon, A. Bracco, and R.A. Broglia. *Giant Resonances. Nuclear Structure at Finite Temperature*. Harwood Academic Publishers, 1998.

[BBB+77] P.F. Bortignon, R.A. Broglia, D.R. Bes, and R. Liotta. Nuclear field theory. *Phys. Rep.*, 30, 1977.

[BFT95] I.N. Borzov, S.A. Fayans, and E.L. Trykov. Gamow-Teller strength functions of superfluid odd-A nuclei and neutrino capture reactions. *Nucl. Phys. A*, 584, 1995.

[BHR03] M. Bender, P.-H. Heenen, and P.-G. Reinhard. Self-consistent mean-field models for nuclear structure. *Revs. Mod. Phys.*, 75, 2003.

[BM69] A. Bohr and B.R. Mottelson. *Nuclear Structure Vol. I. Single-Particle Motion*. W.A. Benjamin, Inc., 1969.

[BM75] A. Bohr and B.R. Mottelson. *Nuclear Structure Vol. II. Nuclear Deformations*. W.A. Benjamin, Inc., 1975.

[BCH06] E. Baldini-Neto, B.V. Carlson, and D. Hirata. Self-consistent Dirac quasi-particle blocking approximation applied to the α-decay scheme of the superheavy element ^{287}115. *J. Phys. G*, 32, 2006.

[BP53] D. Bohm and D. Pines. A collective description of electron interaction: III. Coulomb interactions in a degenerate electron gas. *Phys. Rev.*, 92, 1953.

[BQM07] L. Bonneau, P. Quentin, and P. Möller. Global microscopic calculation of ground state spin and parities for odd-mass nuclei. *Phys. Rev. C*, 76, 2007.

[BS62] D.M. Brink and G.R. Satchler. *Angular Momentum*. Clarendon Press Oxford, 1962.

[C+97] E. Chabanat et al. A Skyrme parametrization from subnuclear to neutron star densities. *Nucl. Phys. A*, 627, 1997.

[C+98] E. Chabanat et al. A Skyrme parametrization from subnuclear to neutron star densities. Part II: nuclei far from stabilities. *Nucl. Phys. A*, 635, 1998.

[C+10] A. Carbone et al. Constraints on the symmetry energy and neutron skins from pygmy resonances in ^{68}Ni and ^{132}Sn. *Phys. Rev. C*, 81, 2010.

[CCG+11] G. Colò, L. Cao, N. Van Giai, and L. Capelli. Self-consistent RPA calculations with Skyrme-type interactions: the `skyrme_rpa` program. *Submitted to Comput. Phys. Commun.*, 2011.

[Col08] G. Colò. The compression modes in atomic nuclei and their relevance for the nuclear equation of state. *Phys. Part. Nucl.*, 39, 2008.

[CRV+02] M. Centelles, X. Roca-Maza, X. Viñas, and M. Warda. Nuclear symmetry energy probed by neutron skin thickness of nuclei. *Phys. Rev. Lett.*, 89, 2002.

[CSB10] G. Colò, H. Sagawa, and P.F. Bortignon. Effect of particle-vibration coupling on single-particle states: A consistent study within the Skyrme framework. *Phys. Rev. C*, 82, 2010.

[DD65] G. Do Dang. Collective excitations in spherical odd-mass nuclei. *Nucl. Phys.*, 62, 1965.

[E+10] J. Endres et al. Isospin character of the pygmy dipole resonance in ^{124}Sn. *Phys. Rev. Lett.*, 105, 2010.

[Ham74] I. Hamamoto. Particle spectra and particle-vibration coupling in the Pb region. *Phys. Rep.*, 10, 1974.

[HP01] C.J. Horowitz and J. Piekarewicz. Neutron star structure and the neutron radius of ^{208}Pb. *Phys. Rev. Lett.*, 25, 2001.

[HPS+01] C.J. Horowitz, S.J. Pollock, P.A. Souder, and R. Michaels. Parity violating measurements of neutron densities. *Phys. Rev. C*, 63, 2001.

[HW01] M.N. Harakeh and A. van der Woude. *Giant Resonances. Fundamental High-Frequency Modes of Nuclear Excitation.* Oxford Studies in Nuclear Physics, 2001.

[K+04] A. Krasznahorkay et al. Neutron-skin thickness in neutron-rich isotopes. *Nucl. Phys. A*, 731, 2004.

[K+07] A. Klimkiewicz et al. Nuclear symmetry energy and neutron skins derived from pygmy dipole resonances. *Phys. Rev. C*, 76, 2007.

[KLT01] S.P. Kamerdzhiev, R.J. Liotta, and V.I. Tselyaev. Random phase approximation for odd nuclei and its application to the description of the electric dipole modes in ^{17}O. *Phys. Rev. C*, 63, 2001.

[KS63] L.S. Kisslinger and R.A. Sorensen. Spherical nuclei with simple residual forces. *Revs. Mod. Phys.*, 35, 1963.

[LCK08] B.-A. Li, L.-W. Chen, and C.M. Ko. Recent progress and new challenges in isospin physics with heavy-ion reactions. *Phys. Rep.*, 464, 2008.

[LP00] J.M. Lattimer and M. Prakash. Nuclear matter and its role in supernovae, neutron stars and compact objects binary mergers. *Phys. Rep*, 333, 2000.

[LR06] E. Litvinova and P. Ring. Covariant theory of particle-vibrational coupling and its effect on the single-particle spectrum. *Phys. Rev. C*, 73, 2006.

[MBB+85] C. Mahaux, P.F. Bortignon, R.A. Broglia, and C.H. Dasso. Dynamics of the shell model. *Phys. Rep.*, 120, 1985.

[NNDC] National Nuclear Data Center (NNDC). `http://www.nndc.bnl.gov`.

[PBR+11] G. Pozzi, M. Brenna, X. Roca-Maza, K. Mizuyama, and G. Colò. Dipole collectivity in even-even nuclei. *Gordon Research Conferences, New London (NH,USA)*, 2011.

[Pie06] J. Piekarewicz. Pygmy dipole resonance as a constraint on the neutron skin of heavy nuclei. *Phys. Rev. C*, 73, 2006.

[PR08] S. Perez-Martin and L.M. Robledo. Microscopic justification of the equal filling approximation. *Phys. Rev. C*, 78, 2008.

[PNV+09] N. Paar, Y.F. Niu, D. Vretenar, and J. Meng. Isoscalar and isovector splitting of pygmy dipole structures. *Phys. Rev. Lett.*, 103, 2009.

[R+02] N. Ryezayeva et al. Nature of the low-energy dipole strength in nuclei: the case of a resonance at particle threshold in ^{208}Pb. *Phys. Rev. Lett.*, 89, 2002.

[RF95] P.-G. Reinhard and H. Flocard. Nuclear effective forces and isotope shifts. *Nucl. Phys. A*, 584, 1995.

[RN10] P.-G. Reinhard and W. Nazarewicz. Information content of a new observable: The case of the nuclear neutron skin. *Phys. Rev. C*, 81, 2010.

[Row70] D.J. Rowe. *Nuclear Collective Motion.* Methuen and co. ltd., 1970.

[RS80] P. Ring and P. Schuck. *The Nuclear Many-Body Problem.* Springer-Verlag, 1980.

[RW73] P. Ring and E. Werner. Distribution of single-particle strengths in the nuclei ^{207}Tl, ^{207}Pb, ^{209}Bi and ^{209}Pb. *Nucl. Phys. A*, 211, 1973.

[SB06] D. Santonocito and Y. Blumenfeld. Evolution of the giant dipole resonance properties with excitation energy. *Eur. Phys. J.*, A 30, 2006.

[SKC06] S. Shlomo, V.M. Kolomietz, and G. Colò. Deducing the nuclear matter incompressibility coefficient from data on isoscalar compression modes. *Eur. Phys. J.*, 30, 2006.

[Sky59] T.H.R. Skyrme. The effective nuclear potential. *Nucl. Phys.*, 9, 1959.

[Sla51] J.C. Slater. A simplification of the Hartree-Fock method. *Phys. Rev.*, 81, 1951.

[SPL+05] A.W. Steiner, M. Prakash, J.M. Lattimer, and P.J. Ellis. Isospin asymmetry in nuclei and neutron stars. *Phys. Rep.*, 411, 2005.

[TB01] S. Typel and B.A. Brown. Neutron radii and the neutron equation of state in relativistic models. *Phys. Rev. C*, 64, 2001.

[TCV08] L. Trippa, G. Colò, and E. Vigezzi. Giant dipole resonance as a quantitative constraint on the symmetry energy. *Phys. Rev. C*, 77, 2008.

[Tho61] D.J. Thouless. Vibrational states of nuclei in the random phase approximation. *Nucl. Phys.*, 22, 1961.

[VB72] D. Vautherin and D.M. Brink. Hartree-Fock calculations with Skyrme's interaction. I. Spherical nuclei. *Phys. Rev. C*, 5, 1972.

[VMK88] D.A. Varshalovich, A.N. Moskalev, and V.K. Khersonskii. *Quantum Theory of Angular Momentum.* World Scientific, 1988.

[W+09] O. Wieland et al. Search for the pygmy dipole resonance in ^{68}Ni at 600 MeV/nucleon. *Phys. Rev. Lett.*, 102, 2009.